



**Politecnico
di Torino**

Politecnico di Torino

Department of Mechanical and Aerospace Engineering

Master's Thesis

In

Mechanical Engineering

A.Y. 2021/2022

April 2022

Finite Element Analysis Of Dental Restorative Adhesives

Supervisors:

Prof. Giorgio Chiandussi

Prof. Alessandro Scattina

Candidate:

Simon Arsene Nsegbe Mgbatou

Dedication

To my mum and my late dad,
forerunners of science in the family

Abstract

In this thesis, 3-Dimensional Finite Element models were developed in LS-PrePost and then run in LS-DYNA in order to simulate three common mechanical tests very useful in the dentistry field. These tests are microtensile bond test, shear bond test and push-out test. For each of these tests, several 3-dimensional finite element models were developed with the aim to compare the experimental results to the results obtained from the numerical models. A particular attention was dedicated to the modelling of the cohesive zone in the different models. From LS-PrePost, the different geometries of the models were completely built then, the tiebreak contact was used as a first approach to model the cohesive zone in our models. The second approach consisted in using cohesive elements to model the cohesive zone in our models. The results obtained from the finite element analysis (FEA) of each model were analysed through the force-displacement curves mainly, and compared to the experimental results of these tests for the validation.

Table Of Contents

1	Introduction	9
1.1	Objectives and Purposes	10
1.2	Method and Tools	10
2	Microtensile Bond Strength Test	12
2.1	Literature Review and Experimental Test Description	12
2.2	Finite Element Model with the Tiebreak Contact	17
2.2.1	Geometry and Mesh	17
2.2.2	Materials	18
2.2.3	Boundary conditions	18
2.2.4	Tiebreak Contact	20
2.2.5	Results	22
2.3	Finite Element Model With Cohesive Elements	26
2.3.1	Geometry and Mesh	26
2.3.2	Materials	27
2.3.3	Boundary conditions	29
2.3.4	Cohesive Elements and Elements Connectivity	29
2.3.5	Results	30
2.4	Comparison between the Tiebreak Contact and the Cohesive Elements	34
3	Shear Bond Strength Test	36
3.1	Literature Review and Experimental Test Description	36
3.2	Finite Element Model With Tiebreak Contact	38
3.2.1	Geometry And Mesh	39
3.2.2	Materials	40
3.2.3	Boundary Conditions	41
3.2.4	Contact Between Parts	42
3.2.5	Results	44
3.3	Finite Element Model with Cohesive Elements	46
3.3.1	Geometry and Mesh	46
3.3.2	Materials	47
3.3.3	Boundary Conditions	48

3.3.4	Contact Between Parts	49
3.3.5	Results	51
3.4	Comparison Between the Different Approaches	53
4	Push-Out Bond Strength Test	55
4.1	Literature Review and Experimental Test Description	55
4.1.1	Literature Review	55
4.1.2	Experimental Test Description	56
4.2	Finite Element Model with the Tiebreak Contact	60
4.2.1	Geometry and Mesh	60
4.2.2	Materials	62
4.2.3	Boundary Conditions	63
4.2.4	Contact Between Parts	64
4.2.5	Results	66
4.3	Finite Element Model With Cohesive Elements	69
4.3.1	Geometry and Mesh	69
4.3.2	Materials	71
4.3.3	Boundary Conditions	72
4.3.4	Contact Between Parts	73
4.3.5	Results	74
4.4	Comparison Between The Different Approaches	77
5	Conclusion	79

List of Figures

2.1	specimens preparation	13
2.2	specimen mounted on the testing machine	14
2.3	adhesive failure of the specimen	16
2.4	mesh of the model	17
2.5	model with boundary conditions	19
2.6	Velocity load curve	19
2.7	contact segments on dentin and ceramic	21
2.8	Tiebreak contact zone: 121 of 121 nodes tied	22
2.9	stress distribution on the structure in [Pa]	23
2.10	Paths on the top surface for stress trend plots	23
2.11	Von Mises stress distribution in [Pa]	24
2.12	Paths on Cerasmart part for stress trend	24
2.13	Experimental and Numerical Force-Displacement curve	25
2.14	Geometry of the model with cohesive elements	26
2.15	cohesive elements: node to node correspondence with surrounding parts	27
2.16	no correspondence node to node	28
2.17	Model with boundary conditions	29
2.18	Von Mises stress distribution on the cohesive node to node model [Pa]	31
2.19	Von Mises stress distribution on the cohesive tied contact model [Pa]	31
2.20	Von Mises stress distribution in [Pa] on parts: cohesive elements with node to node correspondence model	32
2.21	Von Mises stress distribution in [Pa] on parts: cohesive elements with tied contact model	32
2.22	Force-Displacement curves node to node model	33
2.23	Force-Displacement curves tied contact model	34
2.24	Force-Displacement curves	35
3.1	Dimensions of a generic specimen for the micro shear bond test	38
3.2	Specimen mounted on the testing machine for the micro shear bond test	38
3.3	Geometry of the model	39
3.4	Shear bond test model: The mesh	40
3.5	Boundary Conditions enforced on the model	41
3.6	velocity enforced to the indenter	42

3.7	segments sets for the tiebreak contact	43
3.8	Von Mises stress distribution on the model [GPa]	44
3.9	Von Mises stress distribution on each part[GPa]	45
3.10	Force-Displacement curves	46
3.11	Geometry of the model and mesh generated from the geometry	47
3.12	Boundary conditions: Constrained nodes in white	49
3.13	Contact between the indenter and the enamel	49
3.14	segments set defined on the dentin and the adhesive for the tied contact . .	50
3.15	segments sets defined on the enamel and the adhesive for the tied contact .	50
3.16	Von Mises stress distribution on Enamel [GPa]	51
3.17	Von Mises stress distribution on Dentin [GPa]	51
3.18	Force-Displacement curves	52
3.19	Force-Displacement curves	53
4.1	Schematic drawing of the specimen preparation procedure for the micro- push-out bond strength test on 1 mm thick slices. (A)The crowns were removed 2 mm above the cemento-enamel junction (CEJ). (B) After the cleaning-shaping procedure, an adhesive root canal filling was performed. (C) Preparation of the post-space with pre-calibrated burs.(D) Cementa- tion of the fiber post into the root canal.	57
4.2	Schematic drawing of the specimen preparation procedure: slices obtained from each root canal.	58
4.3	Schematic drawing of the specimen mounted on the testing machine	58
4.4	Force-Displacement curve registered for the sample submitted to micro- push-out test.	59
4.5	Geometry of the model exploded with dimensions	60
4.6	Isometric view of the model meshed: the part in red represents the mesh generated from the dentin, the part in green represent the mesh generated from the cement layer, the part in blue represents the mesh generated from the glass post and the part in yellow the mesh generated from the steel rod.	61
4.7	Down view of the model: constrained nodes highlighted in red	63
4.8	velocity curve prescribed to the rod	64
4.9	contact between the rod and the glass post	64
4.10	Tiebreak contact defined on the two subgroups of parts	65
4.11	Von Mises stress distribution on the model in [GPa]	66
4.12	Von Mises stress distribution on the cement and the glass post in [GPa] . .	67
4.13	Von Mises stress distribution on the dentin in [GPa]	68
4.14	Force-Displacement curves	69
4.15	Geometry of the model	70
4.16	Mesh generated from the parts	71
4.17	Partial top view of the model	73
4.18	Von Mises stress distribution on the whole model	74
4.19	Von Mises stress distribution on the glass post and the cement in [GPa] . .	75

4.20	Von Mises stress distribution on the dentin in [GPa]	75
4.21	Stress distribution on the cohesive layers in [GPa]	76
4.22	Force-Displacement curve	77
4.23	Force-Displacement curve	78

List of Tables

2.1	Mechanical properties of the materials	18
2.2	Equivalence between the parameters used by the solver algorithms for the two different approaches. The parameters belonging to the same row have the same physical meaning.	35
3.1	Dimensions of the parts and Mesh size of the elements	39
3.2	Properties of the materials	40
3.3	Equivalence between the parameters used by the solver algorithms for the two different approaches. The parameters belonging to the same row have the same physical meaning.	53
4.1	Mesh properties of the different parts	62
4.2	Mechanical properties of materials	62
4.3	Properties of the mesh for each part	71
4.4	Equivalence between the parameters used by the solver algorithms for the two different approaches. The parameters belonging to the same row have the same physical meaning.	77

Chapter 1

Introduction

Nowadays, restorative dentistry appears to be one of the most developing areas of medical care, principally connected with the commonness of dental caries. By restorative dentistry we refer to any dental procedure that repairs or replaces a tooth. Restorative procedures include cavity fillings, root canals, and even dental implants. There can be two goals in restorative dentistry: the restoration of the function of the teeth and the restoration of the appearance of the teeth. In some cases it's one or the other, and in some cases it's both. Most often, the adhesive materials are used in the dentistry field and greatly contribute to the teeth restoration. MJ Tyas and MF Burrow state that adhesive restorative dentistry originated with the work of Michael Buonocore in 1955 in bonding resin to etched enamel. Buonocore was able to demonstrate that the treatment of enamel with phosphoric acid resulted in a porous surface, which could be infiltrated by resin, to produce a strong micromechanical bond. However, the clinical application of acid etching was not realized until 15 years later when resin composites became available as a result of the work of Bowen's group. In contrast to micromechanical bonding to tooth tissue, chemical bonding was developed by Smith and resulted in the introduction of polycarboxylate cement. Since then, adhesive materials and techniques have developed at a rapid rate. The first chemically adhesive material (zinc polycarboxylate cement) was marketed in the late 1960s, and glass-ionomer cements and dentine bonding agents have since become available [1]. The rapid development by companies of adhesive systems for the restorative dentistry gave birth to the necessity of characterize them in order to have a better knowledge of their properties. The adhesives used in the field of restorative dentistry have several properties but, the properties of interest for us are the mechanical properties. The mechanical properties of the restorative adhesives are evaluated through some tests such as microtensile bond strength test, shear bond strength test and push-out test. These tests are commonly used in the dentistry field for that purpose. The results obtained in the laboratories from these tests are considered to be good enough nevertheless, with the development of numerical methods for the resolution of physical problems described by partial differential equations, numerical models have been increasingly built in recent years in order to have information that would have been difficult if

not impossible to obtain from the experimental tests.

1.1 Objectives and Purposes

The objectives in this thesis work is the analysis via the finite element method of different adhesive systems used in the restorative dentistry. This analysis needed to be performed through the microtensile bond strength test, the shear bond strength test and the push-out test. Therefore, it was necessary to build some numerical models for each of these tests. The building of the numerical model included the construction of the geometries, the generation of the mesh, the definition of all the material models which represent in the best way the real materials, the definition of all the contact experienced by the parts, the definition of the boundary conditions ...etc. Since, the attention was dedicated to the adhesive systems used in these models, the cohesive zones were modelled using two different approaches. The first approach used for the modelling of the adhesive in the model was the Tiebreak Contact. As the second approach, we used cohesive elements to model the adhesive systems in the different numerical models. These two adhesive models allowed us to have information such as the adhesive bond strength, the adhesive stiffness and the stress distribution on the parts surrounding the adhesive. The results obtained from these two adhesive models were compared then. The force-displacement curve obtained from each numerical model was compared to its correspondent experimental force-displacement curve for the validation.

1.2 Method and Tools

In this thesis, the analysis of restorative adhesives was performed via the finite element method. As it is widely known, the finite element method (FEM) is a numerical method widely used nowadays to solve physical problems in the fields like structural mechanics, heat transfer, fluid flow, mass transport, ...etc. Roughly speaking, to solve a problem, the FEM subdivides a large system into smaller and simpler parts from the point of view of the shape that are called finite elements. The finite element method is useful because it can give if well used some information which are accurate enough in particular when we are interested in information or phenomena regarding particular locations of a domain. For this thesis, we opted for the software LS-DYNA to run the different models built in LS-PrePost which is the pre and post processing software of LS-DYNA.

LS-DYNA is an advanced general-purpose multiphysics simulation software package developed by the former Livermore Software Technology Corporation (LSTC), which was acquired by Ansys in 2019. LS-DYNA's potential applications are multiple and can be accommodated to many fields. LS-DYNA is not limited to any particular type of simulation. In a given simulation, any of LS-DYNA's features can be combined to model a wide variety of physical problems. Some features make LS-DYNA one of the main simulation software used to solve physical problems. Being a general purpose multiphysics

software, it can simulate a wide range of problems. Its material library is also a huge advantage for the analysts because it contains a very large material models which allows the analyst to easily find the material model which fit the best reality. Another advantage in using LS-DYNA is the possibility to choose in between several contact algorithms to model the contacts and interactions between parts in a model. The capability to predict accurately events which involve large deformations such as car's behavior in a collision, sheet metal forming...etc makes it one of the softwares most used for these applications in the industry. The main solution method implemented in LS-DYNA is the explicit time integration. The implicit solver is also available but presents a lot of limitations because a lot of features such as contact algorithms, element formulations...etc are not available for the implicit solver. For this work, all the simulations were realized using the version LS-DYNA R9 Finite Element explicit solver.

Chapter 2

Microtensile Bond Strength Test

2.1 Literature Review and Experimental Test Description

Many laboratories use tensile bond tests to compare adhesive systems or evaluate the influence of experimental variables on restorative material-dentin bond strength. Generally, they limit the location of the bond to the center of the occlusal or labial surface of midcoronal normal dentin. The bonded surface is demarcated using a 3 *mm* or 4 *mm* diameter hole punched in sticky tape, or some type of matrix is used that is 3 to 4 *mm* in diameter (7 to 12 *mm*²). These simple tests served well when restorative material-dentin bond strengths were relatively low (circa 10 to 15 MPa). However, as bonding techniques and materials improved, the bond strengths became high enough to cause cohesive failures in dentin or in the restorative material. That is, dentin broke from dentin, leaving the restorative material dentin interface intact or the restorative material broke leaving the dentin-resin bonded interface intact. The frequency of cohesive failures of dentin for instance can be as high as 80% when bond strengths reach 25 MPa. Such failures of the substrates preclude measurement of interfacial bond strengths and limit further improvements in bonding formulations, since the tests can no longer detect improved adhesion. Such cohesive failures in dentin or even in the restorative material do not mean that the restorative material-dentin are uniformly stronger than the intrinsic strength of dentin, but that the way in which the bond is stressed is so non-uniform that it is concentrated or focused at one highly localized region where it opens a crack either in dentin or in the restorative material, that then fails [2]. These stress concentrations often exceed 10 MPa, even though the calculated average bond strength is only 32 MPa.

To avoid cohesive failures of dentin during bond testing, it is necessary to improve stress distributions during testing. This can be accomplished by the microntensile bond testing method. It is a labor-intensive method than the conventional method but avoid inducing cohesive failures in dentin. This method tends to lower the variance associated with testing

to 10% to 25%, instead of the more common 30% to 50% variance seen in conventional testing. Since it may be difficult to obtain extracted teeth, especially intact premolars and

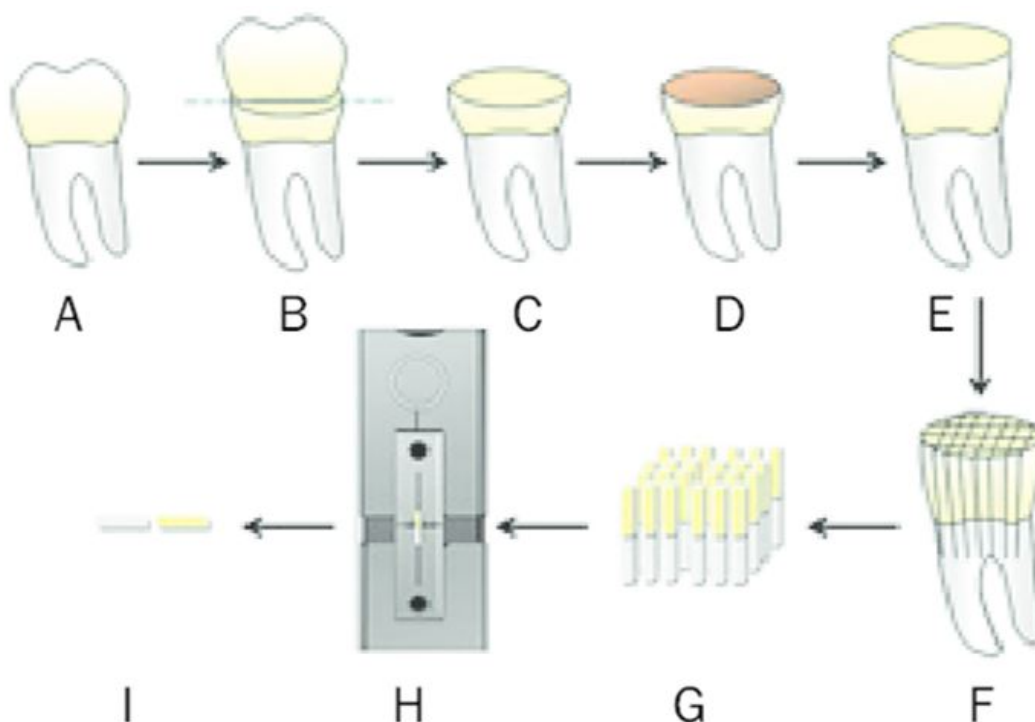


Figure 2.1: specimens preparation

third molars, the microtensile testing method allows multiple specimens to be prepared from each tooth (fig:2.1). Therefore, there is a compromise between the extra labor involved in using this method and the extra data that can be obtained per tooth.

Microtensile bond testing was originally designed to permit evaluation of bond strengths between adhesive materials and small regions of dental tissue(eg, occlusal vs middle vs cervical third of enamel, normal vs adjacent caries-affected dentin, occlusal vs gingival walls of Class vs wedge-shaped lesions). One advantage of the technique is that the bonded interface of small specimens (about $1mm^2$) has a better stress distribution during loading, so that there are fewer cohesive failures in dentin than are found with more conventional testing. This is thought to be due to a reduction in flaw density. Using this method often results in higher apparent bond strengths at failure than are found using large specimens. Since the introduction of the technique, a number of laboratories have made numerous modification to it.

The original microtensile testing was done on mineralized dentin to measure its ultimate tensile strength (UTS) and modulus of elasticity. To measure the ultimate tensile stress, the specimens were trimmed to an hourglass profile to produce uniform stressing of the smallest cross-sectional area. To measure the modulus of elasticity in tension, the need

of a known gauge-length required that the specimens be trimmed to the outline of an "I" beam. That approach has also been used to measure the ultimate tensile stress and elastic modulus of the demineralized dentin matrix by protecting the mineralized ends of the specimens with nail varnish, while the central region was demineralized in EDTA.

Nowadays, several adhesive systems are used in the dentistry field. With the microtensile bond strength test, scientists can measure the strength of the bond due to the adhesive system in the restorative dentistry. The essence of the microtensile test is therefore the division of resin-bonded teeth into slabs 1.0 mm thick that are then trimmed in such a manner that tensile force will be concentrated on the bonded interface during testing. Among the many advantages of the technique as we said are that each tooth produces



Figure 2.2: specimen mounted on the testing machine

multiple specimens. Further, there is no need for a matrix to limit the bonded surface area, since the area is determined by the dimensions of the trimmed specimens.

It is also important to say that so far, no standard test has been approved for measuring the bond strength of dentin and composite using dental adhesive system. Different test methods and parameters used have resulted in discrepancy of the data reported by different researchers on the same adhesive system. The factors affecting the bond strength have been addressed by few researchers before. Pashley et al have listed these factors in a review paper under the broad categories of substrate variables, etching variables, priming variables, bonding variables, storage variables and testing variables. Most of this review has focused on the issues relating to the differences induced by the material properties or the process used in sample preparation. The substrate and adhesive variables induce inherent differences in the material properties. Data reported on the dentin and bovine strength can be up to 50% different depending on the source and part of the dentin or bovine used. The same sort of data spread is reported for demineralized dentin, with some data on the strength being almost one-third of the other test data. The process

used in the preparation of the sample as well such as etching and priming have effect on the interface properties and therefore on the bond strength.

Van noort et al. [3-4] have analyzed the effect of the test method in the bond strength results. They have made a comparison between the microtensile test and shear test in measuring bond strength. Applying FEA they have concluded that the shear test results in unfavorable stresses in the specimen. Consequently, they have recommended the tensile test as a preferred test method for measuring bond strength. While the advantages of the microtensile test were proved, many researchers applied the method to measure the bond strength of dental adhesive [5-6]. Nakabayahsi et al. [7] apply the method to detect defects in the specimen. They study the effect of defects in the failure characteristics of the miniaturized samples. Capel Cordoso et al. [8] use the microtensile bond strength to compare the bond strength of three adhesive systems with the cohesive strength of dentin and composite. In all three systems they find the adhesive bond strength to be much lower than the strength of composite or dentin. Yoshiyama et al. [5] apply the microtensile test to measure the bond strength to different regions of dentin. They have reported higher bond strength on the coronal and apical dentin compared to the bond strength to the cervical root dentin. The effect of specimen size and geometry in the results of the bond strength is studied partly by other researchers[4]. Phrukkanon et al. [9] have investigated specimens with round and rectangular cross sections. For four different adhesive systems they have reported higher bond strength for the circular cross section compared to the rectangular cross section. The second parameter they have considered is the cross sectional area of the samples. For three different cross sections, lower bond strength is estimated for larger cross sections. The results have been explained using FEA to estimate the stress distribution. They have attributed this result to higher stress values for the samples with larger cross section. Other researchers have used Griffith theory to explain the same results. They have reasoned that smaller samples will have smaller flaw size and therefore higher strength. In Phrukkanon's research they have increased the surface area without changing any other part of the sample. If they scale up all parts of the sample with the surface area the FE results would not indicate any changes for different surface areas. Whereas experimental tests still indicate smaller strength for the samples with larger cross sectional area. This shows a second parameter having role in reducing the bond strength for the larger size specimens which is recommended by Griffith's theory. Although the researchers have highlighted the parameters affecting the result of the bond strength in the previous studies, there is little indication of quantifying each effect and systematic study. At the same time most of the previous researches on the factors affecting the result of the bond strength have identified only one or two parameters, ignoring the other parameters. Elaheh Ghassemieh has considered broad range of factors affecting the bond strength and modes of failure. Using finite element analysis he has investigated the effect of each parameter on the general stress distribution in different regions of adhesive, at the interface of the adhesive and composite and at the interface of adhesive and dentin. He has quantified the effect of each variable on the bond strength and modes of failure for the most commonly used geometries of stick, dumbbell and hourglass. He stated that the advantage of using finite element analysis to study

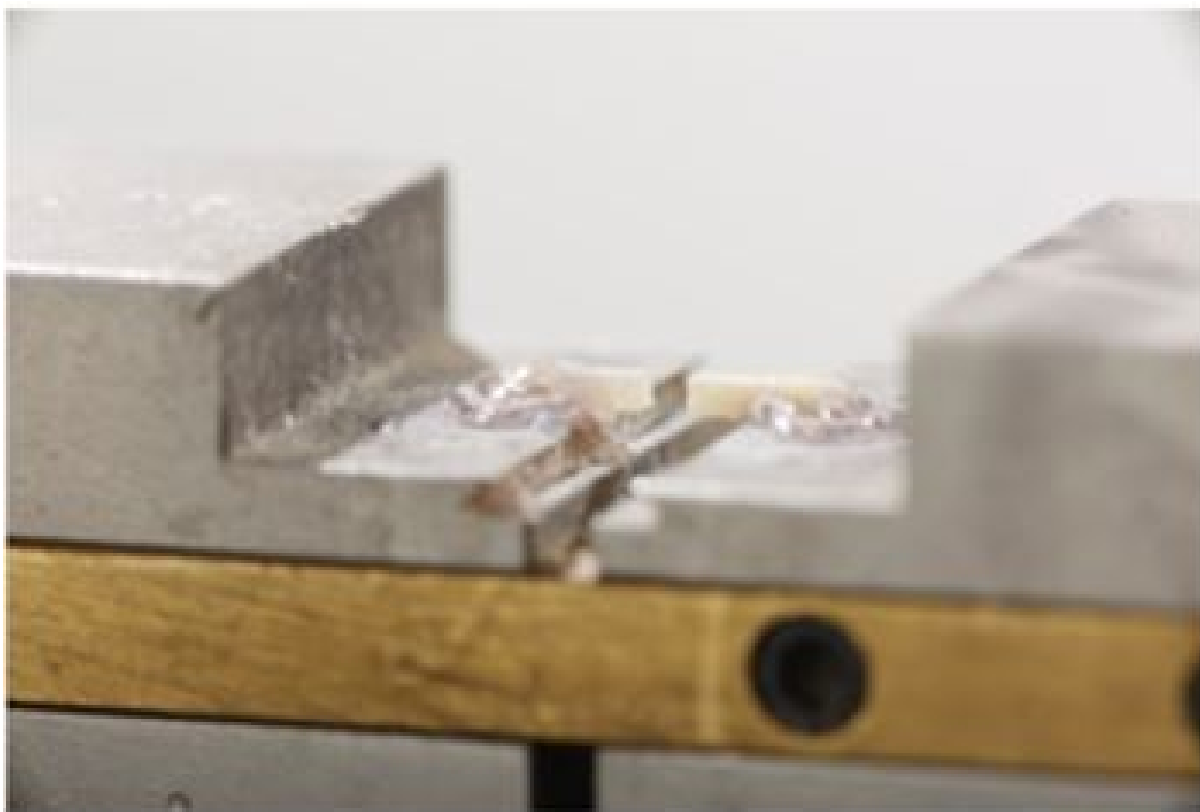


Figure 2.3: adhesive failure of the specimen

and evaluate the sources of uncertainties in microtensile bond strength of dental adhesive system for different specimen geometries is that, it makes separation of the parameters and its effect possible. The experimental tests do not allow to isolate the different factors that might influence the bond strength and therefore, interaction of the variables which influence the microtensile bond strength test is normally unavoidable. The final FEA predictions of bond strength, its variations and modes of failure are derived from bringing together the results of analysis for all the identified individual parameters. Elaheh Ghassemieh [4] performed microtensile bond strength experiments in order to validate the FEA estimation of the mode of failure, bond strength and its standard deviation for the mentioned geometries. His results showed that the experimental measurements of these parameters and the ranking of different geometries in bond strength approve the collective predictions of FEA and confirmed the reliability of the finite element analysis in its estimation of other individual effects as well.

We can say that the microtensile bond strength test consist in mounting a specimen with 1mm X 1mm cross section on a testing machine as shown in figure 2.2.

Then, an axial load is applied to the specimen in other produce a stress state in the specimen which will caused the failure of the specimen. As we already stated, it is necessary to have an adhesive failure (fig2.3) of the specimen in order to evaluate the

tensile bond strength dividing the peak of the axial force registered by the cross section area of the specimen.

2.2 Finite Element Model with the Tiebreak Contact

Two approaches were used to model and simulate the microtensile bond strength test in order to characterize the adhesive system used in restorative dentistry. The main difference between the two models corresponding to the two approaches that we used lies in the modelling of the cohesive zone of our models. Here is the description of the first approach based on the modelling of the cohesive zone of our model with the Tiebreak Contact in LS-DYNA.

2.2.1 Geometry and Mesh

The pre-processing step was performed in LS-PrePost (LSPP) which is an advanced pre- and post-processor and model editor from LSTC, preparing input data for LS-DYNA. Concerning the geometry, the useful information was the dimensions of the parts constituting our model. The experimental test allowed us to have a clear idea on the geometry of our model. Therefore, Two solid parts with dimensions $1mm \times 1mm \times 5mm$ were modelled in LS-PREPOST, then we generated a three dimensional solid mesh from the two parts since they are solid (fig2.4). In order to have a realistic mesh of our model, the meshes generated from the two parts of our model were different from the point of view of the mesh size. This choice was made in order to have a more realistic contact simulation between the two parts as we will see later. Therefore we chose a mesh with a maximum

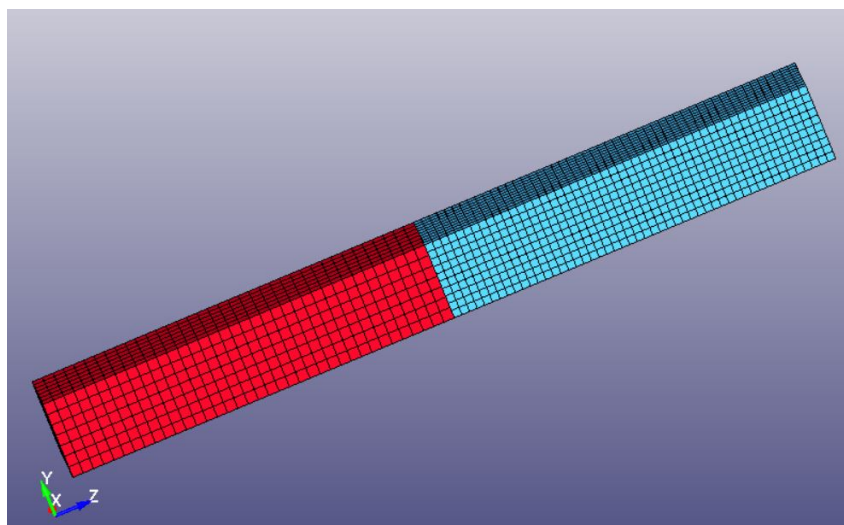


Figure 2.4: mesh of the model

element size of $0.14mm$ for the part in red which represents the dentine while, we chose

a mesh with a maximum element size of $0.1mm$ for the part in blue which represents the enamel. Once we generated the mesh of our model, we assigned to the elements of our model an element formulation among those proposed by LS-PrePost. Being the parts of our model with regular geometries, we opted for hexahedron elements with element formulation ELFORM=3. This choice of the element formulation is justified by the fact that ELFORM 3 are fully integrated solid elements therefore, such elements prevents us from having hourglass modes.

2.2.2 Materials

The model of the experimental test was constituted by dentine, cerasmart and a cement known as PANA VIA V5. In this three dimensional finite elements analysis, all the parts of our model were considered homogeneous, linear, and isotropic. For this reason, in the LS-DYNA material library, all the materials were modelled with the MAT_001 which corresponds to MAT_ELASTIC and is an isotropic elastic material which is available for beam, shell, and solid elements in LS-DYNA. The mechanical properties useful for the finite element analysis are given in the table 2.1.

Materials	Young's Modulus(GPa)	Poisson's Ratio
Dentin	18	0.31
Cement	1	0.30
Cerasmart	69	0.28

Table 2.1: Mechanical properties of the materials

Perfect adhesion between the ceramic (cerasmart) and the cement and between the cement and dentin was assumed. The choice of the material behaviour and properties is motivated by the choice made in all the previous studies that were found in the literature.

2.2.3 Boundary conditions

The definition of the boundary conditions on our model was performed in order to simulate in the best possible way the boundary conditions enforced during the experimental test. It is worth to say that previous studies have been performed in order to understand how the boundary conditions enforced on the numerical model can affect the results of the simulation. These previous studies demonstrated that boundary conditions affect not only qualitatively the results of the microtensile bond strength test, but also quantitatively. In our case, the experimental text allowed us to constrain all the degrees of freedom of the nodes belonging to the elements going from the base to $1mm$ of the dentin just like we can see the nodes highlighted in white in the figure 2.5. Since we opted for an explicit analysis, it was necessary to enforce a displacement law on the nodes belonging to the elements going from $9mm$ to $10mm$ (being the base of the dentine the origin of our frame

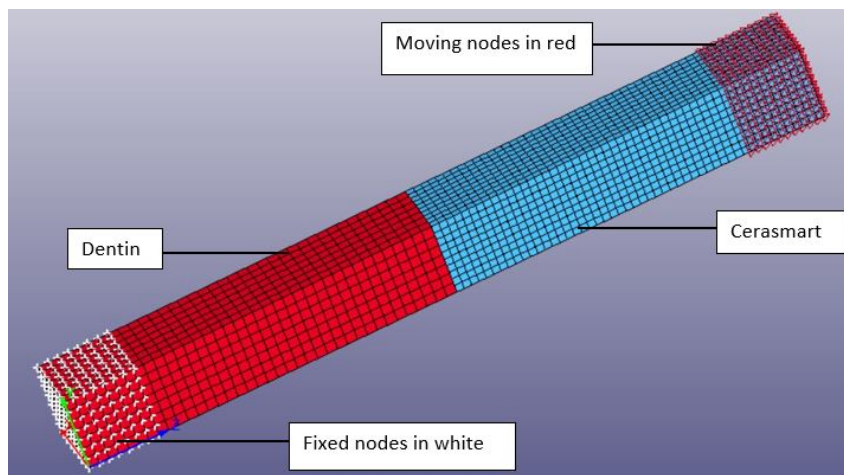


Figure 2.5: model with boundary conditions

of reference). The velocity enforced on those nodes in order to generate the load is shown on the figure 2.6. We had the choice to enforce either a constant velocity on the moving

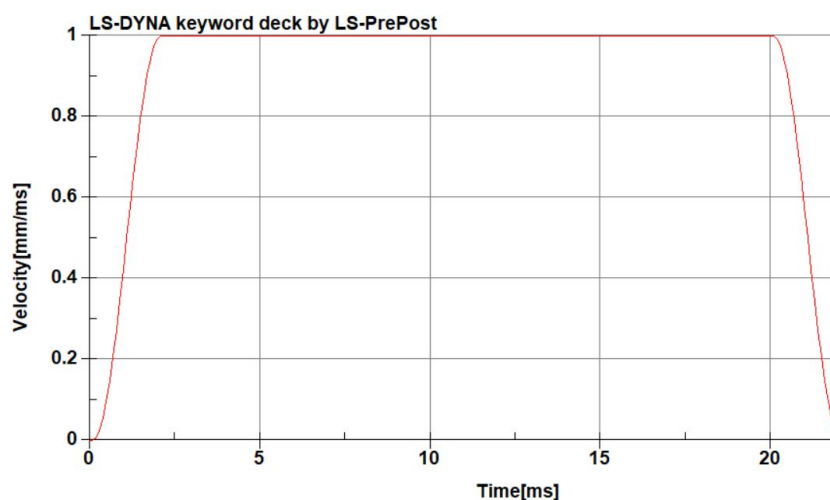


Figure 2.6: Velocity load curve

nodes or a linear velocity, but we opted for a smoothly changed velocity curve. Such a load curve was chosen in order to avoid significant accelerations during the loading of the structure. Significant accelerations during the loading phase would have introduced dynamic effect on the model that we needed to avoid. It is also important to highlight the fact that the experimental test is performed with a loading machine moving at around 5mm/min. Such a velocity is too low for an explicit analysis because it requests a very long simulation time which is directly linked to the CPU time. Therefore, we decided to accelerate the numerical test in order to reduce the CPU time namely reduce the computational cost.

2.2.4 Tiebreak Contact

In order to simulate the adhesive interface between the dentin part and the ceramic part of our model, we opted in a first attempt for a Tiebreak Contact type in LS-PrePost. going to the keyword contact in LS-PrePost, we have the choice between several possibilities of contact.

The CONTACT_AUTOMATIC_SURFACE_TO_SURFACE_TIEBREAK was chosen to model the cohesive zone in our model. In general, to completely model the cohesive zone, several parameters have to be set in the right way. Here follow the parameters that were used to completely define the cohesive zone.

- Option 6: in the contact card we had to chose an option for the contact that we chose. The choice of this option was based on the description given by LS-DYNA_Manual_Volume_I_R12. From the manual volume, we can notice that option 6 is suitable for the use with solids and thick shells elements only. Tiebreak is active for nodes which are initially in contact. Failure stress must be defined for tiebreak to occur. After the failure stress, tiebreak criterion is met. damage is a linear function of the distance between points initially in contact. When the distance is equal to PARAM, damage is fully developed, and interface failure occurs. After failure, this option behaves as a surface-to-surface contact. Since our model is made of solid elements, this option is suitable for our model.
- NFLS: for the option 6 that we have just seen, NFLS represents the normal failure stress of the adhesive. The value of the normal failure stress was unknown but a value of 46 MPa was chosen in order to guarantee the microtensile bond strength given by the experimental test.
- SFSL: it represents the shear failure stress in the contact card. For the microtensile bond strength test, SFSL is not very important because the shear stress in this model is very low therefore, it does not really influence the failure of the contact.
- PARAM: for option 6, PARAM is the critical distance (CCRIT), at which the interface failure is complete. Since we did not have the experimental force- displacement curve, such a parameter was not important for our analysis.
- CT2CN: it represents the ratio of the tangential stiffness of the adhesive to the normal stiffness of the adhesive. This was set to be equal to 1. This parameter was not very important for the analysis since the microtensile bond strength test normally a pure mode.
- CN: is the normal stiffness (stress/length) for OPTION = 6. If CN is not given explicitly, the penalty base approach that we will discuss later on is used to define the normal stiffness dividing the penalty stiffness divided by segment area (default). The manual recommends the use of this option with care, since contact stability can get affected. A value of 18500 GPa/m was assigned on the basis of the Young's modulus of the adhesive systems used during the experimental test.

Now that we have all the variables influencing the cohesive zone in our model, let us see how damage and failure occur in the tiebreak contact option that we chose. The tiebreak failure criterion has normal and shear components and is given by the following relation:

$$\left(\frac{\sigma_n}{NFLS}\right)^2 + \left(\frac{\sigma_s}{SFLLS}\right)^2 \geq 1 \quad (2.1)$$

Whereby σ_n is the tensile normal stress and is taken as zero if the normal stress is compressive while σ_s is the shear stress. Damage initiates when the stress meets the failure criterion. We can easily note from the relation 2.1 that in case the shear stress σ_s is very low, the second term at the right member of the relation will tend to zero therefore, the damage will be ruled almost only by the normal stress σ_s .

In LS-DYNA, in order to define the contact between parts of a model, we need to decide whether the contact will be of type node to node, segment to segment or part to part.

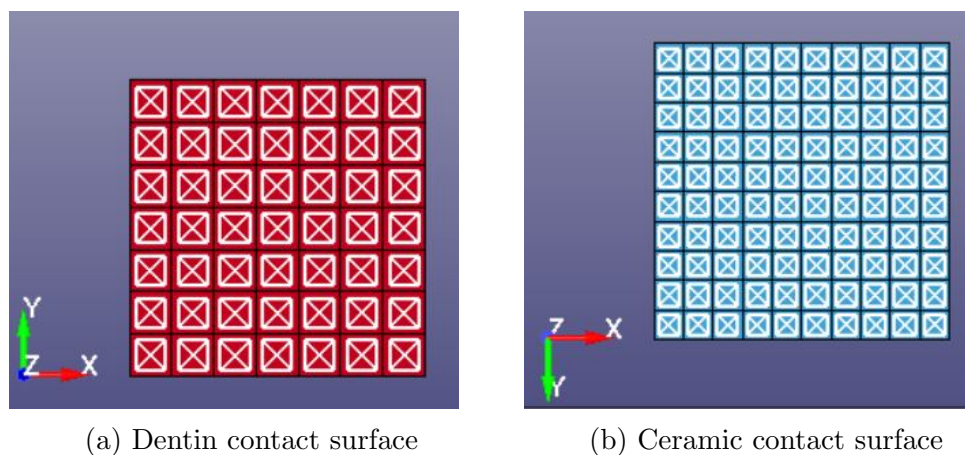


Figure 2.7: contact segments on dentin and ceramic

This has to be defined when we have decide the slave and master side of a contact in general. The right choice depends on the model and on the type of contact the analyst is dealing with. LS-DYNA manual recommends that the slave and master sides of tiebreak contact be defined using segment sets rather than part or part set. By doing this, we can be more selective when choosing which segments are to be tied and ensure that contact stresses calculated from nodal contact forces are not diluted by segments that are not actually on the actual contact surface. We also have more direct control over the contact segment normal vectors when segment sets are used. Segment normal vectors should point toward the opposing contact surface so that tension is properly distinguished from compression.

Checking the contact zone, we can realize that LS-PrePost give the message 121 of the 121 nodes are tied (fig2.8). This means that all the nodes of the part which has a higher mesh density are tied to the surface of the dentin part which has a lower mesh density.

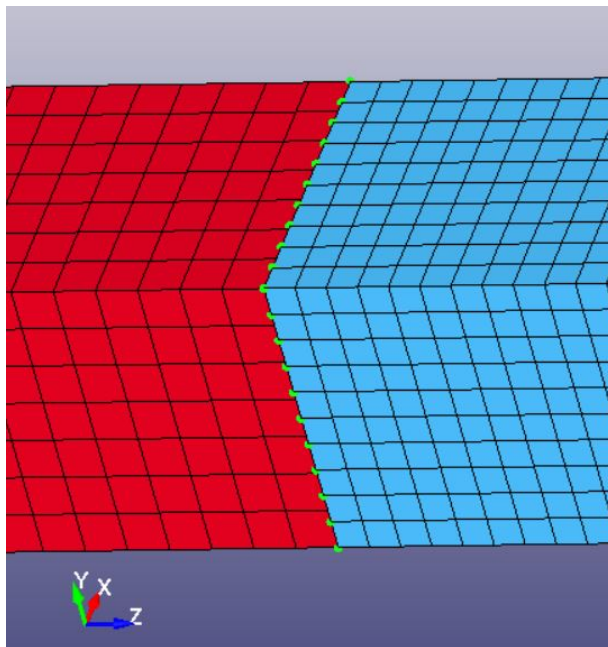


Figure 2.8: Tiebreak contact zone: 121 of 121 nodes tied

2.2.5 Results

After all the pre processing steps performed on LS-PrePost that we just described, the simulation was run through the cluster of the HPC@POLITO, a powerful tool furnished by the Politecnico di Torino and managed by the Department of Automation and Computer Science (DAUIN) of the Politecnico. That corresponds in calculation resources and technical support for academic and didactic research activities using centre systems. The cluster used in this thesis work was Legion cluster. The simulation was completed in 35 minutes and 48 seconds with 64 cores on 2 nodes. Here follow the main results obtained from the simulation after the post processing on LS-PrePost.

2.2.5.1 Stress Distribution

Von Mises stress distribution on the entire model shows that the stress is almost null at the ends of our structure. Then from both the sides of our structure, the closer we are from the cohesive zone of the model, the higher is the stress (fig2.9).

We also plotted Von Mises stress distribution in z direction along all the structure. The first path regards the stress distribution in z direction at almost the center of the model on the top surface as shown in figure 2.10a While the second path was chosen in order to

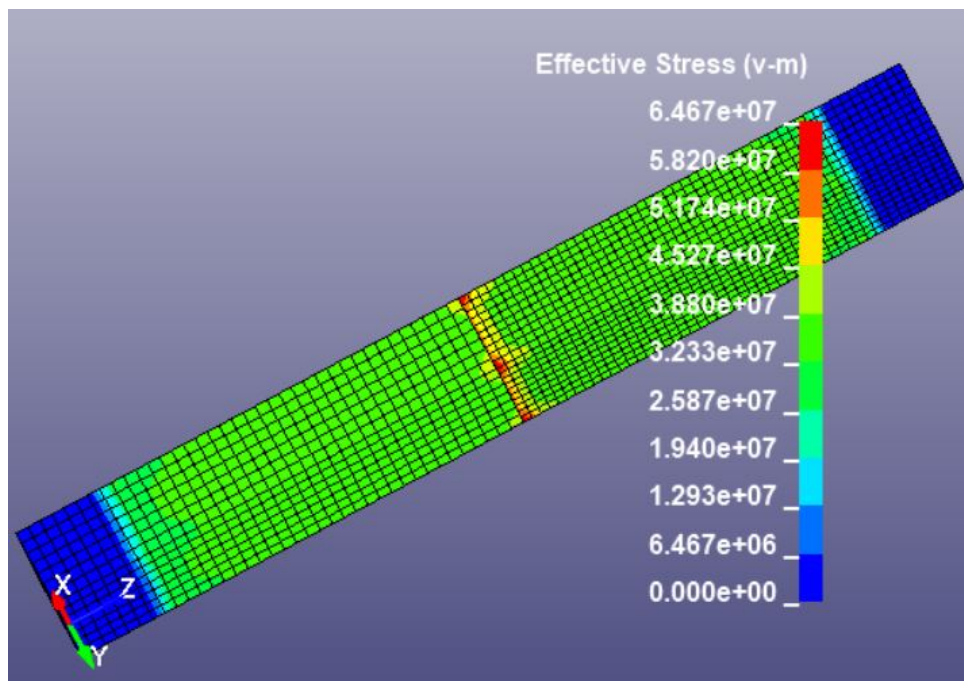


Figure 2.9: stress distribution on the structure in [Pa]

represent the stress distribution in z direction but this time at an edge of the structure (fig 2.10b).

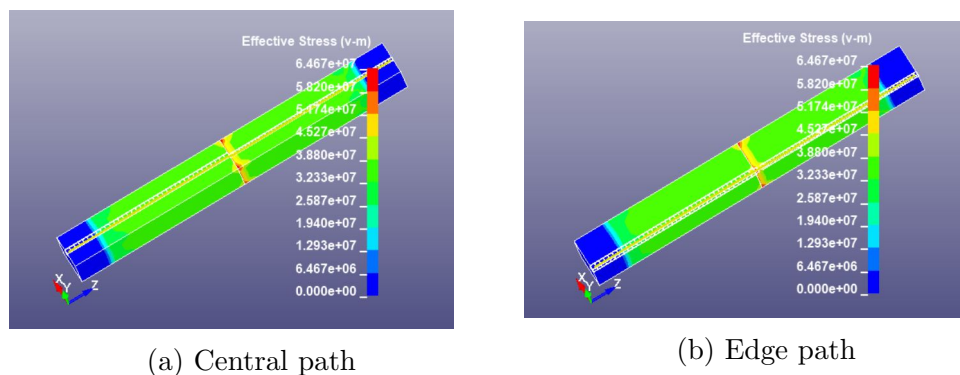


Figure 2.10: Paths on the top surface for stress trend plots

Since the stress distribution is almost symmetric in each part of the model in all the directions, it was not necessary to plot and represents the stress distribution along other paths since the one we represented are already describing the whole structure quite well. The stress trend along the paths we just mentioned shows us that the maximum stress is located at the edge of the structure around the contact interface (at 5mm) as shows figure. In fact we can realize that the green curve which represents the trend at the edge has its maximum at the distance 5mm and the value is 64.7MPa . We can also realised

that along the central path, the maximum stress is around 50 MPa. This result allows us to deduce that the failure begins at the edges of the contact interface. In the same way, we tried to figure out the difference in stress distribution on the parts constituting our model. We realized that the restorative material (Cerasmart) has higher stress values with respect to the dentin.

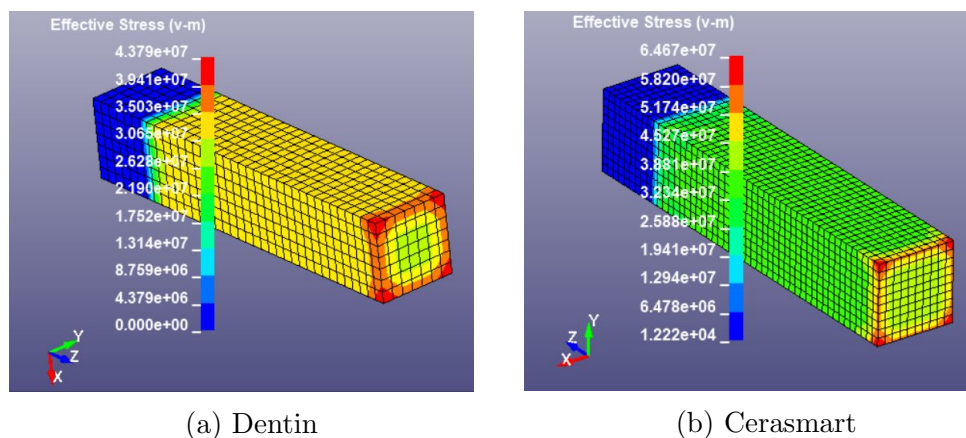


Figure 2.11: Von Mises stress distribution in [Pa]

Since the maximum stress is located on the Ceramic part of the model, we were interested in understanding how is distributed the stress at the tiebreak contact interface on the restorative material. Just like in the case of stress trend in z direction on the top surface, Two paths were chosen in y direction. The first path was chosen in order to represent the stress trend at the center of the contact area while the second one was chosen in order to represent the stress trend at the edge of the contact area.

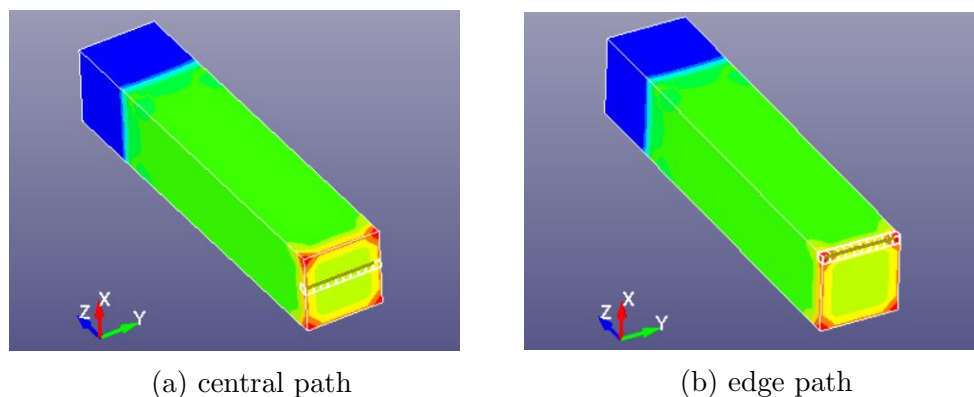


Figure 2.12: Paths on Cerasmart part for stress trend

Due to the symmetry of our model, we know that this two paths that we chose in y direction at the contact surface of our model are enough to have a clear idea on how is distributed the stress at the tiebreak contact interface which simulates the adhesive.

We have a same trend for the dentin part with the only difference that the dentin part is less stressed with respect to the cerasmart part. It worth to precise that the stress trends along all the paths that we plotted is just an indication of the stress distribution on the path. In order to obtain more realistic curves, it its necessary to have a finer mesh in such a way that we can have enough point on the curves.

2.2.5.2 Force-Displacement Curves

From the post processing, the force-displacement curves were also plotted in order to validate the numerical model, by comparing the experimental curve to the numerical curve that we obtained. From the experimental test. From the experimental test, we were able to obtain the adhesive tensile bond strength which is 32,58 MPa for PANAVIA V5. To the value of the tensile bond strength, we were also able to find the adhesive Young modulus which is given in table 2.1. The experimental value of the adhesive Young modulus combined to the value of the tensile bond stress allowed us to have the experimental force-displacement curve. The same value of the adhesive stiffness was introduced in the solver algorithm as the stiffness of the tiebreak contact.

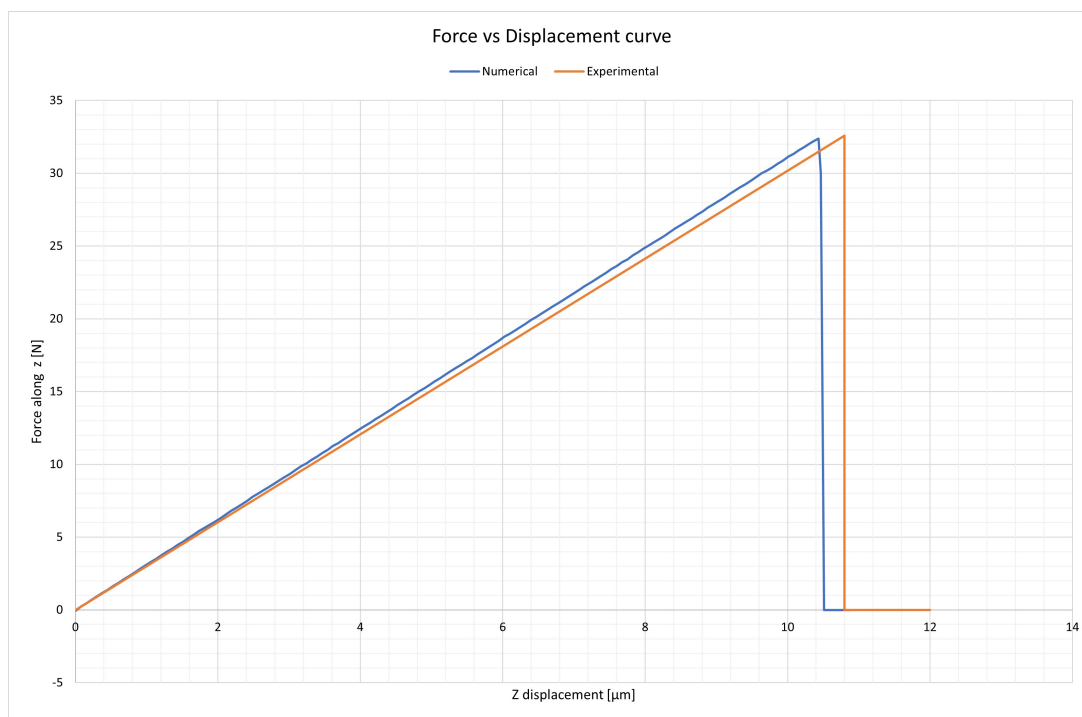


Figure 2.13: Experimental and Numerical Force-Displacement curve

From the figure 2.13 we can realize that the peak of the force obtained from the numerical results is 32,5 N. Considering the contact area of our model which is 1mm^2 , we computed the microtensile bond strength test from the equation and we obtained the value 32,5 MPa. The numerical value of the tensile bond strength is quite close to the value obtained from

the experimental test which is 32,58 MPa. We can also say that the slopes of both the curves which depend on the stiffness of the model are fairly close. For what concerns the peak of the force, it is worth to say that the value of 32,5 N obtained from the numerical results was possible after running the model with different adhesive normal failure stress (NFLS). Therefore, several models were run inserting each time a different value of the adhesive normal failure stress up to reach the right value of the traction peak. Concerning the slope of the numerical force-displacement curve, we realized that by inserting material properties and by setting as the tiebreak contact stiffness the experimental stiffness of the adhesive, the results is quite close to the experimental one without the need of tuning the curve.

2.3 Finite Element Model With Cohesive Elements

The second approach that was used to model the microtensile bond strength test is the use of the cohesive elements within the model. The main difference between this approach with respect to the first one is the use of cohesive elements to simulate the adhesive within the model instead of a contact between the two parts constituting our model.

2.3.1 Geometry and Mesh

The geometry for this model with cohesive elements is almost the same with the previous one because the main parts of the model (dentin and cerasmart) have the same dimensions. However, a new part was inserted in the model in between the two main parts in order to simulate the adhesive. The dimensions of this third part of our model representing

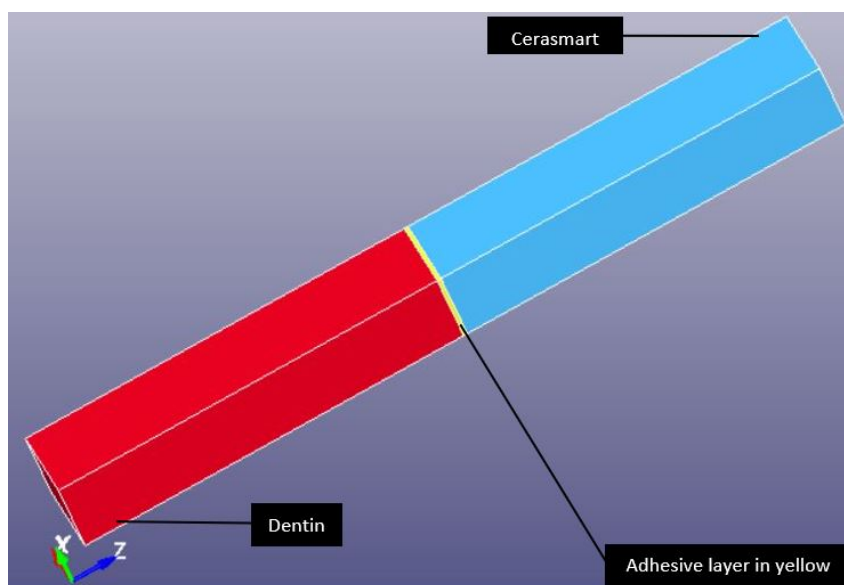


Figure 2.14: Geometry of the model with cohesive elements

the adhesive are $1\text{mm} \times 1\text{mm} \times 0,05\text{mm}$. These dimensions were chosen on the basis of the experimental test since the adhesive thickness during the experiment was $50\ \mu\text{m}$. On this geometry, two different mesh were generated in order to use two different contact algorithms proposed by LS-DYNA when using the cohesive elements. The first mesh we generated from this geometry is comprised of three parts with same element size in the XY plane. This was done in order to have a node to node correspondence between the parts. The second mesh that we generated from the geometry has the three parts of the model with different elements size in the XY plane. This second mesh was generated on the geometry in order to use a tied contact between the three parts. From figure 2.15, we can see that each node of the dentin (part in red) is located exactly in correspondence to a node of the cohesive elements representing the adhesive layer. In the same way, all the faces of the cohesive elements have their nodes which are located exactly in correspondence of the nodes of the ceramic cross section in contact with the adhesive. In this way, after the mesh generation, all these nodes sharing almost the same location were merged and the whole model behaves as a unique part after such a practice. Unlike the node to node

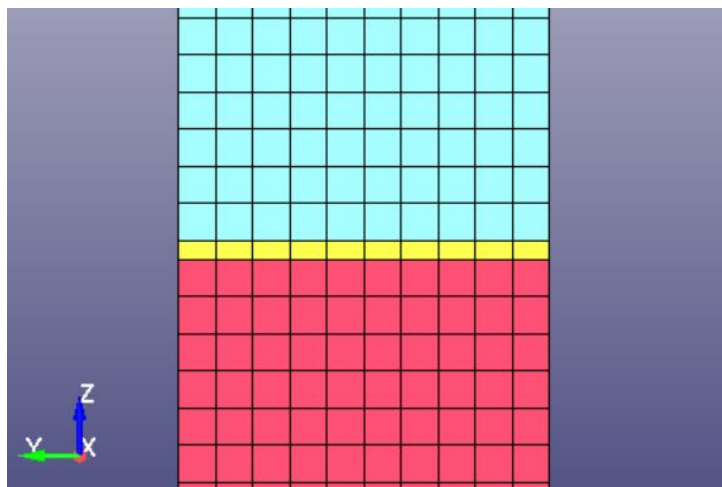


Figure 2.15: cohesive elements: node to node correspondence with surrounding parts

correspondence model, where it is possible to merge the nodes sharing the same position, it is necessary in case we want to have a dissimilar mesh (fig 2.16) to enforce a tied contact in between the parts of the model. If such a practice is not performed, there is no way to use cohesive elements in LS-DYNA in case of non symmetric mesh at the cross section areas.

2.3.2 Materials

The materials used in this approach are almost the same with the one used with the tiebreak contact approach. For the dentin and the ceramic parts, we modelled them as linear elastic isotropic materials as it is recommended in the literature. In LS-PrePost the material model behaving like a linear elastic isotropic material can be chosen under the

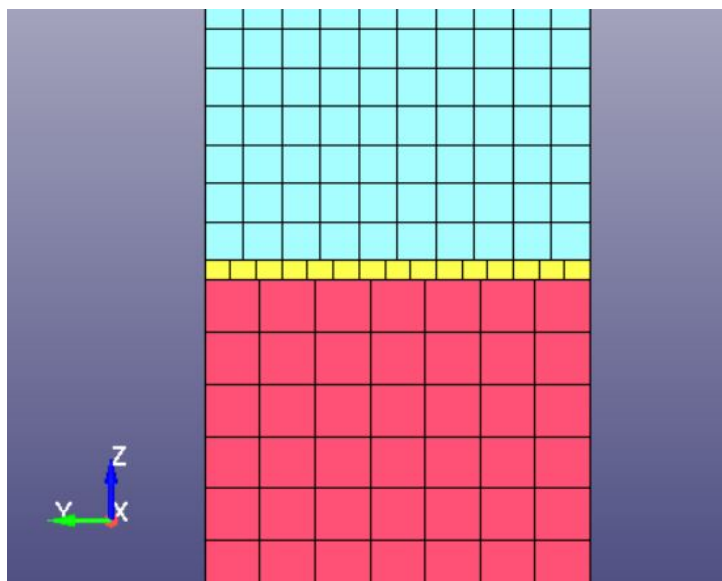


Figure 2.16: no correspondence node to node

keyword MAT as 001-ELASTIC. Concerning the adhesive layer represented by the cohesive elements in the model, we assigned a material model known as 184-COHESIVE_ELASTIC in LS-PrePost. In order to completely define this material the user must give a value for the following properties of the material.

- RO: From the manual user, we know that RO is the mass density. from the literature, we were able to find the value of RO equal to $1200\text{Kg}/\text{m}^3$.
- ROFLG: it is a flag which tells whether density is specified per unit of area or volume. if $ROFLG = 0$, it specifies the density is per unit of volume (default) while if $ROFLG = 1$ specifies that the density is per unit of area for controlling the mass of cohesive elements with an initial volume of zero. This parameter is important because in LS-PrePost, zero thickness cohesive elements can be modelled and usually such a part should have $ROFLG = 1$. In our case, the adhesive thickness is $50\mu\text{m}$ therefore we opted for $ROFLG = 0$.
- INTFAIL: it is the number of integration points required for the cohesive element to be deleted. If it is zero, the element won't be deleted even if it satisfies the failure criterion. The value of INTFAIL may range from 1 to 4, with set INTFAIL=1 because of the recommendation from the manual.
- ET: From the manual, we can read that ET is the stiffness in the plane of the cohesive element. This stiffness is expressed in the unit of stress/length. We can conclude that such a value corresponds to E/L namely the ratio between the adhesive Young's modulus and the thickness of the adhesive. For the microtensile test, ET value is not really important since the traction is mainly normal to the plane of the cohesive element.

- EN: It is the stiffness normal to the plane of the cohesive element (stress/length). From the properties of the adhesive, we set this value equal to 18500GPa/m.
- FN_FAIL: It is the traction in the normal direction for tensile failure. This value was set to be equal to 33 MPa.
- FT_FAIL: FT_FAIL is the traction in the tangential direction for shear failure is necessary in case of cohesive the presence of the shear mode failure. The algorithm does not require this value for the microtensile bond test.

2.3.3 Boundary conditions

The boundary conditions enforced on this model with cohesive elements were the same with the one enforced on the model with the tiebreak contact. Such a choice was made in order to have comparable results between the different approaches. The loading curve

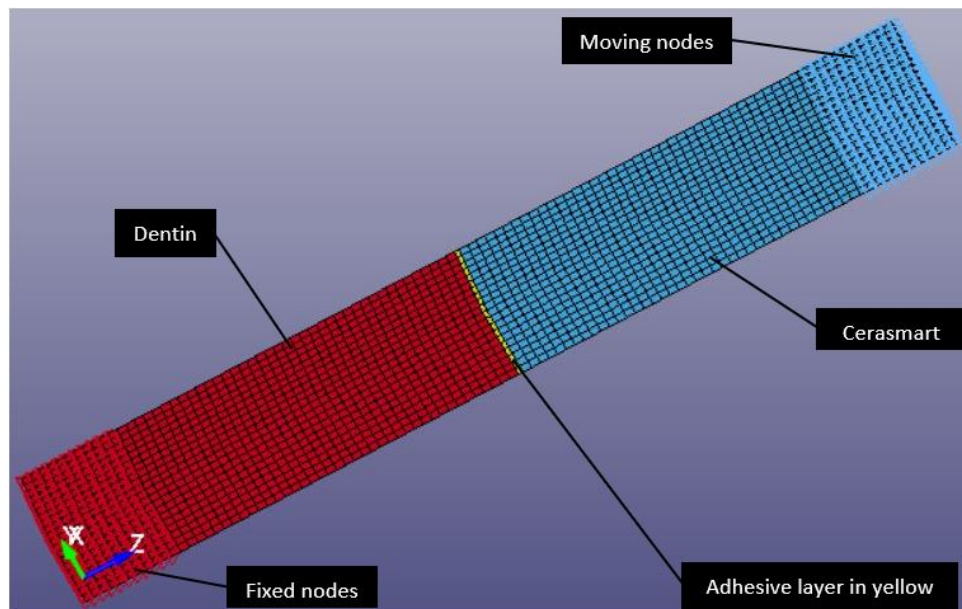


Figure 2.17: Model with boundary conditions

was chosen in order to have a test not too slow in order to reduce the simulation time, but at the same time not too quick in order to reduce dynamic effects during the simulation. We can refer to figure 2.6 for information related to the velocity loading curve for the microtensile bond strength test.

2.3.4 Cohesive Elements and Elements Connectivity

In the LS-DYNA manual user, we have information related to the use of cohesive elements. Among the possible element formulations available in LS-DYNA, just few of them can be used for cohesive elements. We opted for the element formulation ELFORM 19

because such a formulation is recommended in case the adherends are discretized with solid elements.

A cohesive element formulation connects via nonlinear spring elements the relative displacements between the upper and lower surface to a force per unit area. The element is really two dimensional. Instead of strains, the deformation is in terms of the relative displacements between the upper and lower surfaces interpolated to the Gauss points. Unlike strains, the incoming deformations have units of length. The output of the material model is the force per unit area (LS-DYNA manual: traction) at the Gauss points, acting to oppose the displacement.

The two element formulations in LS-DYNA, which can be used with cohesive material models are ELFORM 19 and ELFORM 20. ELFORM 20 transfers moments between the bonded parts, whereas ELFORM 19 does not. The order of the nodes in defining the element is important. For instance if the cohesive element bonds Element A of the first adherend to Element B of the second adherend, nodes 1-2-3-4 of the cohesive element should be shared by Element A or by Element B. In the first case, the normal of face 1-2-3-4 should point towards Element B and nodes 5-6-7-8 should be shared by Element B. In the second case, the normal of face 1-2-3-4 should point towards Element A and nodes 5-6-7-8 should be shared by Element A. Any other kind of connectivity between the cohesive elements and the elements belonging to the adherends will produce errors during the simulation process and lead to the failure of the simulation. It is worth to say that the cohesive element formulations can have zero thickness and even invert without becoming unstable. Therefore, even very thin layer of adhesives can be modelled with these element formulations. Cohesive element is represented in the manual as consisting of three nonlinear springs (one in the normal direction and two in the two shear directions).

2.3.5 Results

Just like for the case of the first approach we have just seen, From the post processing we were able to obtain the stress distribution history and the force-displacement curves.

2.3.5.1 Stress Distribution

From the history of the Von Mises stress distribution, we were interested in the stress distribution on the parts of the model at the instant just before the failure of the structure. The model node to node shows a value of the maximum stress of 43.79 MPa. The model cohesive tied contact instead has a maximum value of the stress equal to 44.16 MPa.

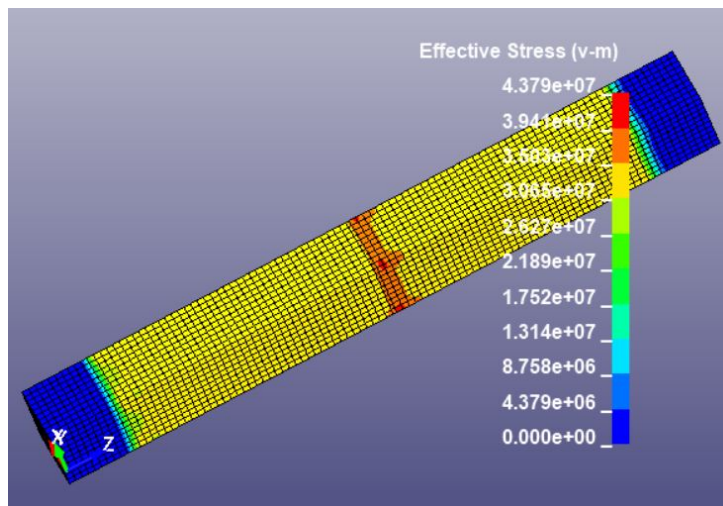


Figure 2.18: Von Mises stress distribution on the cohesive node to node model [Pa]

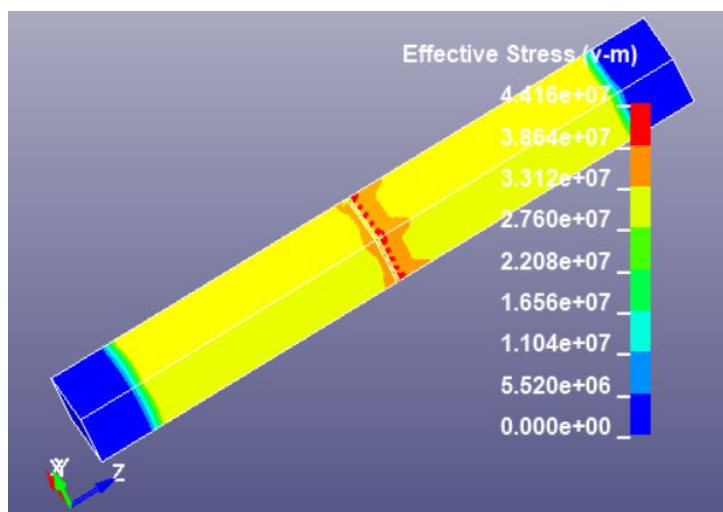


Figure 2.19: Von Mises stress distribution on the cohesive tied contact model [Pa]

Figure 2.18 and figure 2.19 show us that the stress distribution on both the models using cohesive elements is similar at least for what concern the stress distribution on the outer surfaces of the models.

In order to understand better how the stress is distributed on each part at the instant before the failure, and whether there is a difference or not in the stress distribution at the adhesive interfaces, it was necessary to display each part separately. The stress distribution on the parts of the node to node model (2.20) shows us that the maximum stress is located on the cerasmart part. We can also realize that even if the stress is more concentrated on the surfaces edges of the part in contact with the adhesive, there is not a huge difference in between the stress at the edges and the stress at the center of the surfaces. Just like the node to node model, The stress distribution on the cohesive with

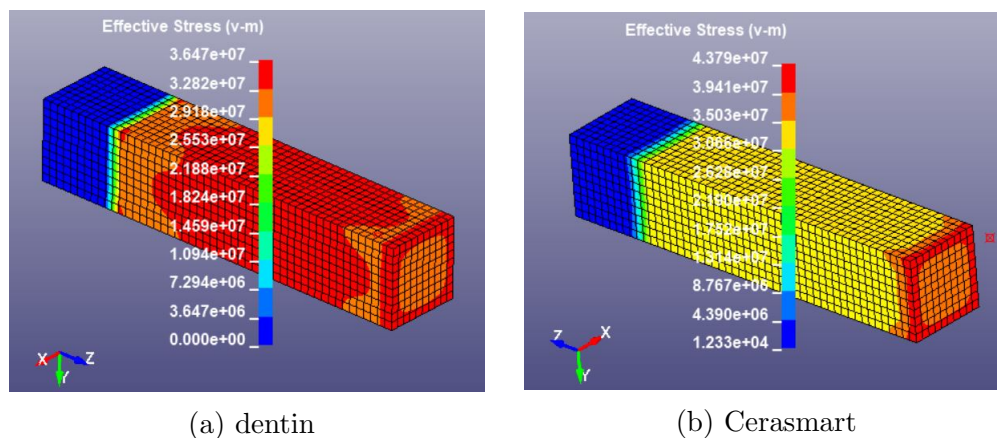


Figure 2.20: Von Mises stress distribution in [Pa] on parts: cohesive elements with node to node correspondence model

tied contact between the parts (fig 2.21) shows us that the maximum stress is localized on the cerasmart. On the surfaces having a physical contact with the adhesive, we note that the stress is concentrated at the edges of those surfaces but the difference between the stress at the edges and the stress at the center is presumably less than 5 MPa.

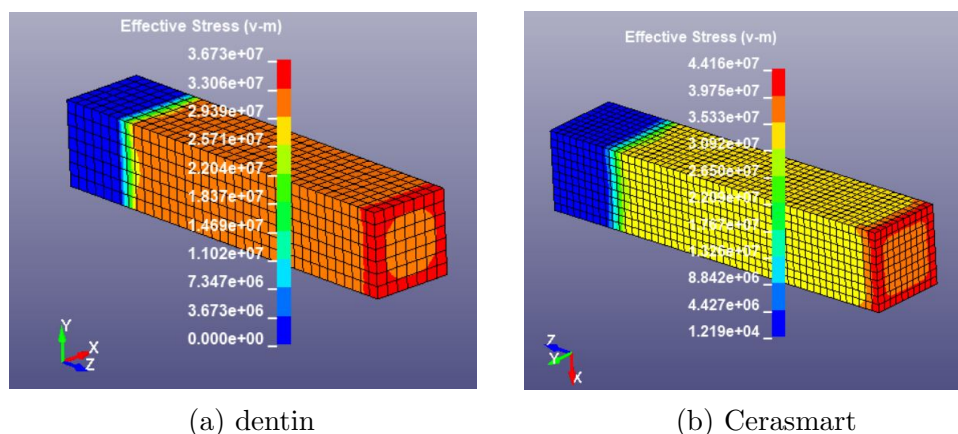


Figure 2.21: Von Mises stress distribution in [Pa] on parts: cohesive elements with tied contact model

2.3.5.2 Force-Displacement Curves

From the post processing, the force-displacement curves were plotted in order to validate the numerical model, by comparing the experimental curve to the numerical curve that we obtained from the experimental test. As we already know, from the experimental test, we were able to obtain the adhesive tensile bond strength which is 32,58 MPa for PANAVIA V5. To the value of the tensile bond strength, we were also able to find the adhesive Young modulus. The experimental value of the adhesive Young modulus combined to the value of the tensile bond stress allowed us to have the experimental force-displacement curve. The same value of the adhesive stiffness was introduced in the solver algorithm as the stiffness of the cohesive material. From the figure 2.22 we can realise that the peak of the force obtained from the numerical results is 32.2 N. Considering the contact area of our model which is 1mm^2 , we computed the microtensile bond strength test from the equation 2.2 and we obtained the value 32.2 MPa.

$$\sigma_{TBS} = \frac{F}{A} \quad (2.2)$$

The numerical value of the tensile bond strength is quite close to the value obtained from the experimental test which is 32,58 MPa. We can also say that the slopes of both

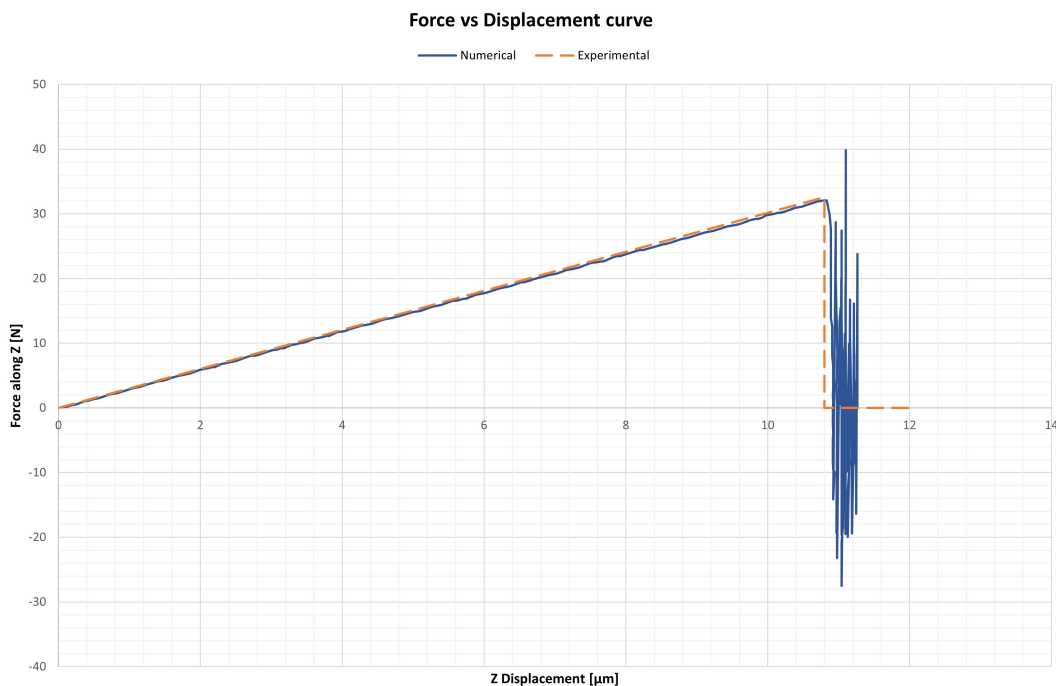


Figure 2.22: Force-Displacement curves node to node model

the curves which depend on the stiffness of the model are almost the same. For what concern the peak of the force, it is worth to say that the value of 32.2 N obtained from

the numerical results was possible after running the model with different adhesive normal failure stress. Therefore, several models were run inserting each time a different value of the adhesive normal failure stress up to reach the right value of the traction peak. Doing the same operation with the cohesive model used with tied contact and setting the same variables for the cohesive material in the algorithm, we obtained a similar force-displacement curve that is shown in figure 2.23. The curve shows a peak of the force equal to 31.9 N which corresponds to a tensile bond strength of 31.9 MPa.

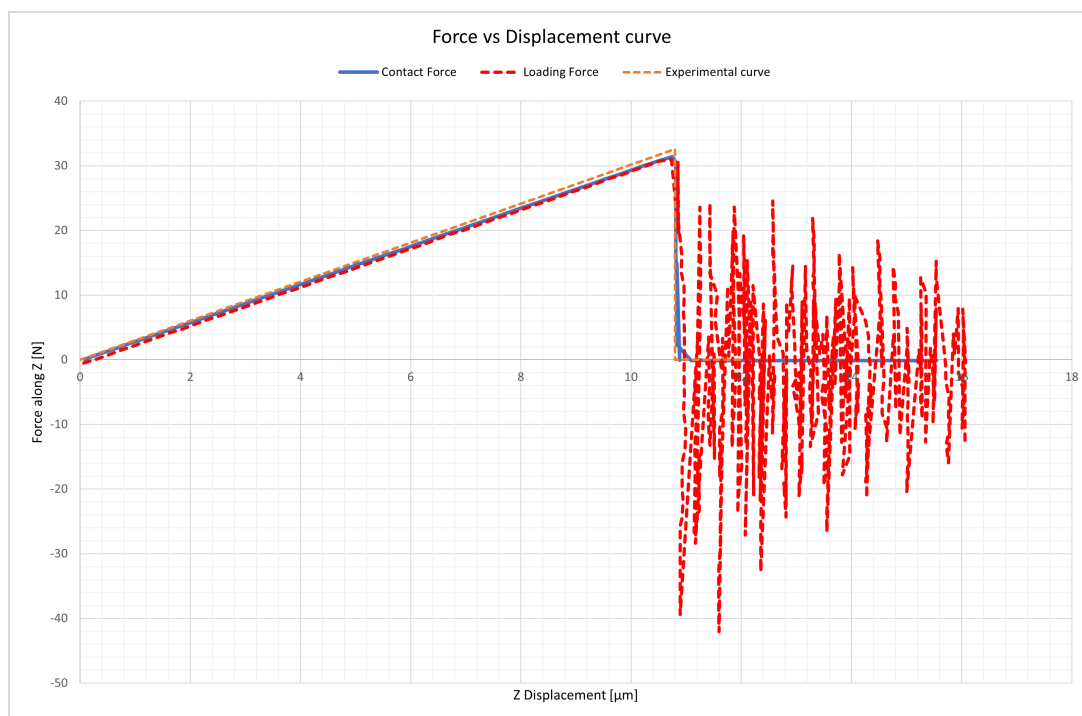


Figure 2.23: Force-Displacement curves tied contact model

2.4 Comparison between the Tiebreak Contact and the Cohesive Elements

We recall that two approaches were used to model the adhesive layer. For each of these adhesive models, it was necessary to define some properties characterizing the model such as the stiffness of the adhesive, its failure stress... etc. Even if these parameters have different names in the manual user for each method, each parameter used to define the tiebreak contact has an equivalent parameter used to model the adhesive with the cohesive elements. The table 2.2 shows us that the main information necessary to model an adhesive with these two approaches are the adhesive failure stress in the normal and tangential direction as well as the adhesive stiffness. These values are enough when using these two approaches because they model adhesives with linear elastic models. We can

Microtensile bond strength test	
Tiebreak contact	Cohesive elements
NFSL=46 MPa	FN_FAIL=33 MPa
SFLS=10 MPa	FT_FAIL=10 MPa
CN=18500 GPa/m	EN=18500 GPa/m

Table 2.2: Equivalence between the parameters used by the solver algorithms for the two different approaches. The parameters belonging to the same row have the same physical meaning.

note from the figure that all the curves have almost the same slope.

The figure 2.24 shows us the force-displacement curves obtained from the numerical analysis for different approaches. We can deduce from this that both the methods are suitable to define the adhesive stiffness since the slope of each curve depends on the adhesive stiffness. Another observation is that the peak forces are almost the same. If we look

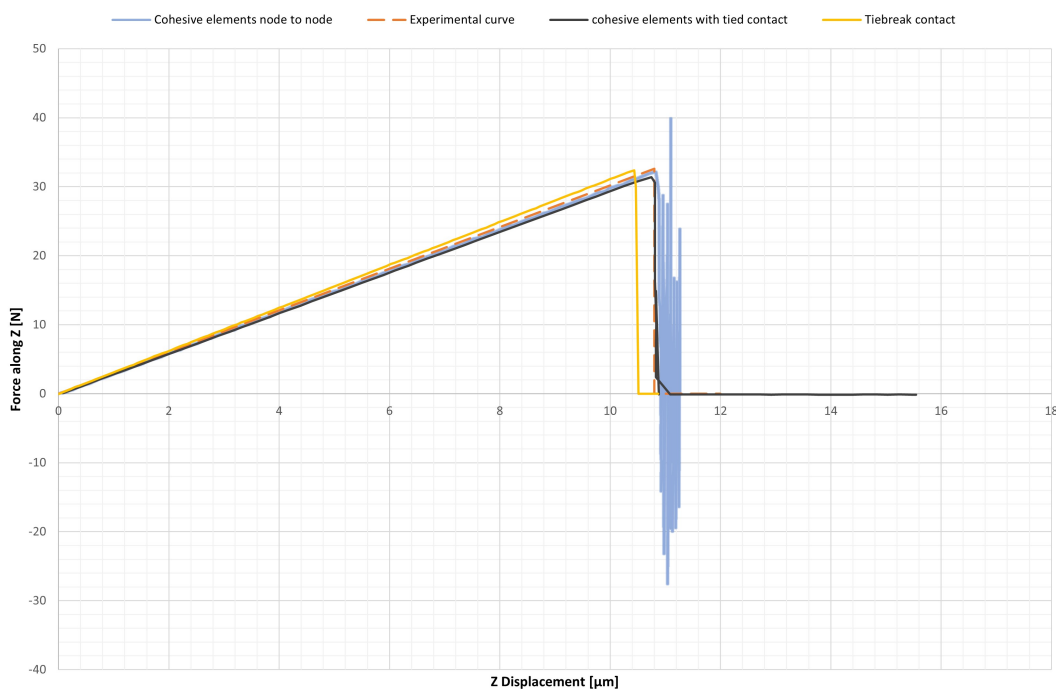


Figure 2.24: Force-Displacement curves

at the equivalence between the parameters (tab 2.2 used to simulate the adhesive layer, for the adhesive normal failure stress (NFSL) a value of 46 MPa was assigned whereas a value of 33 MPa was assigned with the cohesive elements approach to obtain the same peak force. From this observation we can say that the adhesive failure stress is probably between the two values.

Chapter 3

Shear Bond Strength Test

3.1 Literature Review and Experimental Test Description

In-vitro mechanical tests of dental restorative materials provide dental practitioners with guidance as regards material selection criteria and identifying patterns of optimal clinical use of material. In vitro tests play a significant role in providing the necessary information regarding the effectiveness of new materials with less cost and in a short period of time, whereas clinical studies would provide information only after the use for long period. The quality of adhesive material bonding is frequently verified by various laboratory tests, using shear and tensile efforts under certain limitations [10-11]. In 1997, a study evaluated 50 studies that used laboratory tests to quantify the bond strength at the bond interface, and observed that 80% used the shear bond strength test in its several forms [12]. Today, use of the micro shear bond strength tests have increased considerably. However, several recent studies still use the shear bond strength test to evaluate adhesive material bonding. In some situations, sectioning of the specimen for micro shear bond induces its loss due to failure before the test, and micro shear bond strength test cannot be used because of the difficulty of making specimens with some materials. In these cases, the shear bond strength test may be used to evaluate adhesive material bond strength. It is important to consider the changes in the test procedures commonly applied in different investigations that have the same aim: to determine the bond strength. For this reason, analyses of the same material inevitably produce different bond strength data [11,13-16].

Bond strength is obtained from the load at failure divided by the cross-sectional area of the bonded interface, and is referred as ‘nominal’ or ‘average’ bond strength. Shear bond strength tests have been widely used, mainly because of their relative simplicity when compared to tensile bond strength tests, in which it is difficult to align the specimen in the testing machine without creating deleterious stress distribution [17-19]. Advantages in shear tests include ease of specimen preparation and simple test protocol. However,

problems related to the validity of obtained measurements started to arise as cohesive failures in the substrate were frequently observed with new adhesives that yield improved bond strengths. Although some authors speculated that the bonding had surpassed the cohesive strength of the substrate with no further need for improvement, the actual conclusion was that this test had turned out to be unsuitable to determine the true strength of a bonded interface [9,20]. According to Della Bona and van Noort [3], the real explanation for this fact was that stresses were mostly concentrated in the substrate, thus causing its premature failure prior to the interface itself. Another point that has drawn fundamental criticism regards to the non-uniform nature of stress distributions along tested interfaces [19]. According to a study performed by van Noort et al. [21] using finite element analysis to compare shear and tensile tests, the nominal bond strength may vary with specimen geometry, loading configuration and material properties, such as elastic modulus. In other words, the nominal bond strength misrepresents the actual maximum shear or tensile stresses the specimen resisted at failure. As this sensitivity is more pronounced in the shear test set-up, it was concluded that tensile bond strength tests were still preferable. Moreover, although a shear loading is applied during testing, it was demonstrated that tensile stresses produced by the bending moment are responsible for fracture initiation[22]. Amidst this controversy, shear tests were almost completely substituted by the microtensile test, introduced by Sano et al. [26]. The main characteristic of this test is the reduced specimen size. It is also verified that different values are achieved for different bonding areas: the smaller the area, the higher the bond strength [23]. More recently, a new test method using specimens with reduced dimensions has been advocated by some authors [24,25] as a substitute for the conventional shear test: the so-called ‘microbond’ or ‘micro-shear’ bond strength test. According to them, this test would allow for testing of small areas, thus permitting a regional mapping or depth profiling of different substrates, and preparing multiple specimens from a same tooth, as in microtensile tests, but without sectioning procedures to obtain sticks or trimming to achieve dumbbell or hour-glass shaped specimens, laboratory procedures that may by themselves induce early micro cracking within the specimen. Studies on stress distribution in conventional shear tests cannot be applied to the micro-shear method. One of the reasons may be the lack of proportionality between the geometrical aspects of both tests, whereas composite and dentin diameters may vary, the adhesive layer thickness will always remain constant. Considering the importance of knowing what a test is actually measuring to ensure proper interpretation of obtained data, finite element analysis becomes of great usefulness to elucidate the stress states found in bonded interfaces and provide information on the nature of stresses generated within the specimen.

The micro shear bond strength test consist in mounting a specimen with cross section not exceeding $4mm^2$ on a testing machine as shown in figure. Then, a load is applied in the radial direction of the restorative material in other produce a stress state in the specimen which will caused the failure at the adhesive interface of the specimen. As we already stated, it is necessary to have an adhesive failure (fig2.3) of the specimen in order to evaluate the tensile bond strength dividing the peak of the shear force registered by

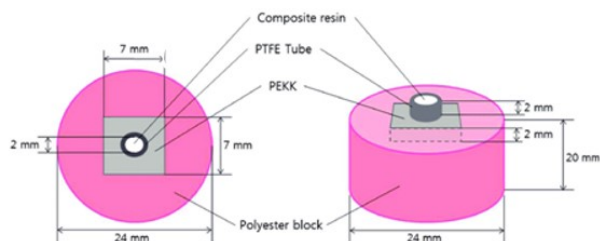


Figure 3.1: Dimensions of a generic specimen for the micro shear bond test

the cross section area of the restorative material. This is done because the restorative material cross section represents the area on which the adhesive is applied and only that area will stick to the dentin. The load is generated by the displacement of the cross head speed of the universal testing machine whose velocity during the test ranges usually from 1mm/min to 5mm/min.

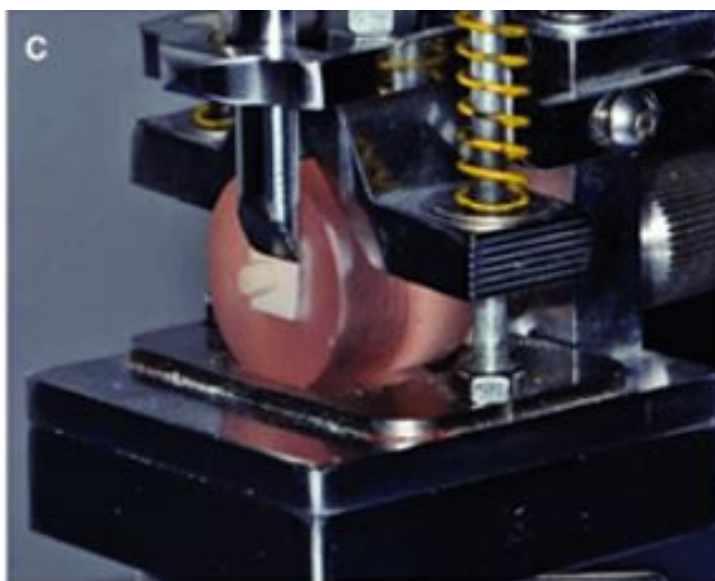


Figure 3.2: Specimen mounted on the testing machine for the micro shear bond test

3.2 Finite Element Model With Tiebreak Contact

Two approaches were used to model and simulate the shear bond strength test in order to characterize the adhesive system. Just like for the case of the microtensile bond strength test, the main difference between the two models built for the shear bond strength test

and corresponding to the two approaches that we used lies in the modelling of the cohesive zone of our models. Here is the description of the first approach based on the modelling of the cohesive zone with the contact known as Tiebreak Contact in LS-DYNA.

3.2.1 Geometry And Mesh

The experimental test allowed us to have a clear idea on the geometry of our model. We can see from figure how the experimental test was performed. Therefore, Three solid parts were modelled in LS-PREPOST, then we generated a three dimensional solid mesh from the three parts. In order to have a realistic mesh of our model, the mesh generated

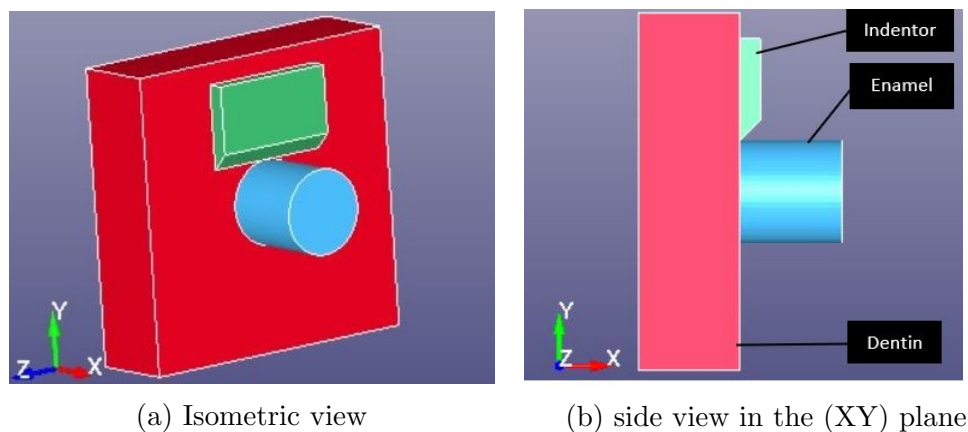


Figure 3.3: Geometry of the model

from the three parts of our model was different from the point of view of the mesh size. The table summarizes the mesh size and the dimensions of the main parts of the model. A coarse mesh was generated from the indenter geometry because we were not interested in any information related to the indenter part such as deformation, stress...etc. A finer mesh instead was generated from the block part representing the dentin and the cylindrical part representing the enamel. This was done in order to have a better contact between the dentine and the enamel. The table 3.1 summarizes the information related to the dimensions on the geometry and the mesh size of each part of the model. In the table, r is the radius of the enamel part while l is the length of the enamel. The indenter was

Parts	Dimensions	Mesh size
Dentin	$7mm \times 7mm \times 2mm$	$0.1mm$
Enamel	$r = 1mm, l = 2mm$	$0.05mm$
Indentor	not important	/

Table 3.1: Dimensions of the parts and Mesh size of the elements

modelled in order to reproduce in the best possible way the steel rod which transmits the loading to the specimen. It was necessary to have a knife edge at the indenter tip. The

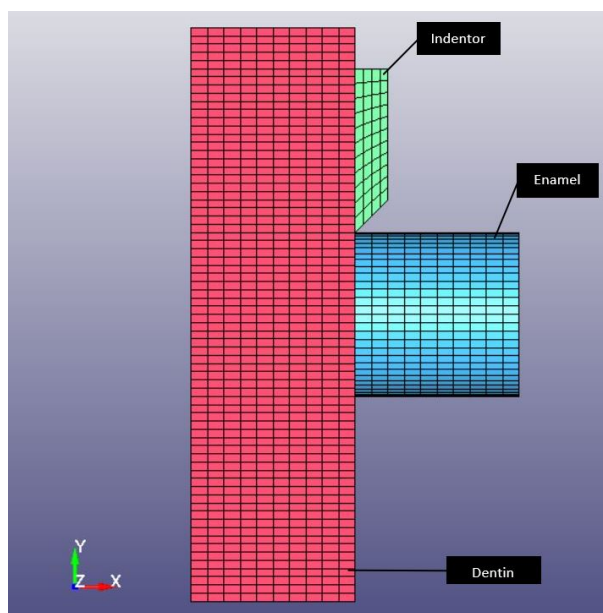


Figure 3.4: Shear bond test model: The mesh

dimensions related to the indenter were not really important nevertheless, the position of the indenter with respect to the contact area was chosen in order to minimize or even avoid a moment load on the enamel part which would have changed the shear bond strength test to flexural bond strength test.

3.2.2 Materials

The experimental model comprises the dentin, the enamel and the indenter which is a steel rod. The dentin and the enamel were considered as linear, homogeneous and isotropic materials and modelled with the material 001-ELASTIC in LS-DYNA. The indenter was considered as a rigid material considering its very high elastic modulus with respect to the two other parts elastic modulus (Tab:3.2). It is worth to precise that by modelling

Parts	Young's Modulus [GPa]	Poisson's Ratio
Dentin	18	0.31
Enamel	69	0.28
Indenter (Steel)	210	0.30

Table 3.2: Properties of the materials

the indenter as a rigid material in LS-DYNA, the indenter will not deform during the simulation and no data related to the indenter will be available during the post processing step. In the other hand, even if the indenter is defined as rigid material, it is necessary to define its mechanical properties such as Young Modulus and Poisson's ratio for the solver algorithm. This is done in order to compute the contact stiffness between the enamel

and the indenter which is a steel in realty. The adhesive system in this model was not considered as a part just like it is in the realty but, as a specific type of contact between the dentin and the enamel. The table summarizes the material properties of the material used in this model. The choice of the material constitutive laws was motivated by the results that we found in the literature in which previous studies were performed with the aim to define the mechanical properties of these parts.

3.2.3 Boundary Conditions

In this numerical model, some nodes of the dentin were constrained as shows the figure. The constraints enforced on a set of nodes on the dentin aim to prevent the nodal displacements along x, y, and z directions. These constraints prevent also the nodal rotations around the x, y and z axis of the reference frame. For what concerns the loading, a motion

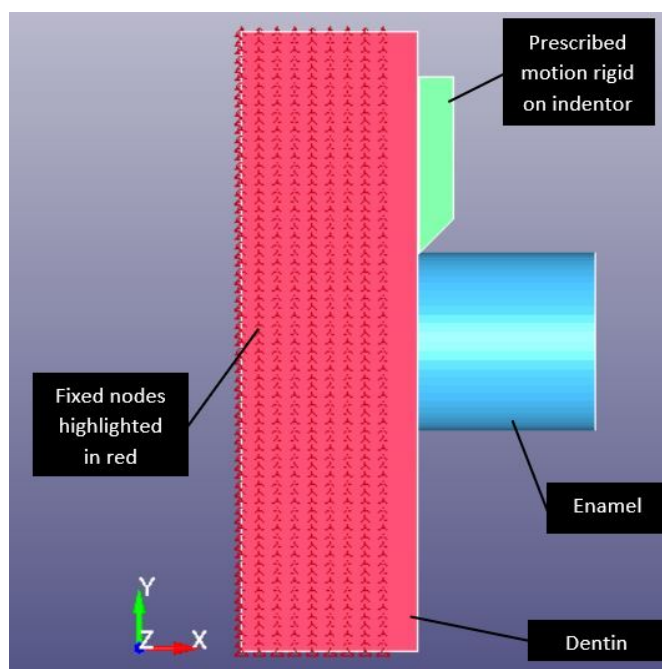


Figure 3.5: Boundary Conditions enforced on the model

at a velocity defined on figure 3.6 was prescribed to the indenter in order to simulate the loading condition enforced to the steel rod. It was necessary to constrain all the displacements and rotations of the indenter except the translational degree of freedom in the y direction. This was done in order to have the loading force only in the Y direction just like it happens during the experimental test. The velocity of the indenter was chosen in order to accelerate the simulation time and maintained under a certain value at the same time in order to avoid the influence of dynamic effects. Let us recall that the experimental test is performed at a constant velocity of the steel rod equal to 5mm/min while the indenter in the numerical model moves at a velocity which starts from zero and smoothly

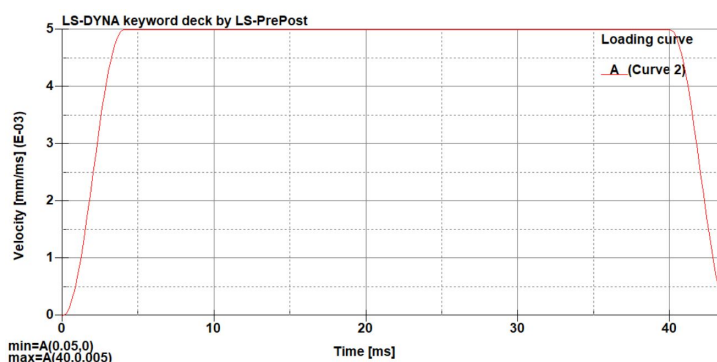


Figure 3.6: velocity enforced to the indenter

increases up to reach a maximum value (5mm/s) and remains constant at that value. The simulation is ended before the deceleration of the indenter which is represented by the descendent part of the velocity curve.

3.2.4 Contact Between Parts

3.2.4.1 Contact Between the Indenter and the Enamel

The contact between the indenter and the enamel was defined in order to have the transmission of the load to the enamel. Without a proper definition of the contact in between some parts having a physical contact in the reality, The solver ignores the interaction between the parts and penetration between the parts does happen. Therefore, In LS-DYNA, a contact is defined by identifying (via parts, part sets, segment sets, and/or node sets) what locations are to be checked for potential penetration of a slave node through a master segment. A search for penetrations, using any of a number of different algorithms, is made every time step. In our case, we defined an `AUTOMATIC_SURFACE_TO_SURFACE` contact type between the indenter and the enamel. This choice was made because the contact search algorithms employed by automatic contacts make them better-suited than older contact types to handling disjoint meshes.

3.2.4.2 Tiebreak Contact Between the Dentin and the Enamel

The tiebreak contact is one of the most important of this model because it is the one allowing to simulate the adhesive within the model. Therefore, the cohesive zone was modelled using the tiebreak contact. Everything that was said related to the tiebreak contact in the chapter one remains valid for this model. Here are the parameters that we set for the tiebreak:

- `NFLS` : `NFLS` represents the normal failure stress of the adhesive. The value of the normal failure stress was unknown but a value of 39 MPa was chosen based on the microtensile bond strength of the adhesive.

- SFLS : it represents the shear failure stress in the contact card. For the shear bond strength test, SFLS one of the most important parameter because the shear stress is the one causing the failure in the shear bond test. It is easy to realise that the failure depends mostly on the shear stress just by looking at the failure criterion that given by the relation 2.1. A value of 50 MPa was chosen in order to guarantee the shear bond strength obtained from the experimental test.
- PARAM : for option 6, PARAM is the critical distance (CCRIT), at which the interface failure is complete. Since we were not able to have the experimental force-displacement curve, such a parameter was not important for our analysis.
- CT2N : it represents the ratio of the tangential stiffness of the adhesive to the normal stiffness of the adhesive. This was set to be equal to 1. By setting CT2N=1 we defined the tangential stiffness of the adhesive equal to the normal stiffness.
- CN : is the normal stiffness (stress/length) for OPTION = 6. If CN is not given explicitly, the penalty based approach that we will discuss later on is used to define the normal stiffness dividing the penalty stiffness divided by segment area (default). The manual recommends the use of this option with care, since contact stability can get affected. A value of 10020 GPa/m was assigned on the basis of the Young's modulus of the adhesive system given in table 3.2.

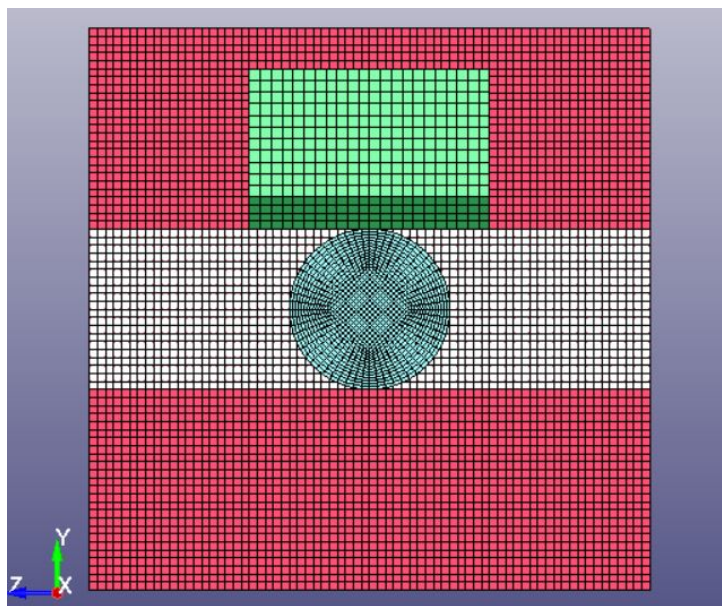


Figure 3.7: segments sets for the tiebreak contact

Practically speaking, in order to define a tiebreak contact between the enamel and the dentin, two set of segments were defined. The first set of segments was defined on the enamel and represents the slave segments. The second set was defined on the dentin and represents the master segments set. In this way the contact algorithm checks at each step

time the penetration of a slave nodes in master segments of the dentin. The figure shows a blank band belonging to the dentin which represents the master segments set defined for the contact with the enamel.

3.2.5 Results

The results obtained from the numerical simulation allowed us to have information related to the stress distribution on the parts and the force-displacement curve necessary to characterize the adhesive.

3.2.5.1 Stress Distribution

the interest for the stress distribution lies in the fact that it is useful on one hand for the comparison to the experimental results for the validation and on the other hand it is useful for the comparison to the stress distribution obtained from other adhesive systems from previous studies. In our case, the interest lies mainly in the possibility to compare from the qualitative point of view how the stress is distributed at the adhesive interface at the instant before the failure. The figure 3.8 shows the stress distribution on the whole

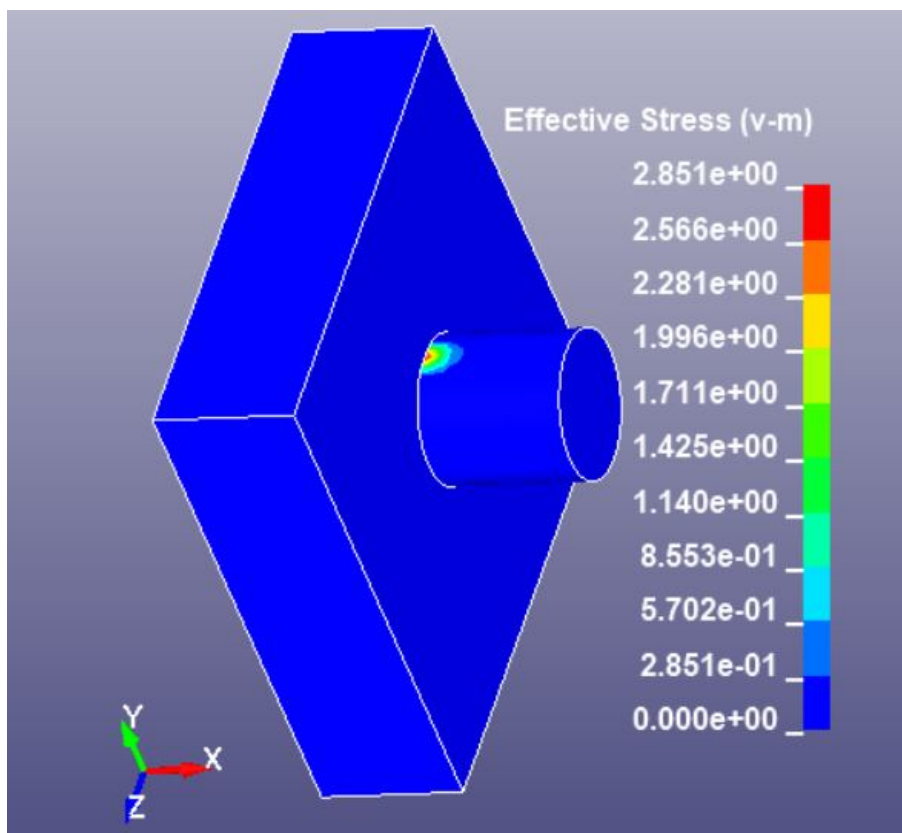


Figure 3.8: Von Mises stress distribution on the model [GPa]

model. We can realise that the maximum stress on the model at the instant before the

failure is around 2851 MPa. Such a value is very high given the shear failure stress of the adhesive. In order to understand how Von Mises stress is distributed on the dentin and the enamel, we separated the parts and tried to analyse the stress distribution on each part. We were particularly interested in the maximum stress on each of these parts. The figure 3.9 shows that the maximum stress on the model that we just saw and which is equal to 2851 MPa is located on the enamel. We can realise that on the dentin part the stress is maximum stress is lower with respect to what we have on the enamel. In fact the maximum stress on the dentin is about 49,29 MPa. This value is 58 times lower than the maximum stress on the model located on the enamel. The high value of the stress on the

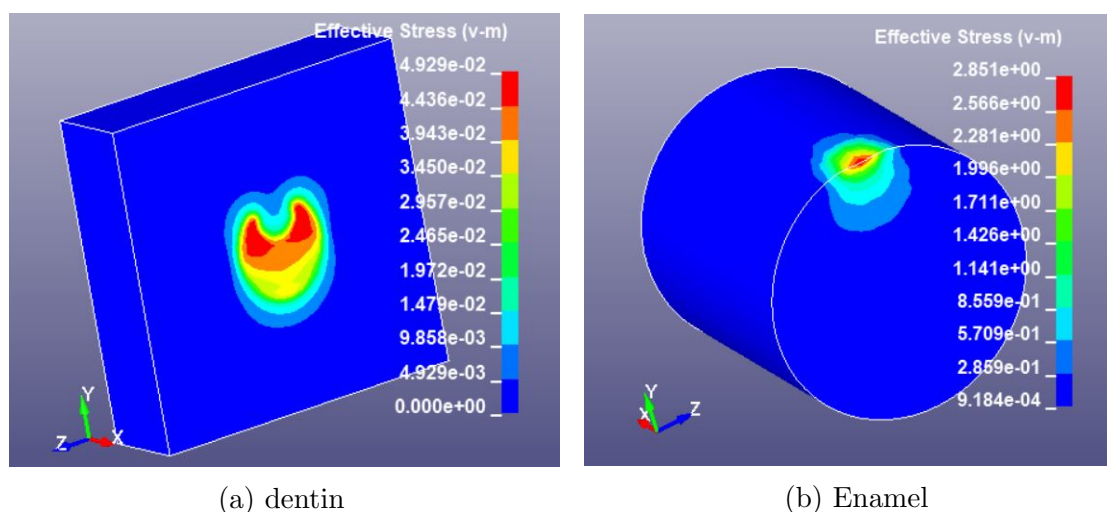


Figure 3.9: Von Mises stress distribution on each part[GPa]

enamel is certainly due to the cutting edge of the indenter and to the small chock that occurs when the indenter experiences the contact with the enamel part. That is why the dentin which does not experience the contact with the indenter has a maximum stress which is close to the value of the shear failure stress of the adhesive (SFLS=50 MPa).

3.2.5.2 Force-Displacement Curves

The force-displacement curve obtained from the numerical analysis was also plotted in order to validate the model. To achieve this, the first step consisted in plotting the experimental curve of the test using two main information which are the tensile bond strength value and the adhesive young modulus. From the tensile bond strength, we were able to define the maximum loading force registered during the experimental test through the formula from which we can have the force knowing the contact area and the shear bond strength of the adhesive. This was possible using the equation 3.1

$$\tau_{SBS} = \frac{F}{A} \quad (3.1)$$

Where τ_{SBS} represents the shear bond strength of the adhesive and A is the contact area. In our case, having a contact area of $3.14mm^2$ and a shear bond strength of 22.29 MPa, the peak force resulted to be equal to 70 N. The adhesive Young's modulus was useful to determine the steepness of the curve by computing the whole structure stiffness. After plotting the experimental force-displacement curve, we tried to obtain a similar curve from the numerical model. It is worth to say that before obtaining a numerical result fitting the experimental one, several simulations were run by changing each time the adhesive shear stress failure value in the solver algorithm. This was done in order to obtain the correct peak force from the force-displacement curve. The curve in the figure 3.10 was obtained by setting the adhesive shear failure stress (SFLS) equal to 50 MPa. The force-displacement curve obtained from the numerical analysis reach its maximum at

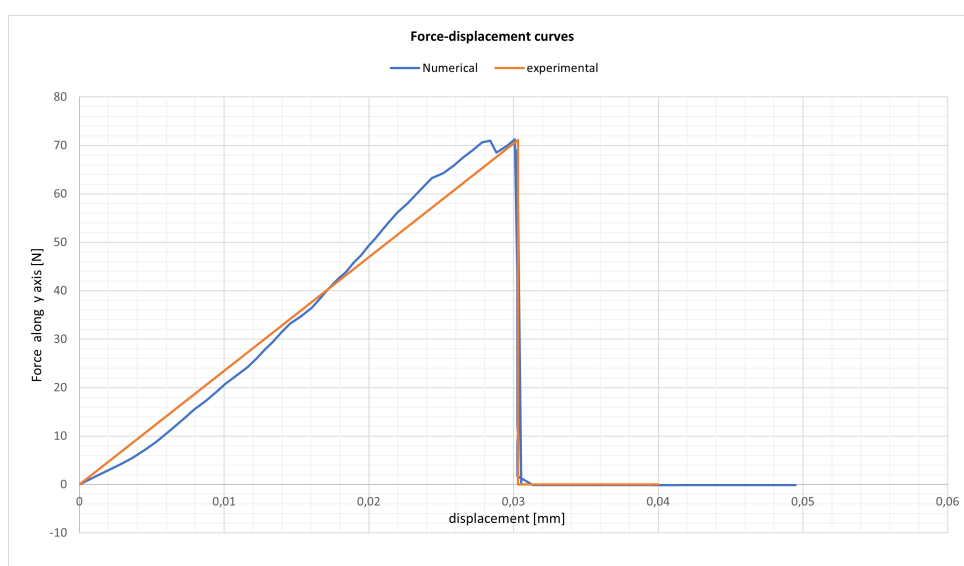


Figure 3.10: Force-Displacement curves

a value corresponding to 71.9 N which corresponds to a shear bond strength of 22,9 MPa. The experimental results and the numerical results are quite close as the figure shows us.

3.3 Finite Element Model with Cohesive Elements

Once the cohesive zone in the shear bond strength test was modelled with the tiebreak contact, another approach was adopted via the use of the cohesive elements. Here are the steps we followed in order to run the simulation and analysed the results.

3.3.1 Geometry and Mesh

The geometry that was designed in LS-PREPOST for the model with cohesive elements is almost the same that was designed for the model with the tiebreak contact. The only

difference with this model is the presence of a new part which represents the adhesive. From the experimental test, we were able to know the adhesive thickness which is $10\ \mu\text{m}$. For this reason, a new part having the diameter of the enamel and a thickness of $10\ \mu\text{m}$ was added to the model (fig3.11a). From such a geometry, a mesh was generated on each part. During the mesh generation process on each part, we made sure that the elements size of this model were the same with the model with the tiebreak contact. This was done in order to easily compare the simulation time and understand also better how the results depends on the mesh size. In fact we realized that the contact depends also on the mesh size of the parts experiencing the contact. For this reason in order to have a fair comparison between the two approaches, it was necessary to have the same mesh size at least between the main two parts which are the dentin and the enamel. The figure 3.11 shows us on one side the geometry with a new part included representing the adhesive. on the other side, the same figure represents the mesh generated from the geometry. All the

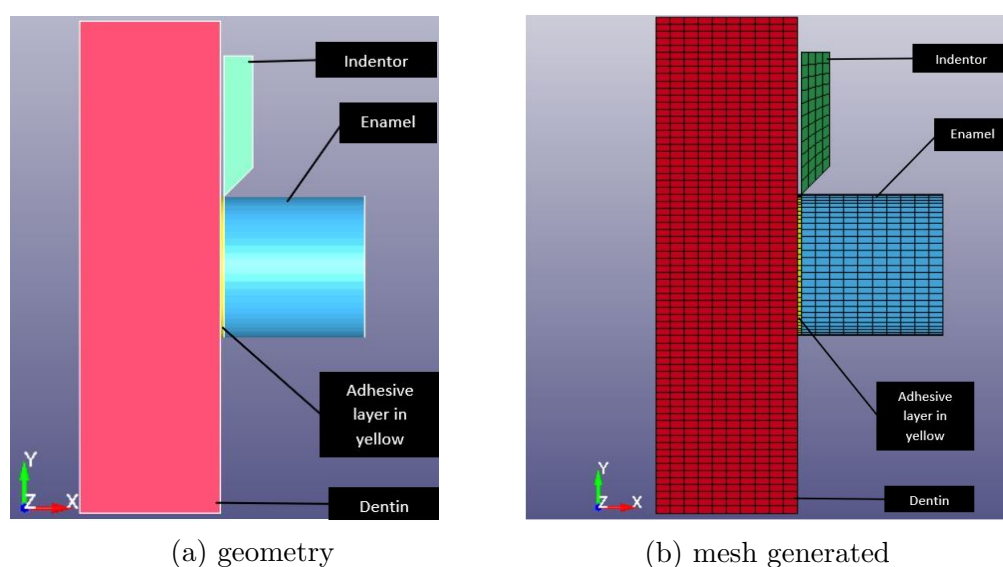


Figure 3.11: Geometry of the model and mesh generated from the geometry

information related to the mesh size can be found in the table 3.1. The size of the cohesive elements was defined on the basis of the contact that we used between the parts as we will see later on. For what concerns the element formulation, ELFORM3 formulation which corresponds to 8 nodes solid elements was chosen for the dentin and the enamel. The adhesive layer was modelled with ELFORM19 formulation which is suitable for all the applications involving the contact between an adhesive and solid elements.

3.3.2 Materials

As we know, the part that was added to this model is the part which simulates the adhesive. This means that for enamel and dentin parts we can refer to the material properties given in the table 3.2. For what concerns the adhesive layer, we opted for the

material model MAT_184 which is known as MAT_COHESIVE_ELASTIC. MAT_184 is suitable for the modelling of adhesives. The properties that was assigned to this material model are the following:

- $RO=1200Kg/m^3$. RO is the mass density of the material.
- ROFLG: it is a flag which tells whether density is specified per unit OF area or volume. if $ROFLG = 0$, it specifies the density is per unit of volume (default) while if $ROFLG = 1$ specifies that the density is per unit of area for controlling the mass of cohesive elements with an initial volume of zero. This parameter is important because in LS-PrePost, zero thickness cohesive elements can be modelled and usually such a part should have $ROFLG = 1$. In our case, the adhesive thickness is $10\mu m$ therefore, we opted for $ROFLG = 0$.
- INTFAIL: it is the number of integration points required for the cohesive element to be deleted. If it is zero, the element won't be deleted even if it satisfies the failure criterion. The value of INTFAIL may range from 1 to 4, with set INTFAIL=1 because of the recommendation from the manual.
- $ET=10.02\text{ GPa/mm}$. ET is the Stiffness in the plane of the cohesive element namely the tangential stiffness. This stiffness is expressed in the unit of stress/length.
- EN: It is the stiffness normal to the plane of the cohesive element (stress/length). We assumed its value equal to the tangential stiffness ET.
- $FN_FAIL = 39\text{ MPa}$: It is the traction in the normal direction for tensile failure.
- $FT_FAIL = 67\text{ MPa}$: It is the traction in the tangential direction for shear failure is necessary in case of cohesive the presence of the shear mode failure. This value is the most important for the failure criterion.

3.3.3 Boundary Conditions

The boundary conditions enforced to this model are almost the same with the one enforced to the model with the tiebreak contact. The nodes that were constrained on the dentin part in order to prevent all their displacements in the directions x, y, z and all their rotations around the axis x, y, z are the same for this model. The slight difference in this model regards the position of the indenter. In fact, the presence of cohesive elements between the dentin part and enamel part constrained us to move the indenter in the X direction of our reference frame for about $11\mu m$. This was done in order to have a contact between the enamel and the indenter. The velocity enforced to the indenter was exactly the first we enforced to the first model (fig3.6).

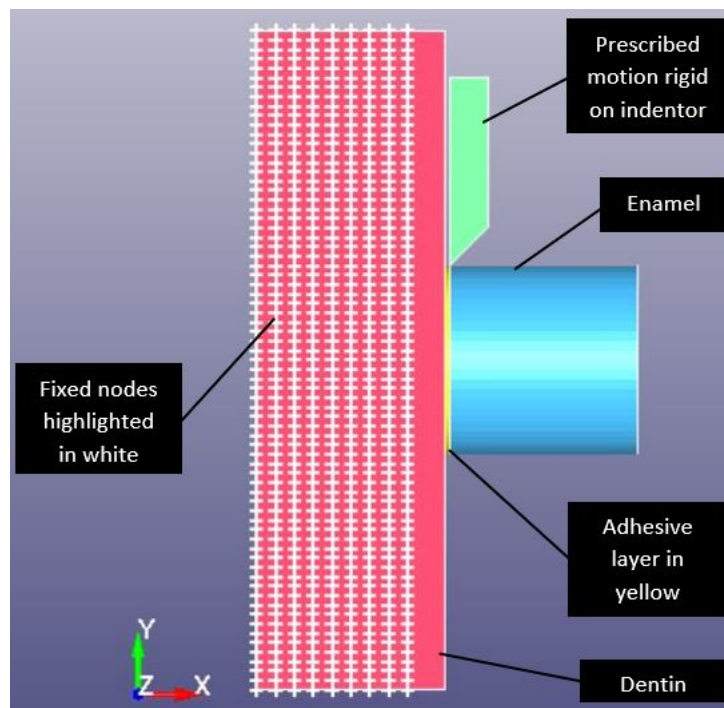


Figure 3.12: Boundary conditions: Constrained nodes in white

3.3.4 Contact Between Parts

It was necessary to define the contact between the parts of this model. The first contact defined was the contact between the enamel and the indenter. In order to have a good

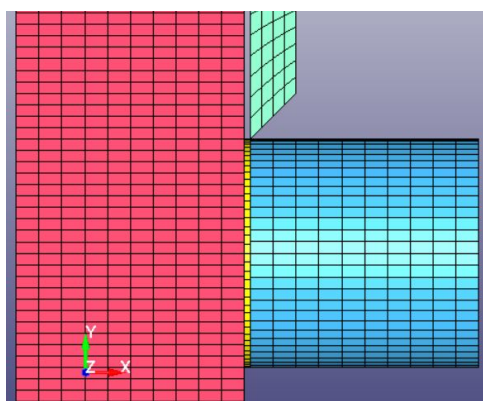


Figure 3.13: Contact between the indenter and the enamel

interaction between these two parts and have the transmission of the load, a contact `AUTOMATIC_SURFACE_TO_SURFACE` type was defined. For this contact we identified by the two parts the location to be checked for potential penetration of a slave node through a master segment. Due to the shape (cutting edge) of the indenter and the difference in

the stiffness between the enamel and the indenter, it was necessary to care very well about this contact. Since the adhesive bonds the dentin to the enamel, it was also necessary to define a contact between the cohesive elements and the two other parts. Usually, when

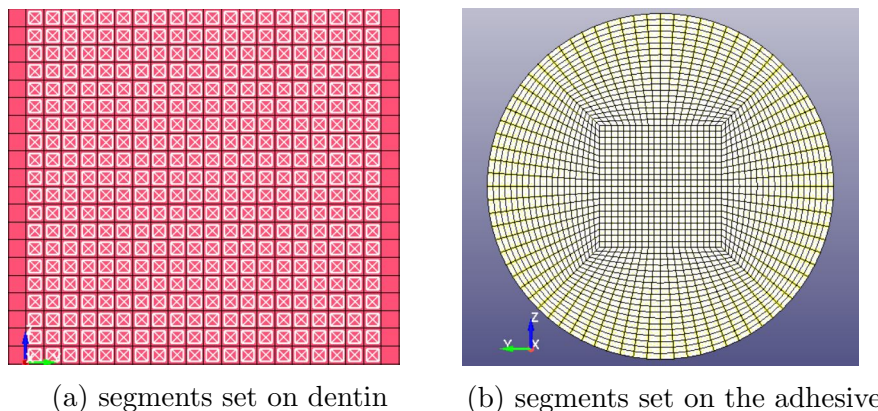


Figure 3.14: segments set defined on the dentin and the adhesive for the tied contact

dealing with cohesive elements, it is not necessary to define a contact between the cohesive elements and the part in contact with. The contact is not necessary because when the meshes are generated on the parts in such a way that the parts have a correspondence node to node with the cohesive elements, it is sufficient to merge the nodes. In this case, due to the impossibility of having a node to node correspondence between the parts (the shapes of the parts do not allow it) it was necessary to define tied contacts between these parts. In order to define tied contacts, we needed to define on the parts segments sets that were used then to define the region where the contact algorithm has to check the contact between the parts.

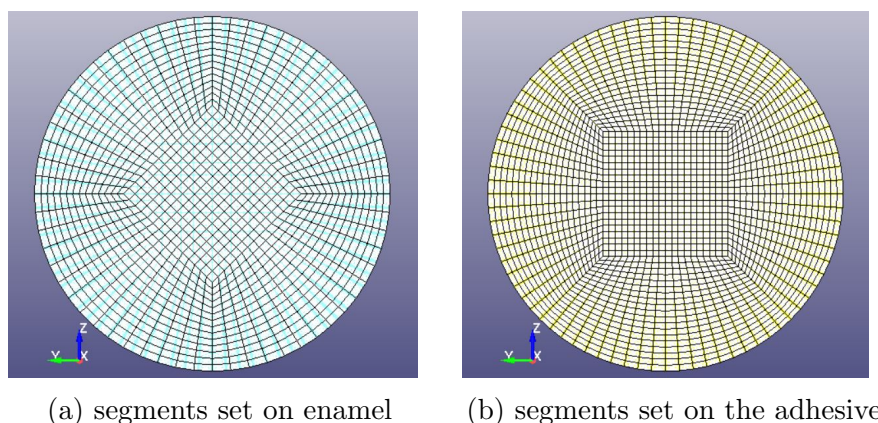


Figure 3.15: segments sets defined on the enamel and the adhesive for the tied contact

3.3.5 Results

The results obtained from the numerical simulation comprised mainly the stress distribution on the parts and the force-displacement curves of the test.

3.3.5.1 Stress Distribution

The stress distribution on the parts obtained with this approach is similar (qualitatively) with the one we obtained using the tiebreak contact to model the cohesive zone. In fact

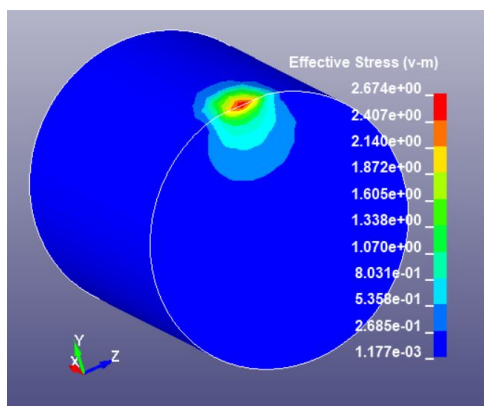


Figure 3.16: Von Mises stress distribution on Enamel [GPa]

we can realise from the figure 3.9 and the figures 3.16 and 3.17 how the stress distribution on each part looks similar qualitatively speaking. The stress distribution on enamel

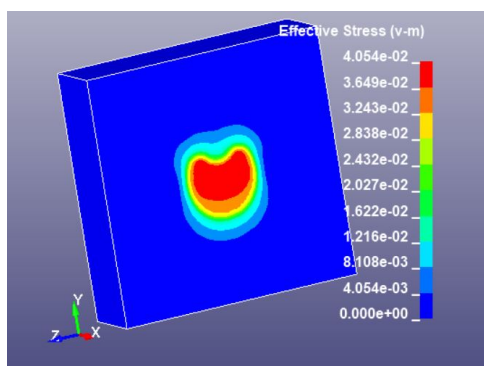


Figure 3.17: Von Mises stress distribution on Dentin [GPa]

shows us that the maximum stress is located at the zone where the indenter and the enamel are in contact. The maximum stress is equal to 2674 MPa and corresponds to the maximum stress of the whole structure. The Von Mises stresses on the dentine are mainly distributed in the central region of the dentin. We can see from figure 3.17 how the farther we are from the central zone of the dentin the lower is the stress. If we refer the the geometry of our model, it is easy to note that the central zone of the dentin corresponds

to the zone where the cohesive elements and the dentin are in contact namely the zone where the adhesive and the dentin are in contact. Focusing on the central zone of the dentin, we can realise that the stress is non homogeneously distributed on that zone. The maximum stress is equal to 40.54 MPa. The maximum stress on the dentin is quite close to the traction in the tangential direction for shear failure that we set as equal to 67 MPa.

3.3.5.2 Force-Displacement Curves

The force-displacement curve for this model was plotted in order to validate the model. During the post processing, the loading force transmitted to the enamel by the indenter was plotted as well as the contact force between the cohesive elements and the parts in contact with. We realised as we expected that the y component of the contact force was almost equal to the force generated by the displacement of the dentin as shows the figure 3.10. From the adhesive Young's modulus and the adhesive shear bond strength value, we were able to plot the experimental force-displacement curve shown by the figure 3.10. The procedure followed in order to obtain the experimental force displacement curve was

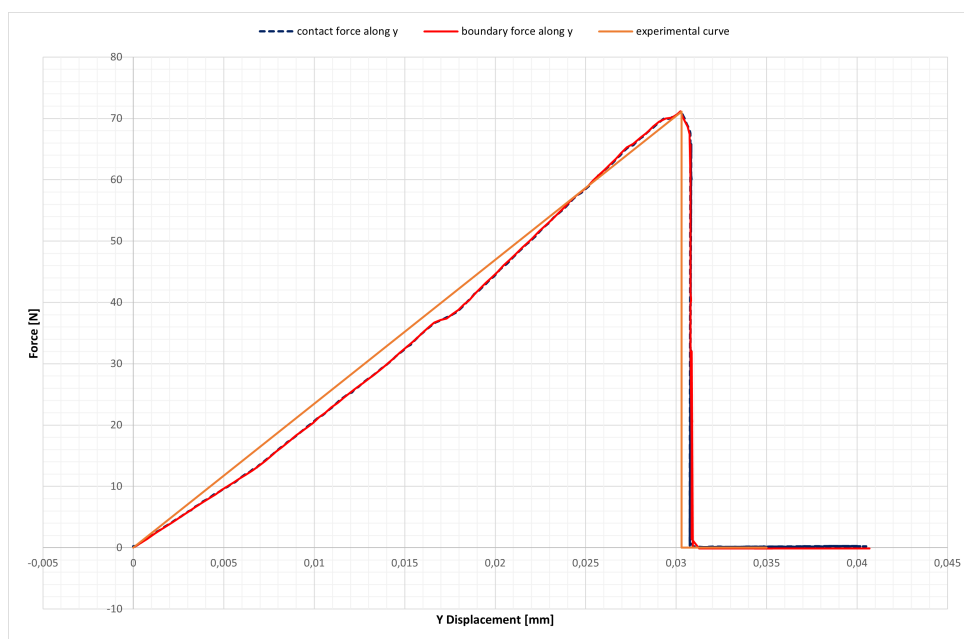


Figure 3.18: Force-Displacement curves

already explained in the sub-subsection 3.2.5.2 on page 45. The force-displacement curve obtained from the numerical analysis shows a maximum force equal to 71.6 N. Considering a contact surface of 3.14mm^2 circa, such a force corresponds to a bond strength equal to 22.8 MPa. The experimental results gave us a mean shear bond strength test of 22.29 MPa. By looking at the curves from figure 3.18, we can note that both the numerical results and experimental curve are quite close. For this reason, the model with cohesive elements was validated. Just like with the tiebreak contact, several simulations were run

by changing each time the adhesive shear failure stress in the solver algorithm. We just recall that the adhesive shear failure stress (FT_FAIL) which gave the results fitting the most with the experimental curve is equal to 67 MPa.

3.4 Comparison Between the Different Approaches

We recall that two approaches were used to model the adhesive layer. For each of these approaches, it was necessary to define some properties characterizing the adhesive such as the stiffness of the adhesive, its failure stress (in the normal and tangential direction)... etc. Even if these parameters have different names in the manual user for each method, each parameter used to define the tiebreak contact has an equivalent parameter used to model the adhesive with the cohesive elements.

Shear bond strength test	
Tiebreak contact	Cohesive elements
NFSL = 39 MPa	FN_FAIL = 39 MPa
SFSL = 50 MPa	FT_FAIL = 67 MPa
CN = 10020 GPa/m	ET = 10020 GPa/m

Table 3.3: Equivalence between the parameters used by the solver algorithms for the two different approaches. The parameters belonging to the same row have the same physical meaning.

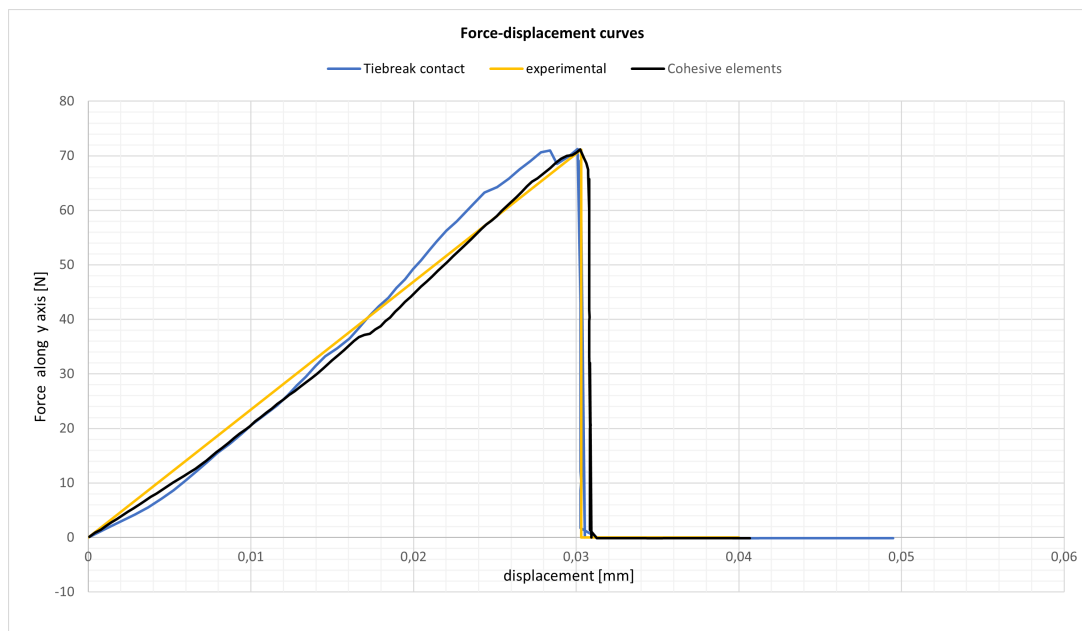


Figure 3.19: Force-Displacement curves

The table 3.3 shows us that the main information necessary to model an adhesive with these two approaches are the adhesive failure stress in the normal and tangential direction as well as the adhesive stiffness. These values are enough when using these two approaches because they model adhesives with linear elastic models.

The figure 3.19 shows us the force-displacement curves obtained from the numerical analysis for different approaches. All the curves have almost the same slope therefore, We can deduce that both the methods are suitable to define the adhesive stiffness since the slope of each curve depends on the adhesive stiffness. Another observation is that the peak forces are almost the same. If we look at the equivalence between the parameters (tab 3.3 used to simulate the adhesive layer, for the adhesive shear failure stress (SFSL) a value of 50 MPa was assigned whereas a value of 67 MPa was assigned when using the cohesive elements approach to obtain the same peak force. From this observation we can say that the adhesive failure stress is probably between the two values.

Chapter 4

Push-Out Bond Strength Test

4.1 Literature Review and Experimental Test Description

4.1.1 Literature Review

The restoration of endodontically treated teeth is guided by strength and aesthetic requirements. The goal is to transfer a bio mechanically favorable stress distribution from the coronal and root restoration to the remaining tooth structure. The quantity and character of the remaining coronal and root dentin, the materials employed, as well as the bonding interaction between the tissues and biomaterials will influence the longevity of the restoration. Studies have concluded that post materials that more closely match the Young's modulus of tooth structures, such as luted carbon and glass fiber posts, demonstrate more favorable outcomes. Several different mechanical testing methods have been used to measure the bond strength of a glass post to intraradicular dentin, to include: microtensile bond strength test, pull-out and push-out tests. The microtensile test has been stated to permit a more uniform stress distribution along the bonded interface due to the small specimen size and has been used to evaluate the regional bond strength throughout the length of the canal. Following these principles the "micro-push-out" method was developed and has been used to evaluate the adhesion of a glass post to root dentin. Although intraradicular bonded surface areas greater than $1mm^2$ are commonly evaluated, the use of term 'micro' will be continued in the present paper. The micro push-out method was shown to have fewer premature specimen failures and a lower data distribution variability compared to both trimmed and untrimmed microtensile specimens during the bond strength evaluation of glass fiber posts to intraradicular dentin and has been suggested to more closely simulate the clinical conditions. Bonding to root canals might be difficult, because of the handling characteristics of the adhesive system, root anatomy, tooth position, the presence of coronal residual tissue, the use of a light-curing technique, the experience and skill of the operators, etc [27]. Self-adhesive cements were introduced

in 2002 as a new subgroup of resin cements. They were designed with the intent of integrating the favorable characteristics of different cement classes into a single product. Their main advantage is the simplicity of clinical use. These cements are expected to offer properties analogous to those of resin cements. Many *in vitro* studies have investigated the different factors affecting the interfacial shear strength at the dentin – post interface. Some of these factors are represented by the intracanal irrigant as well as the endodontic cement used to seal the root canal. Chemical irrigants are essential for successful debridement of root canals during shaping and cleaning procedures. They are used not only as antimicrobial agents but also to lubricate the dentinal walls and to dissolve organic and inorganic components of the smear layer. Sodium hypochlorite (NaOCl) has long been proved to present capacity of dissolution of organic tissues and neutralization of toxic products while chlorhexidine (CHX), in addition to capacity of dissolution, has also been shown to possess bactericide properties because of its ability to precipitate and coagulate bacterial intracellular constituents. Irrigants might affect the characteristics of the dentin surface and therefore, might trigger or inhibit the chemical (e.g. covalent bonds, metallic bonds, etc), physical (e.g. van der Waals forces, hydrogen bonds, etc) and mechanical (e.g. entrapment of a material into another body, within natural or artificial cavities) attraction forces which are involved in the process of adhesion of the post to the dentin.

4.1.2 Experimental Test Description

According to Antonio Boccaccio[27], forty human single-rooted teeth were collected and used in the present study. All teeth were extracted for orthodontic reasons and kept, according to Jainaen et al.[28], in 1 % chloramine T (pH 7.8) at 4 °C until use. By using a high speed carbide bur and water spray, the dental crowns were removed obtaining approximately 15 mm long root segments. The obtained roots were then randomly assigned to four groups (n=10) according to the irrigating solution used as well as to the type of endodontic cement employed to seal the root canal space. Canal patency and working length were established by inserting K file #15 (DENTSPLY Maillefer, Oklahoma, USA) to the root canal terminus. All canals were prepared at working length 0.5 mm short of the patency length using 0.04 taper Profile instrument (DENTSPLY Maillefer, Oklahoma, USA) to master apical rotary (MAR) size 35–45. In order to remove the smear layer left by every file, the root canals were abundantly

irrigated with chlorhexidine 0.2 % . Canals were dried using paper points. Apexit canal sealer (IVOCLAR VIVADENT, Naturno(BZ), Italy), cement based on calcium hydroxide, was used to seal the root canal. After mixing the sealer, a gutta-percha master cone was lightly coated with sealer and inserted to the working length. A System B plugger size fine medium was used to condense the master cone to within 5 mm from the working length. Gutta-percha and sealers were removed with Gates-Glidden (DENTSPLY Maillefer, Oklahoma, USA) instruments and a 4÷5 mm thick layer was left on the root canal terminus so to guarantee its sealing. Then, root canals were abundantly irrigated with

sodium hypochlorite; paper points were again used to dry their surface. Fiberglass posts were inserted according to the protocol prescribed by the posts' Manufacturer (MC Italia, Milano, Italy). The choice of the post was made according to the size of the root canal. Using a Surgi Shaper cutter disk, the post was adapted apically. The root canal walls were treated with the Surgi Gel acid solution (phosphoric acid 37 %) for sixty seconds to etch dental tissues and obtain a stronger adhesion. The acid was accurately removed by water spray. Paper points were again used to dry the root canal. However, this time, the dentinal surface was left wet. By using a micro-brush, a first layer of dual adhesive Surgi Primebond Base + Surgi Primebond Activator (MC Italia, Milano, Italy) was applied on the root canal walls. Then, the layer was radiated by a halogen lamp for twenty seconds. A second layer of dual adhesive was applied, but, this time, the adhesive was not radiated (to avoid the formation of an additional thickness that would push the post in the direction of the crown). The dual adhesive was also applied on the post surface. The Surgi Dual Flò Core cement (MC Italia, Milano, Italy) was slowly extruded within the root canal thus filling it completely. The post was finally inserted; the excessive amounts of cement that came out of the root canal were radiated by a halogen lamp for forty seconds to stabilize the emergent part of the post. All the operations were carried out by a single experienced operator[27]. For each of the collected roots, approximately 5÷6

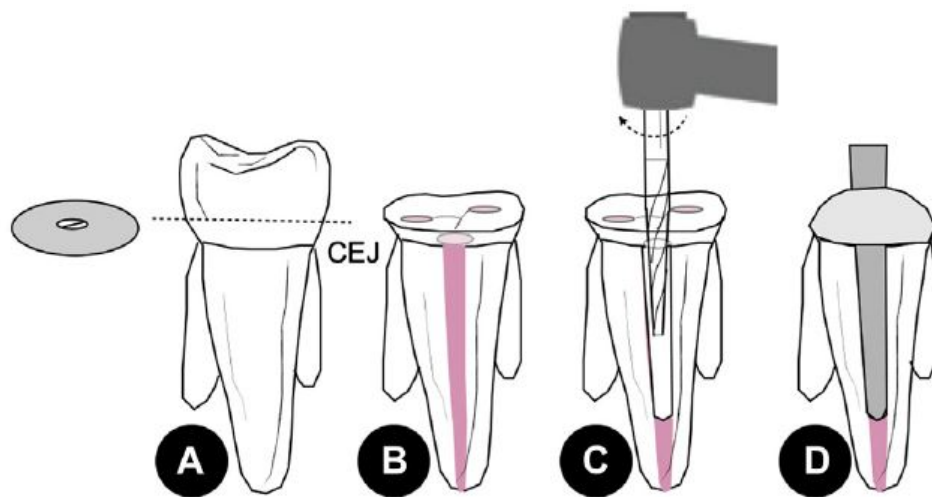


Figure 4.1: Schematic drawing of the specimen preparation procedure for the micro-push-out bond strength test on 1 mm thick slices. (A) The crowns were removed 2 mm above the cemento-enamel junction (CEJ). (B) After the cleaning-shaping procedure, an adhesive root canal filling was performed. (C) Preparation of the post-space with pre-calibrated burs. (D) Cementation of the fiber post into the root canal.

1000 micrometri thick sections have been obtained; a total of 220 sections were therefore submitted to micro-push-out-test. The micro-push-out test was performed on a 3343 Instron universal testing machine with a load cell of 500 N. Following Teixeira et al [29], the crosshead speed was set equal to 1 mm/min. A couple of guides firmly fixed to the

grips (controlled by a hydraulic system) of the testing machine, guaranteed the exact vertical positioning of a steel rod. The rod had a circular transverse section; according to Hashem et al [30], the diameter of the steel rod was set equal to 0.8 mm. The specimens were placed onto an aluminium plate 10 mm thick with a 2 mm diameter circular hole. The plate was fixed, in turn, by means of a supporting frame, to the bottom grips of the testing machine. All tested specimens included posts possessing a transverse section with a diameter greater than the rod diameter. For each sample, the force-displacement curve was traced thus distinguishing four different regions.

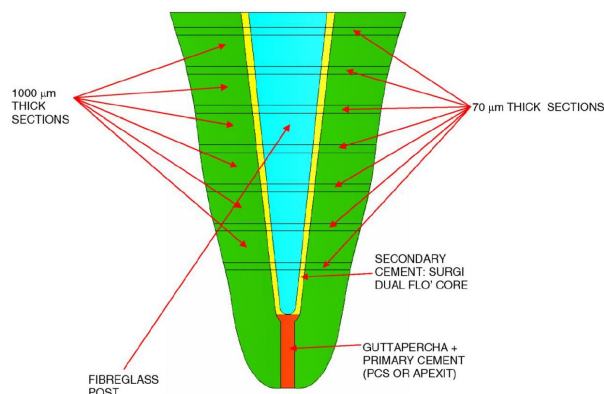


Figure 4.2: Schematic drawing of the specimen preparation procedure: slices obtained from each root canal.

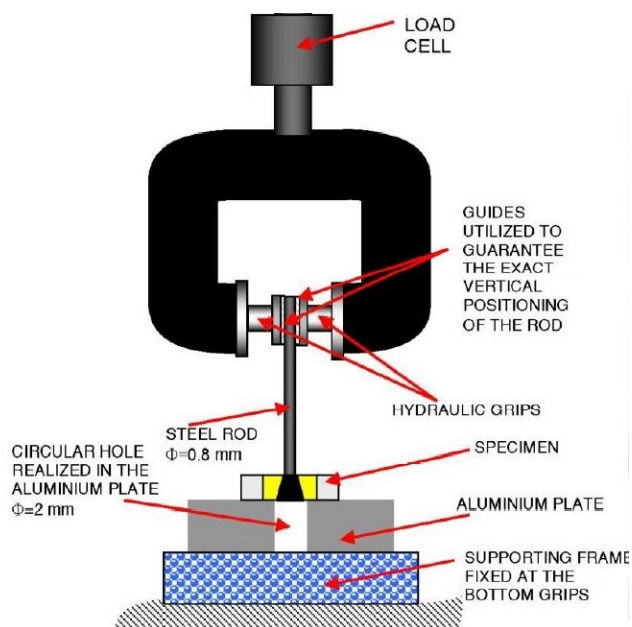


Figure 4.3: Schematic drawing of the specimen mounted on the testing machine

An initial region (highlighted in red in which, due to the clearance existing between the

sample and the aluminium plate, as well as the rod tip and the sample, small values of force were registered against large displacement values; a second region where a quasi-linear increase of the force with the displacement was observed; a third region (highlighted in green 4.2) where a sudden decrease of the force was recorded, which indicates that the critical condition of failure have been reached; a fourth region where, due to the fact that the portions of the adhesive area at the post-cement interface that did not fail yet opposed the further displacement of the rod, a small increase of the force was observed. The interfacial shear strength was computed as the ratio between the maximum value of

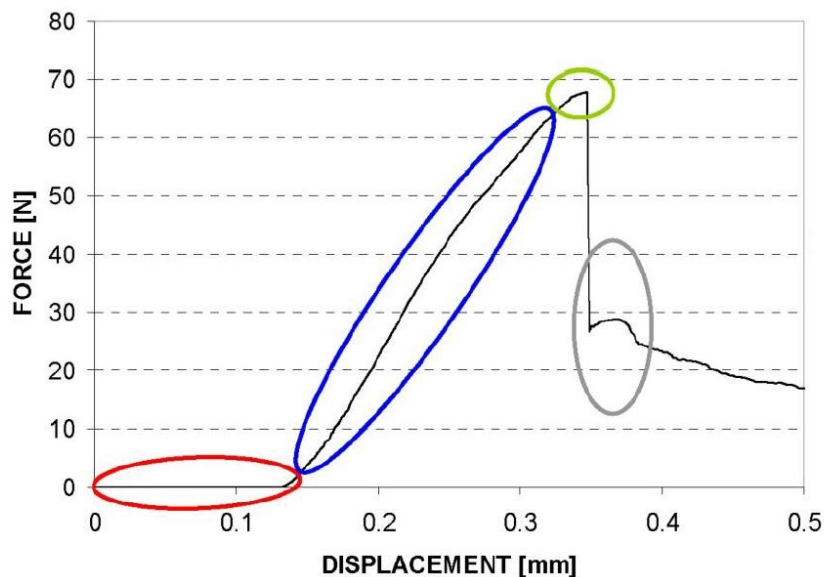


Figure 4.4: Force-Displacement curve registered for the sample submitted to micro-push-out test.

force (registered in the third region) and the bonding area at the dentin – post interface. The bonding area was accurately measured through the histomorphometric images of the 70 micrometri thick samples immediately adjacent (to the 1000 micrometri thick section under analysis). The test was considered not acceptable in each of the following cases:

1. failure of the dentin occurring before the failure of the cement;
2. failure of the PMMA occurring before the failure of the cement;
3. failure of the dentin and of the PMMA occurring before the failure of the cement;
4. penetration of the rod within the post without failure of the cement.

The samples to be tested have been randomly chosen. This is how the experimental test was conducted in the laboratory and the force-displacement curve that was obtained from this test is shown in the figure 4.4

4.2 Finite Element Model with the Tiebreak Contact

Just like for the microtensile test and the shear bond test, two approaches were used to model and then simulate the micro-push-out test in order to characterize the adhesive system that was used for the experimental test. The main difference between the two models built for the micro-push-out test and corresponding to the two approaches that were used lies in the modelling of the cohesive zone in our models. Here is the description of the first approach based on the modelling of the cohesive zone with the Tiebreak Contact in LS-DYNA.

4.2.1 Geometry and Mesh

The first step in the building of the finite element model was the construction of the different geometries corresponding to the different parts which comprised the model. Basing on the dimensions of the parts used for the experimental testing, the geometry represented in the figure 4.5 was designed. We thought that for this approach with the tiebreak contact, a model with four parts was able to fully describe and represent the micro-push-out test. Some dimensions of the parts are shown in the figure 4.5. For what concerns the height

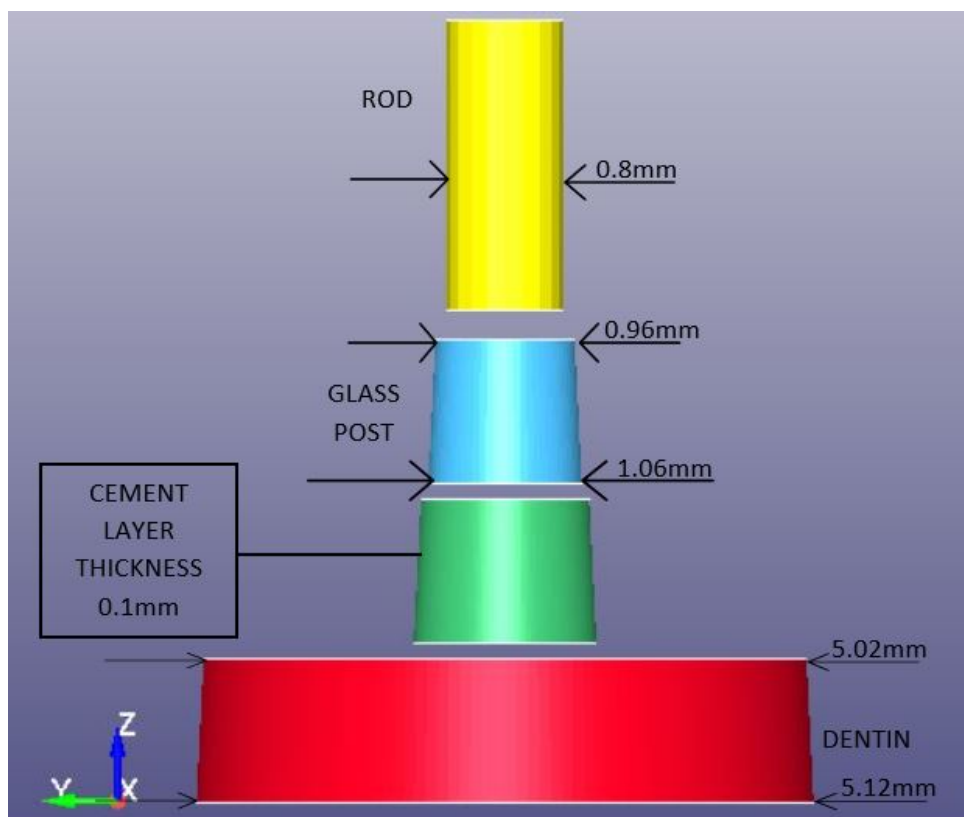


Figure 4.5: Geometry of the model exploded with dimensions

of the parts which constitutes with the radii the dimensions of interest, we designed the

glass post, the cement layer and the dentin with a height equal to 1 mm in order to be coherent with the specimen preparation before the experimental test. The steel rod was designed with a height equal to 2 mm because we thought that the most important dimension related to the steel rod in order to have a realistic model of the micro-push-out test was the steel rod diameter. Having this geometry, the next step was the generation of a mesh on each of the four parts. Being the dimensions of each part different, the elements size was different from one part to another. The mesh density of the pusher was lower with respect to the mesh density of the other parts. This was done because our main interest regarded the zone where parts are in contact with the adhesive cement. At the same time, it was necessary that the mesh generated on the pusher is fine enough in order to transmit the load in the right way as recommends us LS-DYNA manual user. All

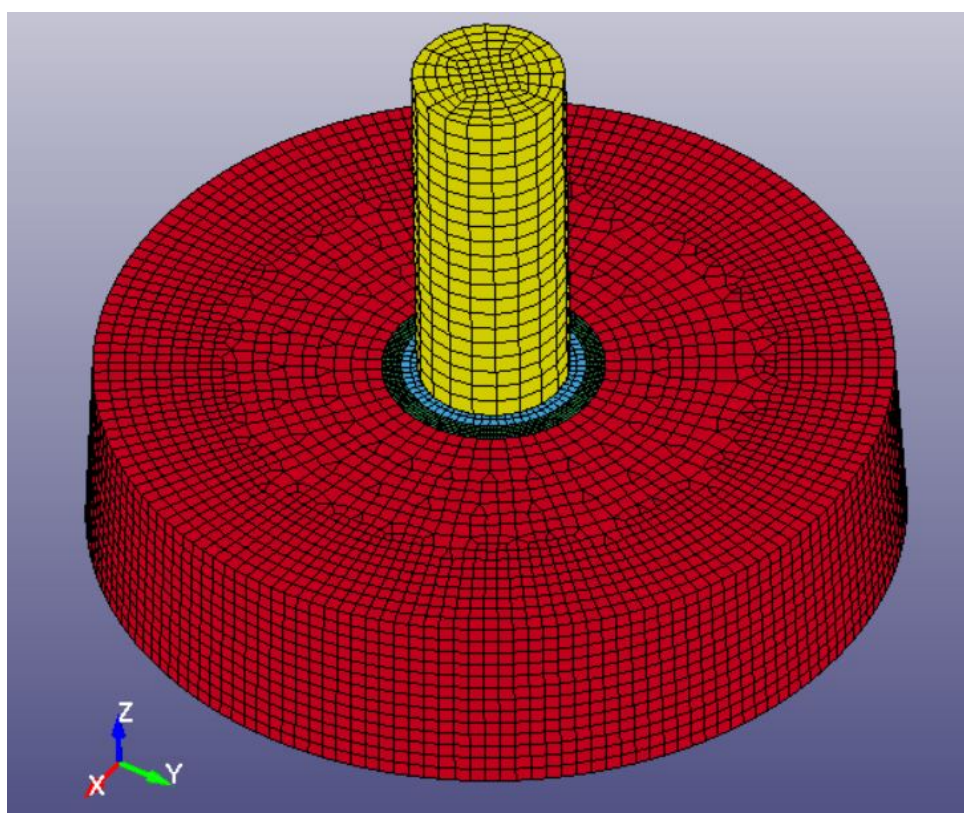


Figure 4.6: Isometric view of the model meshed: the part in red represents the mesh generated from the dentin, the part in green represent the mesh generated from the cement layer, the part in blue represents the mesh generated from the glass post and the part in yellow the mesh generated from the steel rod.

the parts were meshed with solid elements with element formulation ELFORM3. Such an element formulation corresponding to fully integrated quadratic 8 node element with nodal rotations were suitable for this model because were able to prevent the hourglass modes occurrence. The table 4.1 gives us some information about the mesh generated from the parts. We can easily note that the cement layer is the part having more elements

Parts	Maximum element size	Number of elements	Number of nodes
Dentin	0.08 mm	29315	32620
Cement	0.02 mm	46000	55437
Glass Post	0.05 mm	9200	10248
Rod	0.04 mm	2100	2436

Table 4.1: Mesh properties of the different parts

and therefore more nodes. The choice of having a fine cement mesh was made in order to have a better analysis of the tiebreak contact on this model. Having the information related to the mesh of each part, we can have the total number of elements which comprises the model as well as the total number of nodes of the model. The sum leads us to a total number of elements equal to 86615 and a total number of nodes equal to 100741.

4.2.2 Materials

The choice of the material model for this numerical model was based essentially on the literature. The dentin and the cement were modelled as linear elastic isotropic materials whereas the glass post was modelled as a linear elastic orthotropic material. The steel rod which transmits the load to the model, it was modelled as a rigid material. It is worth to precise that the a linear elastic isotropic material is model with the material 001-ELASTIC while a linear elastic orthotropic material is modelled with the material 002-ORTHOTROPIC_ELASTIC. The material 020-RIGID was used to model the steel rod in this model. The material properties used for this model are given in the table 4.2. Let's precise that the principal material directions are the one shown in the figure 4.5.

Parts	Young's Modulus [GPa]	Poisson's Ratio
Dentin	18.6	0.31
Cement	15	0.27
Steel rod	210	0.30
Glass post	$E_{xx} = 9.5, E_{yy} = 9.5, E_{zz} = 37$	$\nu_{yz} = 0.27, \nu_{xy} = 0.27, \nu_{xz} = 0.34$

Table 4.2: Mechanical properties of materials

A particular attention was dedicated to the material direction since the data collected in the literature have different reference frame. The material 020-RIGID used for the the modelling of the steel rod was chosen because LS-DYNA manual user recommends such a material for parts that are considered to belong to a rigid body (for each part ID). In our specific case, even if the rod made from steel is not a rigid material, it was considered as rigid because it has a very high elastic modulus with respect to the other materials elastic modulus. In order to properly define a rigid material in LS-DYNA, a part from the mechanical properties, center of mass constraints and global translational constraints of the body modelled with the material must be defined. Constraint directions for rigid

materials (CMO equal to +1 or -1) are fixed, that is, not updated, with time.

4.2.3 Boundary Conditions

The Boundary conditions enforced on this model consisted in fixing some nodes belonging to the dentin and prescribe a motion to the rod through a velocity curve. Some nodes were constrained at the base of the dentin because the experimental test shown us how a portion of the dentin base surface is in contact with the aluminium plate which behaves as support for the specimen. For this reason, instead of including in the model the aluminium

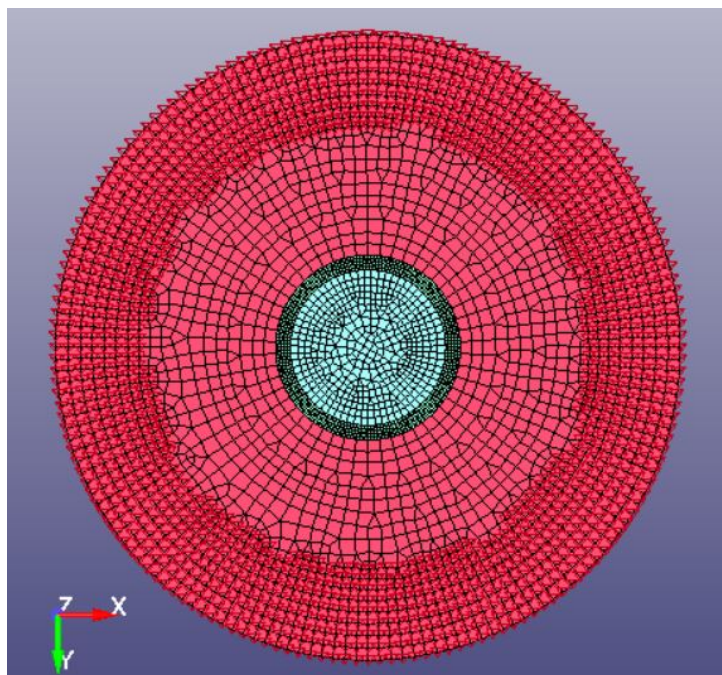


Figure 4.7: Down view of the model: constrained nodes highlighted in red

plate and the supporting frame as shows us the figure 4.3, the nodes belonging to that portion of the dentin base in contact with the aluminium plate were constrained. The constraints enforced on these nodes consisted in preventing all the nodal displacements along x, y, z axis, and all the nodal rotations around x, y, z axis. Another reason of such a choice is the fact that we were interested mainly in the dentin-cement and cement-glass post interfaces. The incorporation of other parts in this model would have made the simulation longer and more complex without giving us interesting results for our purpose. The decision of prescribing a motion to the rigid body (steel rod) in order to have the load transmission was made because it reflects in a realistic way what happens during the test in the laboratory. The displacement law enforced to the rod through a velocity curve is shown in the figure 4.8. Such a curve starts from zero and smoothly increases up to reach a maximum value corresponding to 10mm/s and then remains constant during all the simulation time. A velocity curve that smoothly increases was chosen in order to

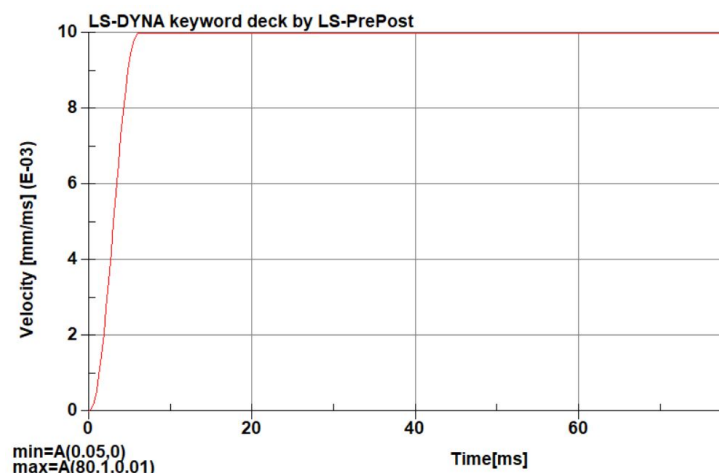


Figure 4.8: velocity curve prescribed to the rod

avoid rapid huge acceleration on the model. The maximum velocity reached by the curve was set in order to reduce the simulation time.

4.2.4 Contact Between Parts

For this model, two main types of contact were used:

1. The CONTACT_AUTOMATIC_SURFACE_TO_SURFACE
2. The CONTACT_AUTOMATIC_SURFACE_TO_SURFACE_TIEBREAK

The CONTACT_AUTOMATIC_SURFACE_TO_SURFACE was used to model the contact between the rod and the fibreglass post. This contact resulted to be suitable to model the contact between the two and is available for the massive parallel processing (MPP) and explicit analysis. Given the shape and the material properties of the parts

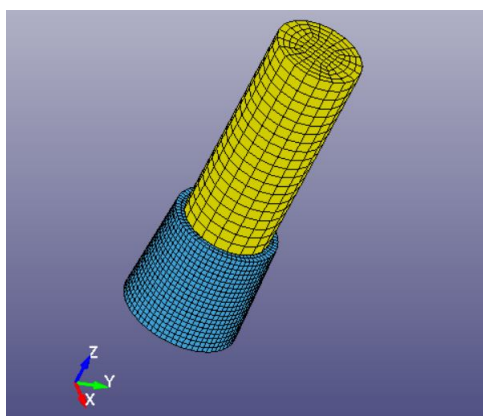
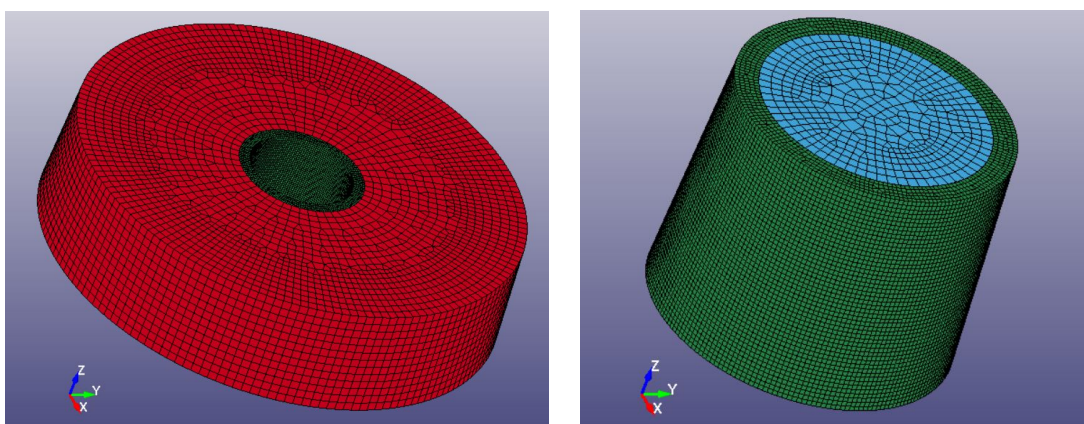


Figure 4.9: contact between the rod and the glass post

experiencing the contact, this contact did not present any issue during the simulation and the load was transmitted to the specimen in the right way.

The `CONTACT_AUTOMATIC_SURFACE_TO_SURFACE_TIEBREAK` was used to model the contact between the cement and the dentin on one hand and the contact between the cement and the glass post on the other hand. As we have already mentioned, the use of the tiebreak contact was used as the first approach also for the micro-push-out test model. The tiebreak contact is recommended by LS-DYNA manual user to model adhesive behavior. The first step to model this contact was the definition of segment sets on the contact surfaces that we just cited. Some of the segment sets were defined as master segments and the others as slave segments on the parts during the definition of these contacts. The second step in order to completely define this contact is the definition



(a) contact between cement and dentin (b) contact between cement and glass post

Figure 4.10: Tiebreak contact defined on the two subgroups of parts

of some variables useful for the modelling of the cohesive zone. The variable defined for the modelling of the cohesive zone were changed from one simulation to another up to reach the results matching with the experimental ones. These variables are:

- **NFLS** : NFLS represents the normal failure stress of the adhesive. For the micro-push-out test we chose a value equal to 20 MPa.
- **SFSL** : it represents the shear failure stress in the contact card. For the micro-push-out test, a value of 24 MPa was chosen in order to guarantee the shear bond strength obtained from the experimental test.
- **PARAM** : for option 6, PARAM is the critical distance (CCRIT), at which the interface failure is complete. Since we were not able to have the experimental force-displacement curve, such a parameter was not important for our analysis.
- **CT2N** : it represents the ratio of the tangential stiffness of the adhesive to the normal stiffness of the adhesive. This was set to be equal to 1. By setting $CT2N=1$ we defined the tangential stiffness of the adhesive equal to the normal stiffness.

- CN : is the normal stiffness (stress/length) for OPTION = 6. The manual recommends the use of this option with care, since contact stability can get affected. A value of 220 GPa/m was assigned in order to guarantee the right slope to the force-displacement curve.

It is worth to precise that all these variables were assumed to be equal for the contact definition on both the parts. In fact, by doing such an assumption, we were expecting the failure to occur on the interface cement - glass post because since both the contact have the same adhesive failure stress, the interface to fail is supposed to be the one with a minor area. The interface with the minor area satisfies the contact failure criterion first. This happens because when the load force reaches the peak value, the shear stress at the cement - glass post interface is higher than the shear stress at the cement - dentin interface therefore, the failure criterion is satisfied at that interface but not at the cement - dentin interface.

4.2.5 Results

After running the simulation, we were interested in the stress distribution and the force-displacement curve. The stress distribution was useful to understand how the failure occurs at the cement - glass post interface whereas the force-displacement curve was useful for the validation of this model.

4.2.5.1 Stress Distribution

The Von Mises stress distribution on all the parts except the rod was analysed. The figure 4.10 shows us how the stress is distributed on the whole model. We can note that the maximum stress is equal to 171 MPa. In order to analyse better the information

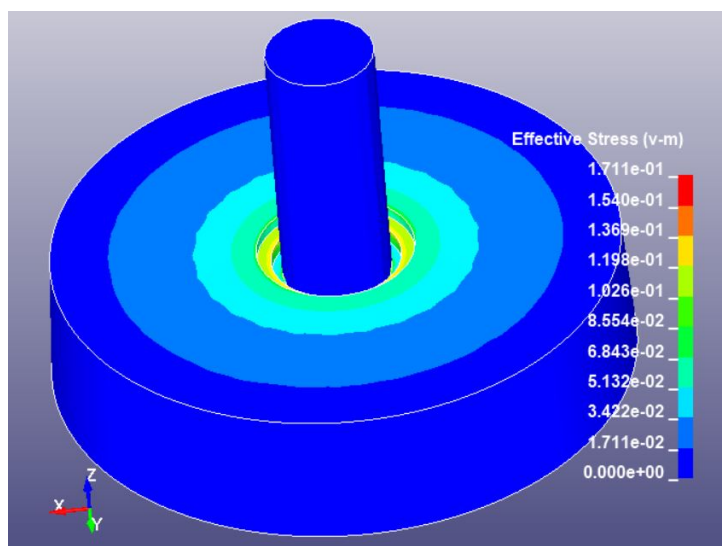


Figure 4.11: Von Mises stress distribution on the model in [GPa]

related to the stress distribution, it was necessary to separate the parts. The main parts of interest were the cement and the glass post because the adhesive bond strength was measured considering the cement - glass post interface as the reference surface area. The stress distribution on these two parts when separated shows us that the maximum stress on the glass post corresponding to 171 MPa is located at the top surface of the glass post. We note also that the maximum stress is located at a diameter corresponding to circa 0.8 mm of the top surface center. We recall that such a diameter is the rod diameter. Such a results let us think that those isolated points are due to the contact between the glass post and the rod. The stress distribution on the cement shows that the maximum

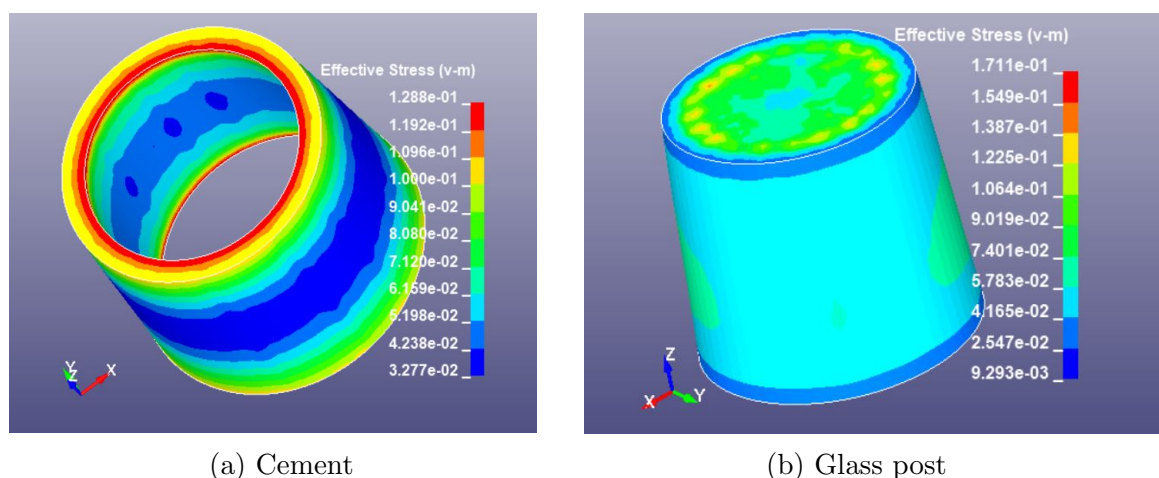


Figure 4.12: Von Mises stress distribution on the cement and the glass post in [GPa]

stress is located at the internal contact surface of the cement layer and precisely at the top edges and the bottom edges of the internal surface. The Von Mises stress value at these zones is around 128 MPa. The stress distribution also shows us that the stress is more concentrated at these zones. For this reason, we can presume that the failure starts at these zones.

We can see that starting from the middle height of the cement layer, the stress gradually increases almost in a symmetric way up to reach the maximum value at the internal surface top edge and at the internal surface bottom edge. As we were expecting, the external surface shows the same stress distribution from the point of view of the quality whereas quantitatively speaking, the stress values are smaller at the external surface of the cement layer. From the figure 4.13 we can see more clearly how the Von Mises stress is distributed on the dentin. The first thing that we can remark is that the maximum stress on the dentin is equal to circa 82.86 MPa. The maximum stress is located at the dentin internal surface top edge. The fact that we have a smaller value of the maximum stress on the dentin makes sense because the contact area of the cement - dentin interface is larger.

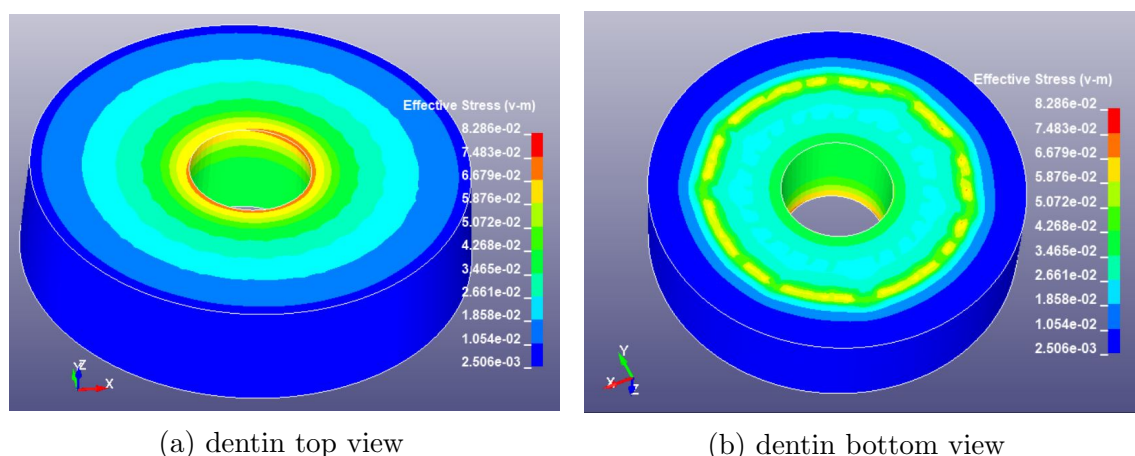


Figure 4.13: Von Mises stress distribution on the dentin in [GPa]

4.2.5.2 Force-Displacement curves

For the validation of the numerical model, the experimental curve was compared to the numerical curve that we obtained after the post processing. As we already know, from the experimental test, we were able to obtain the force-displacement curve. Having the experimental force-displacement curve, we were able to compute the bond strength of the adhesive system. To compute the bond strength of the adhesive system, it is enough to have the area of the glass post lateral surface which is in contact with the cement layer namely the internal surface of the cement layer. The knowledge of the glass post geometry is enough to compute the area of its lateral surface which is given by the equation whereby

Having that area, it is enough to read the value of the peak force on the experimental force-displacement curve shown in the figure 4.4. Having these two values, the adhesive system bond strength was given by the ratio between the peak force and the contact area. This procedure allowed us to have an average bond strength equal to 19.79 MPa. The adhesive system bond strength was useful because the first simulation was run by setting the value of the adhesive system bond strength equal 19.79 MPa in the tiebreak contact algorithm. The value 19.79 MPa set in the tiebreak contact algorithm as the adhesive system failure stress gave a force-displacement curve with a peak force that was lower than what we have had from the experimental test. In order to increase the peak force, the adhesive failure stress was slightly increased from one simulation to another up to reach the value of the adhesive failure stress equal to 22 MPa which gave us a numerical force-displacement curve very close to the experimental one as shows the figure 4.14. The curve obtained from the numerical analysis has a peak force equal to 69 N. considering the contact area, this peak force correspond to and average bond strength equal to 20.29 MPa. The numerical curve just like the experimental one, has a first part where the force remains equal to zero even if there is a displacement of the rod. This is due to the initial clearance between the rod and the glass post. The second part of the curve shows a linear

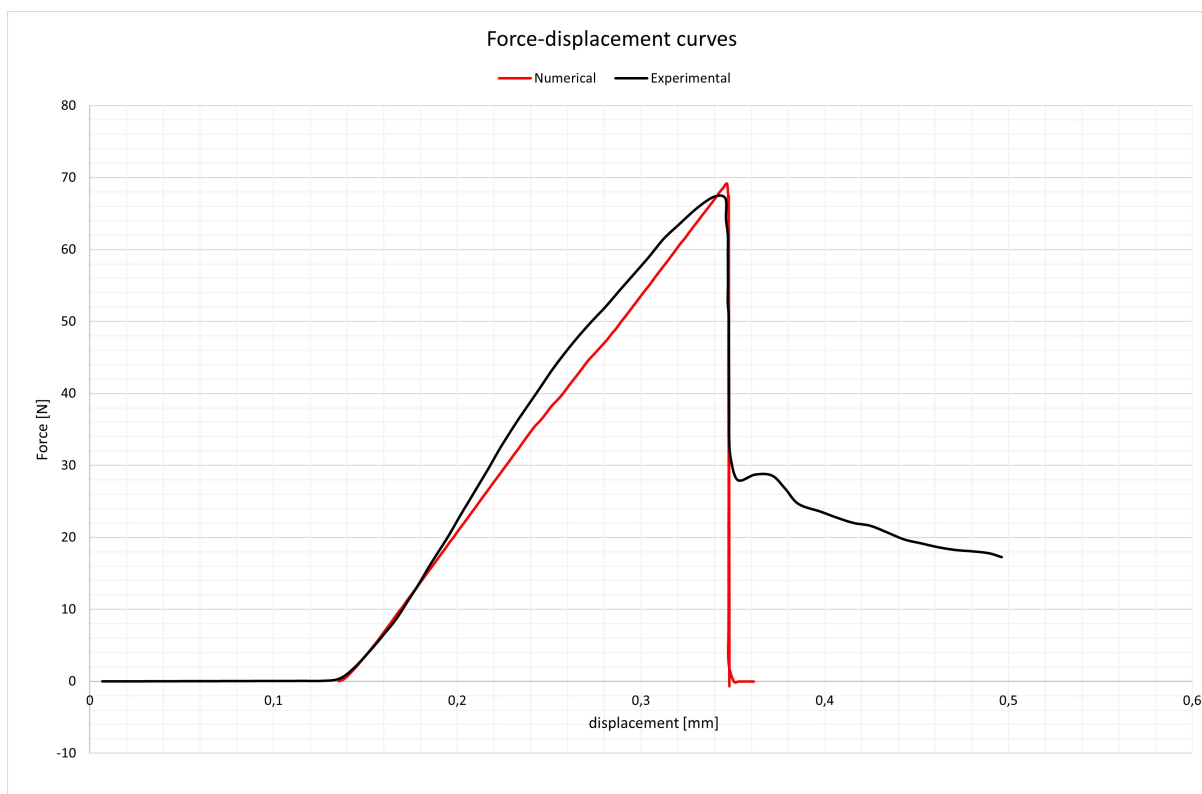


Figure 4.14: Force-Displacement curves

increase of the curve starting from the value of the force equal to zero (instant where the rod starts experiencing the contact with the glass post) up to a maximum value known as the peak which corresponds to the instant in which the adhesive failure occurs. Just after the failure, the force returns to zero. This is due to the elastic model of the adhesive that we used for the modelling of the cohesive zone.

4.3 Finite Element Model With Cohesive Elements

The second approach used for the modelling of the micro-push-out test consisted in using the cohesive elements to simulate the adhesive in the model. The main difference between the two approaches lies on the fact that these are two different way of modelling the cohesive zone. With the use of the cohesive elements, the adhesive is considered as a part which needs to be meshed with a specific type of elements. Here are described the steps followed to build and run this numerical model.

4.3.1 Geometry and Mesh

The geometry used for this model was almost the same with the geometry shown in the figure 4.5. The dimensions are the same for the parts such as the steel rod, the glass post,

the cement layer and the dentin with the one used in the previous section. The only parts added are two layers of thickness 0.01mm which represents the adhesive system used for the cementation of the glass post. Therefore, one of these layers was inserted between the dentin and the cement layer and another one was inserted between the cement layer and the glass post. From this geometry the meshes were generated on each part. The fact that the parts are concentric gave us the possibility to have coincident nodes at the interfaces whereby the parts experience the contact. By having coincident nodes in between the parts, it was possible to merge them. The mesh generated on this model is shown in the figure 4.16 and all the information related to the mesh generated on the parts are reported in the table 4.3.

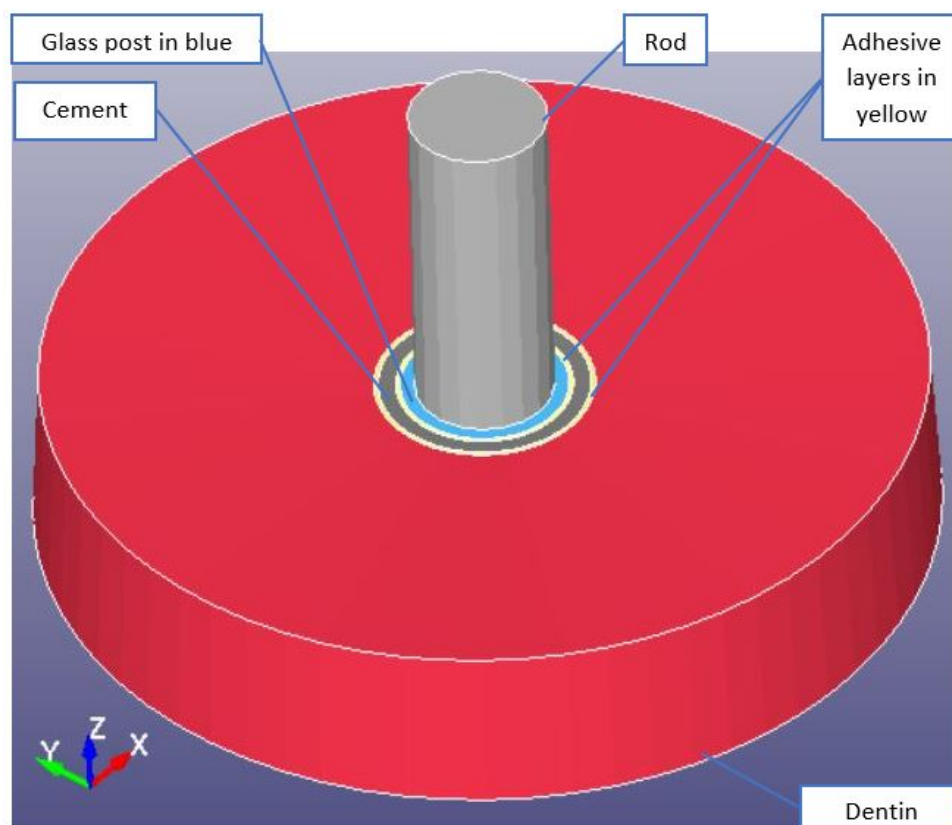


Figure 4.15: Geometry of the model

In the table 4.3, cohesive layer (1) stands for the layer of cohesive elements existing between the glass post and the cement whereas the cohesive layer (2) stands for the layer of cohesive elements existing between the dentin and the cement. We can realise that the two cohesive elements layer have the same number of elements and the same number of nodes this is because there is a node to node correspondence between the parts. We can also note from the mesh that the the glass post is the part with a higher mesh density because it has the smallest maximum element size. From the information related to the mesh properties, we were able to totalize a total number of elements for the whole model

Parts	Maximum element size	Number of elements	Number of nodes
Dentin	0.08 mm	26800	29547
Cement	0.02 mm	4020	5628
Glass Post	0.05 mm	9200	10248
Rod	0.04 mm	2100	2436
cohesive layer (1)	0.05	1340	2814
cohesive layer (2)	0.05	1340	2814

Table 4.3: Properties of the mesh for each part

equal to 44800 and a total number of nodes equal to 47859. For this model, the ELFORM3 was chosen as the element formulation for all the parts except the cohesive layer parts for which the ELFORM19 was chosen. The ELFORM19 element formulation is suitable whenever cohesive elements have to be used with solid elements.

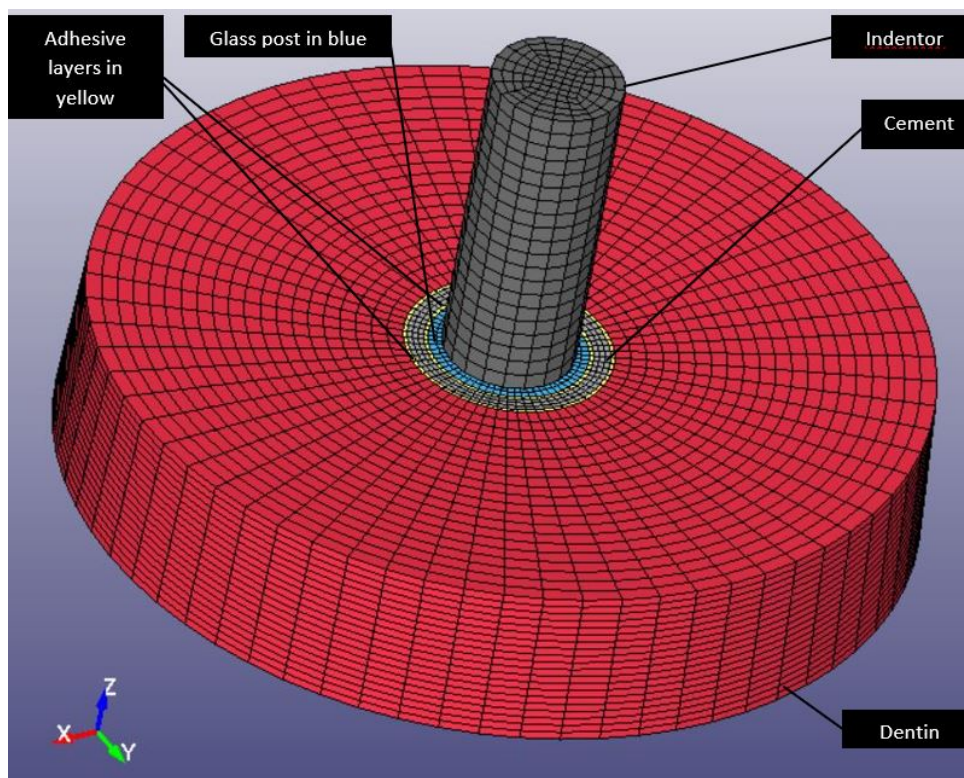


Figure 4.16: Mesh generated from the parts

4.3.2 Materials

For the materials used for this model, we will refer mainly to the subsection. The slight difference here is due to the presence of a new part in the model which requires

the definition of a new material model. Being the new parts the adhesive layers, it was necessary to define a material model able to well define the adhesive system used for the cementation of the glass post. Among the possible cohesive materials available for the modelling of cohesive zones in the LS-DYNA material library, we opted for the material 184 known as cohesive elastic material. This material has the advantage of being simpler for the modelling of the cohesive. This is due to the fact that it is an elastic model of the cohesive zone. To complete definition of this material model properties requires the knowledge of the following parameters:

- $RO=1200Kg/m^3$. whereby RO is the mass density of the material.
- ROFLG: it is a flag which tells whether density is specified per unit of area or volume. if $ROFLG = 0$, it specifies the density is per unit of volume (default) while if $ROFLG = 1$ specifies that the density is per unit of area for controlling the mass of cohesive elements with an initial volume of zero. This parameter is important because in LS-PrePost, zero thickness cohesive elements can be modelled and usually such a part should have $ROFLG = 1$. In our case, the adhesive thickness is $10\ \mu m$ therefore we opted for $ROFLG = 0$.
- INTFAIL: it is the number of integration points required for the cohesive element to be deleted. If it is zero, the element won't be deleted even if it satisfies the failure criterion. The value of INTFAIL may range from 1 to 4, we set INTFAIL=1 because of the recommendation from the manual.
- $ET=0.22\ GPa/mm$. ET is the Stiffness in the plane of the cohesive element namely the tangential stiffness. This stiffness is expressed in the unit of stress/length.
- EN: It is the stiffness normal to the plane of the cohesive element (stress/length). We assumed its value equal to the tangential stiffness ET.
- FN_FAIL= 20 MPa: It is the traction in the normal direction for tensile failure.
- FT_FAIL= 24 MPa: It is the traction in the tangential direction for shear failure is necessary in case of cohesive the presence of the shear mode failure. This value is the most important for the failure criterion.

4.3.3 Boundary Conditions

The boundary conditions are exactly the same that we have seen in the subsection 4.2.3 where the boundary conditions were described for the model using the tiebreak contact approach. Nothing new related to the boundary conditions was added to this model built with the cohesive elements.

4.3.4 Contact Between Parts

In this model, we defined the contact AUTOMATIC SURFACE TO SURFACE CONTACT to model the contact between the glass post and the steel rod. In order to well define this contact, we only needed to define the zone where the penetration between the two parts has to be checked. In this case, Since a rigid material (material model used to model the steel rod) was involved in the contact, we prescribe the whole parts as zone where to check the penetration. Therefore, a the steel rod was defined as the master part and the glass post was defined as the slave part in the contact algorithm. This contact is shown in the figure.

The contacts experienced by the other parts such as the contact between the glass post and the first adhesive layer, the contact between the cement layer and the adhesive layer as well as the contact between the dentin and the adhesive layer were modelled with a different method. In fact, whenever it is possible to generate the mesh on the parts and have node to node coincidence between the cohesive elements layer and the parts in contact with, it is possible to use the merge option in order to unite the coincident nodes belonging to different parts. When coincident nodes belonging to different parts

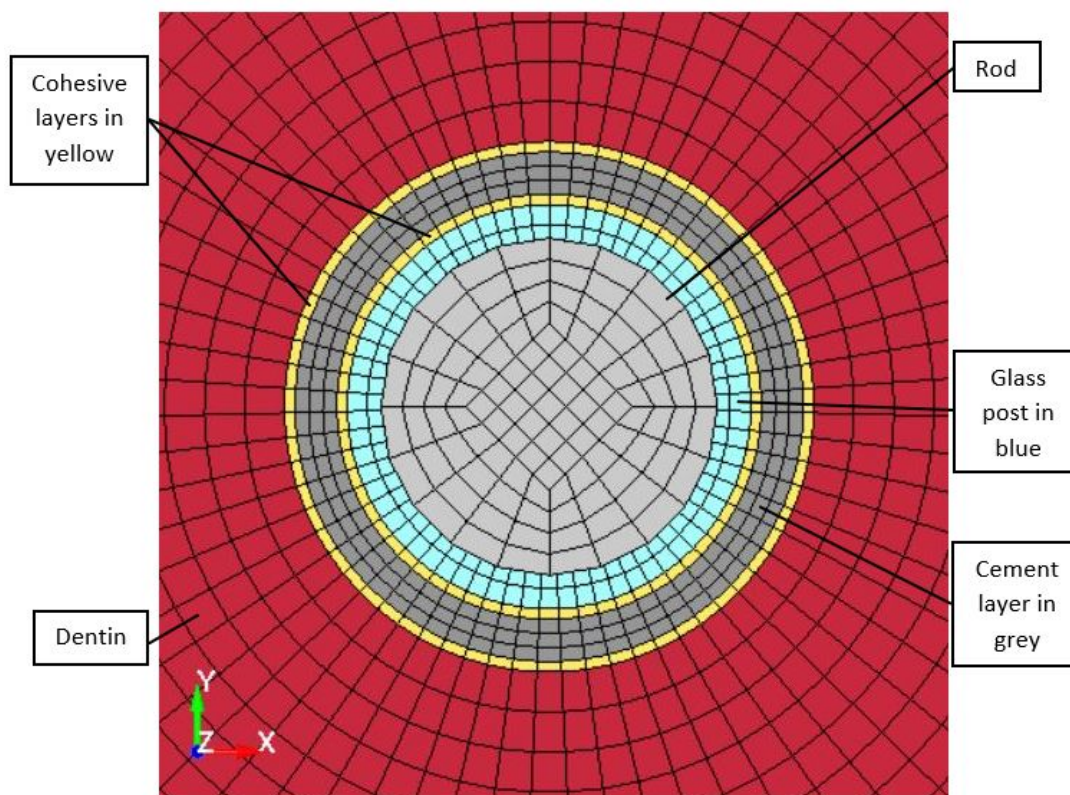


Figure 4.17: Partial top view of the model

are united by the merge option, the parts behave as if they were bonded therefore, no

other contact is needed. In the figure 4.17, we can clearly see how the nodes which are concentric to the glass post have the nodes coincident to the nodes of the surrounding parts.

In case the mesh does not allow to have coincident nodes between a cohesive layer and a part experiencing the contact with, the tied option can be used to define the physical contact which occurs between the parts. For this reason, While generating the mesh on the parts, we paid attention to how the nodes would be at the contact surfaces between the adhesive layers and the surrounding parts. We also recall that the cohesive elements layers, in particular the one to which are assigned the element formulation ELFORM19, must be generated within the model in such a way that all their elements must have on one side of the contact their four nodes lying on an element of the other part involved in the contact and the four other elements must have their element lying on an element belonging to another part involved in the physical contact. The figure summarises how the mesh was generated on the concentric parts. We can clearly realise that the adhesive layers have just one layer of elements in the radial direction.

4.3.5 Results

After running this model, we were mainly interested in the stress distribution on the parts which allows us to have an idea on how the failure occurs and the force-displacement curve which is useful for the validation of the model.

4.3.5.1 Stress Distribution

The Von Mises stress distribution on the whole model is shown in the figure . The figure reveals us that the maximum stress is equal to 198.4 MPa. This results need to be analysed in deep. this is why the stress distribution was analysed on the single parts. In

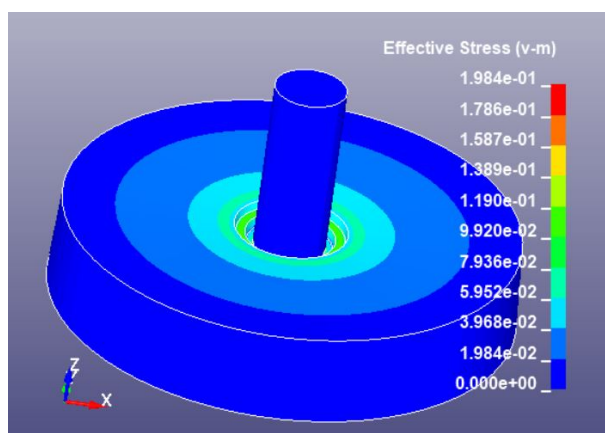


Figure 4.18: Von Mises stress distribution on the whole model

the figure 4.19b we can see how the Von Mises stress is distributed on the glass post. The

maximum stress on the glass post is equal to 198.4 MPa. It is the highest stress value on the whole model. This stress is located at the top surface of the glass post. The location

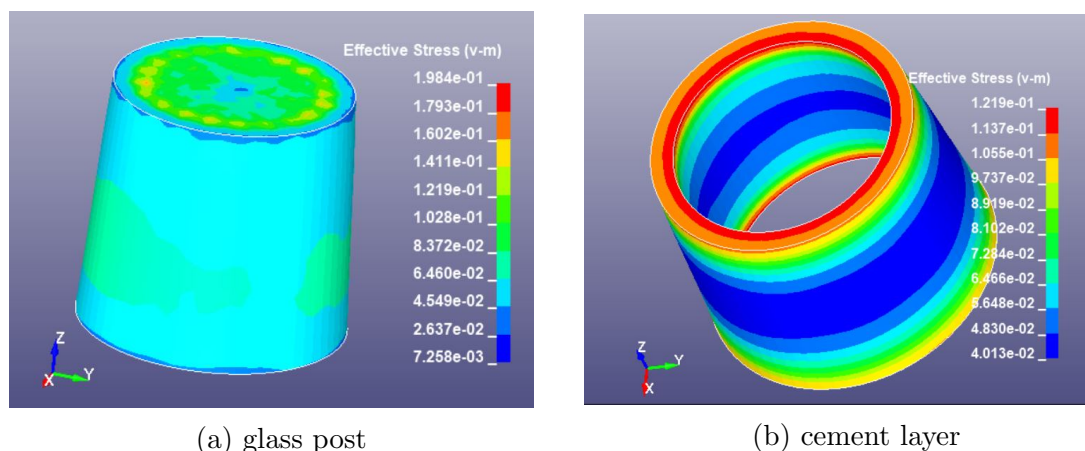


Figure 4.19: Von Mises stress distribution on the glass post and the cement in [GPa]

of the maximum stress allows us to deduce that such a value of stress is due to the contact between the steel rod and the glass post. The stress is almost uniformly distributed on the lateral surface of the glass post. That lateral surface corresponds to the area in contact with the cohesive elements layer. The figure 4.19b instead, shows us a stress concentrated at the top and the bottom edge of the internal surface of the cement layer. The stress concentration at the edges of the cement internal surface highlights the zone where the failure starts. In the same way, the stress analysis on the dentin shows that the stress distribution on the dentin is not uniform. We have in particular a concentration of the

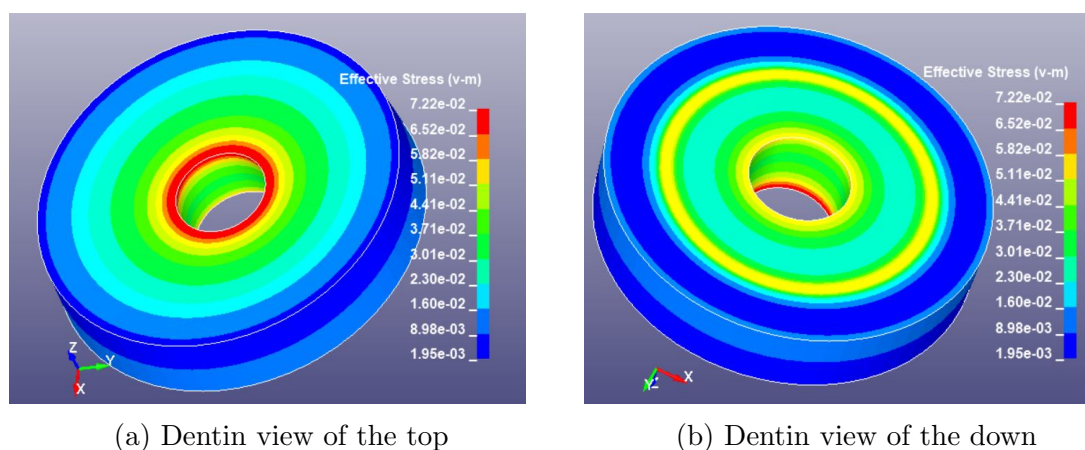


Figure 4.20: Von Mises stress distribution on the dentin in [GPa]

stress at the top edge of the dentin internal surface. From the configuration of the parts we know that the dentin internal surface is the surface which experiences the contact with the adhesive in reality. We can also realise that unlike the cement layer on which

the maximum Von Mises stress is equal to 121 MPa, the maximum stress on the dentin is equal to around 72.2 MPa. This result is the consequence of the fact that the dentine internal surface is larger than the cement layer internal surface. The stress distribution

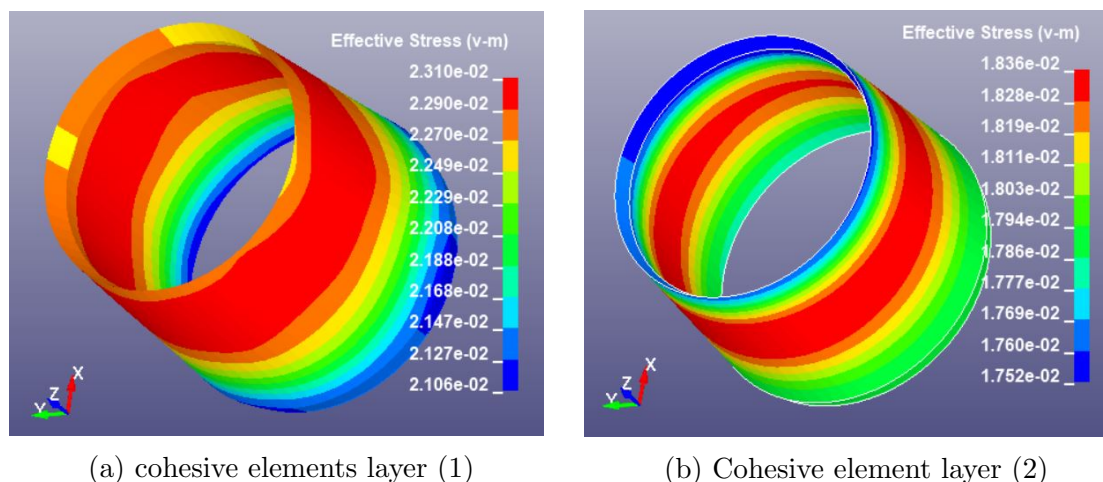


Figure 4.21: Stress distribution on the cohesive layers in [GPa]

on the cohesive elements layers was also analysed. From the figure 4.21a we can see how the stress is distributed on the cohesive layer in contact with the glass post. We can see that at the instant before the failure, the maximum stress is equal to 23.1 MPa. This value is close to the adhesive shear failure stress that we set to be equal to 24 MPa. We can also see how the stress is almost uniformly distributed on the adhesive internal and external surface. Unlike the cohesive elements in contact with the glass post, the one in contact with the dentin is less stressed. In fact we can see from the figure 4.21b that the maximum stress on that cohesive layer is equal to circa 18.36 MPa. This value is lower than the adhesive shear failure stress therefore, the failure will not occur at that contact interface.

4.3.5.2 Force-Displacement curves

The force-displacement curve was plotted and from the figure 4.22 we can read that the peak force obtained from the numerical analysis is equal to 75.7 N. Considering the lateral surface of the glass post, we can deduce from the formula that adhesive bond strength is equal to 22.26 MPa. Such a value is enough close to the experimental result which gives an adhesive bond strength value equal to 19.79 MPa. We can see from the figure that both the curves have the same steepness. This is due to a good estimation of the adhesive stiffness for the numerical analysis. The trend of the curve is similar to what the experimental results gave us. This trend is justify by the reasons we gave in the results subsection of the model with the tiebreak contact. The fact that the numerical force-displacement curve was enough similar to the experimental force-displacement curve allowed us to validate this adhesive model.

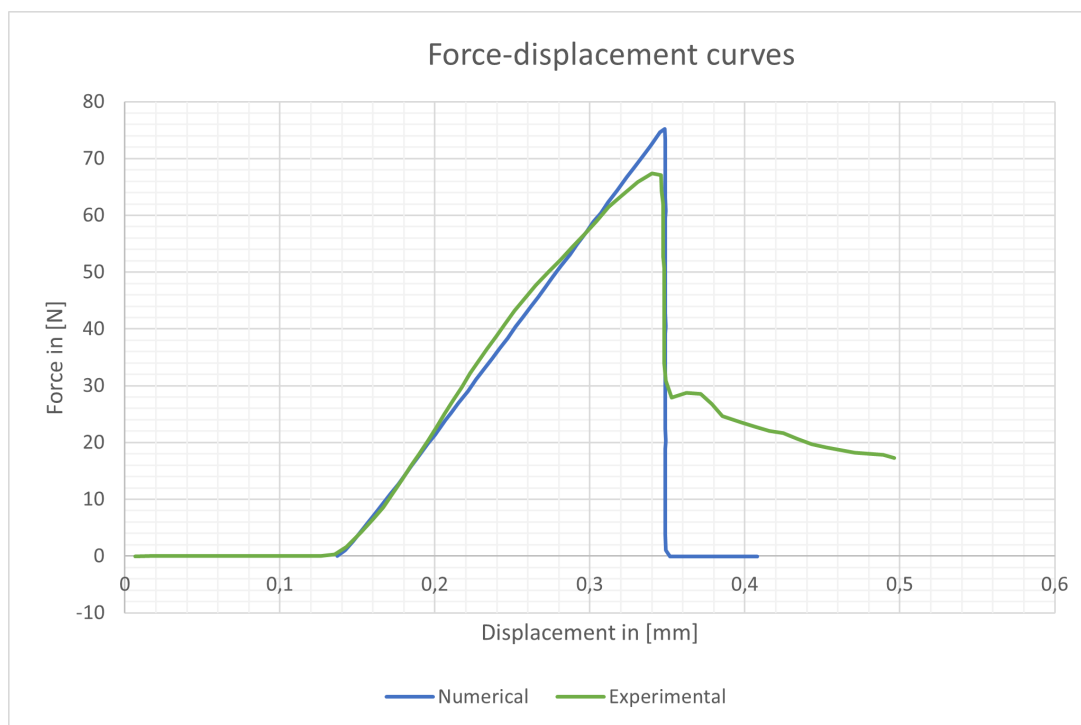


Figure 4.22: Force-Displacement curve

4.4 Comparison Between The Different Approaches

We recall that two approaches were used to model the adhesive layer. For each of these approaches, it was necessary to define some properties characterizing the adhesive such as the stiffness of the adhesive, its failure stress (in the normal and tangential direction)... etc. Even if these parameters have different names in the LS-DYNA manual user for each method, each parameter used to define the tiebreak contact has an equivalent parameter used to model the adhesive with the cohesive elements. The table 4.4 shows us that the

Push-out bond strength test	
Tiebreak contact	Cohesive elements
NFSL=20 MPa	FN_FAIL=20 MPa
SFSL=24 MPa	FT_FAIL=24 MPa
CN=220 GPa/m	ET=220 GPa/m

Table 4.4: Equivalence between the parameters used by the solver algorithms for the two different approaches. The parameters belonging to the same row have the same physical meaning.

main information necessary to model an adhesive with these two approaches are the adhesive failure stress in the normal and tangential direction as well as the adhesive stiffness. These values are enough when using these two approaches because they model adhesives

with linear elastic models.

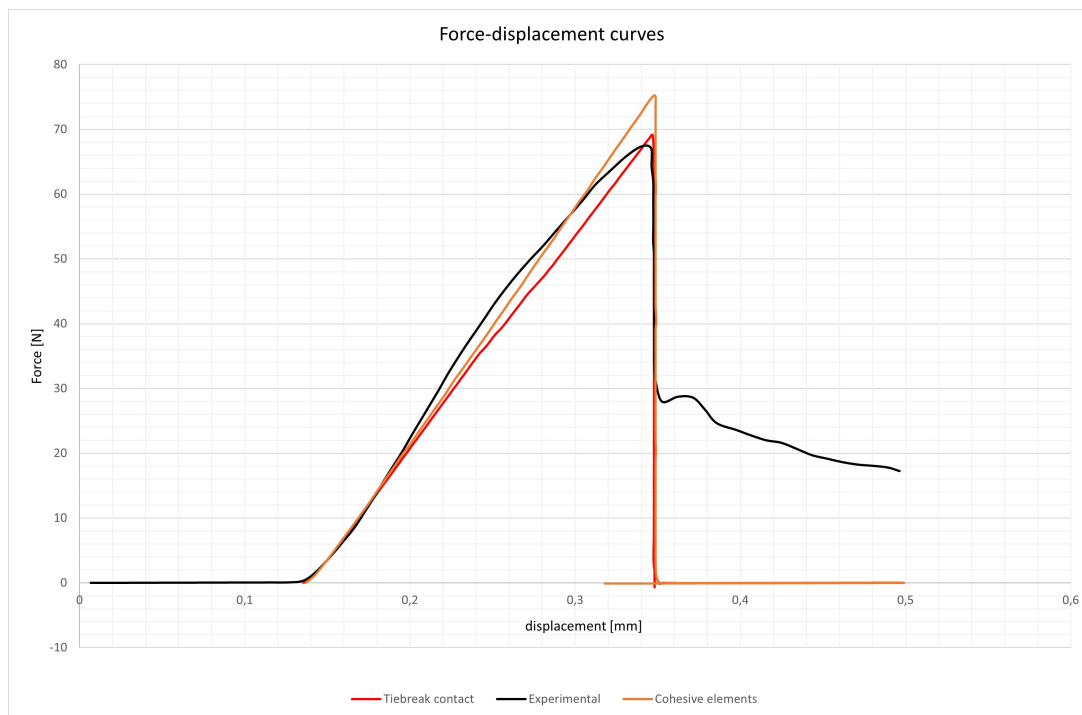


Figure 4.23: Force-Displacement curve

The figure 3.19 shows us the force-displacement curves obtained from the numerical analysis for different approaches in comparison with the experimental force-displacement curve. All the curves have the same slope therefore, We can deduce that both the methods are suitable to define the adhesive stiffness since the slope of each curve depends on the adhesive stiffness. We can also observe that the peak forces which depends on the adhesive failure stress (in normal and tangential direction) are almost the same even if the peak force is a little bit higher in the case of the cohesive elements. If we look at the equivalence between the parameters (tab 4.4 used to simulate the adhesive layer, for the adhesive shear failure stress (SFSL) a value of 24 MPa was assigned and the same value was assigned when using the cohesive elements approach but we obtained the peak forces which are a little bit different.

Chapter 5

Conclusion

In this thesis, the finite element analysis of restorative adhesives was performed through three in vitro tests widely used in the dentistry field which are:

1. The microtensile bond strength test.
2. The shear bond strength test.
3. The Push-out test.

The analysis of the restorative adhesives via these experimental tests required the building of numerical models able to represent the laboratory experiments. Our interest for the characterization of the adhesives and the validation of the experimental tests lead us to the adoption of two different approaches proposed by the software LS-DYNA to model cohesive zones. First, we opted for the Tiebreak contact to simulate the adhesive presence in each of these models making sure to have a force-displacement curve enough close to the one obtained from the experimental curve. As a second step, the adhesives were simulated with the cohesive elements in each of the models making sure to obtain from the results the force-displacement curves very close to the experimental force-displacement curves. The results obtained from the two approaches were analysed and compared. The two approaches that were used for the simulation of the adhesives are based on linear elastic models which are:

1. The AUTOMATIC_SURFACE_TO_SURFACE_TIEBREAK_CONTACT
2. The MAT_184 namely MAT_COHESIVE_ELASTIC.

Since these two models are linear elastic models, the parameters required by the solver to run these simulations were the same. They are called differently in the LS-DYNA manual user, but they correspond to the same material properties as we showed in the equivalence tables. These parameters are mainly the normal and the shear adhesives failure stress, the normal and the tangential adhesives stiffness which depend respectively on the adhesives Young's modulus and the adhesives shear modulus.

The comparison between the properties which characterize the adhesive in the two approaches shows that apart from the adhesives stiffness (either in the normal direction or in the tangential direction), all the other properties gave the results slightly different from one approach to another. We noted that both the approaches are able to well simulate the adhesive stiffness based on the adhesives Young's modulus and adhesives shear modulus. In fact with the same value of the stiffness assigned, both the approaches gave the force-displacement curves with the same slopes. On the other hand, we also realized that the peak of the forces which depends on the adhesive normal failure stress and the adhesive shear failure stress were almost the same in both the approaches provided that the adhesive failure stresses were tuned so that the numerical curve can fit the experimental one. For this reason, the adhesive failure stress assigned were different from one approach to another. Such a result prevented us from having the same value of the adhesives failure stresses. We noted that for what concerns the adhesives failure stresses the modelling of the adhesive with the cohesive elements gives the results which are more realistic.

Bibliography

- [1] MJ Tyas, MF Burrow. Adhesive restorative materials: A review. *Australian Dental Journal* 2004; 49:(3):112-121.
- [2] David H. Pashleya, Ricardo M. Carvalhob, Hidehiko Sano, Masatosiii Nakajima, Masahiro Yoshiyama, Yasuo Shono, Carios A. Fernandes, Franklin Tay. The Microtensile Bond Test: A Review. *J Adhesive Dent* 1999; 1:299-309.
- [3] Van noort R, Della Bona A. Shear vs. tensile bond strength of resin composite bonded ceramics. *J Dent Res* 1995;74(9):1591-6.
- [4] Elaheh Ghassemieh. Evaluation of sources of uncertainties in microtensile bond strength of dental adhesive system for different specimen geometries. *dental materials* 24 (2 0 0 8) 536-547.
- [5] Yoshiyama M, Carvalho RM, Sano H, Hornerg JA, Brewer PD, Pashley DH. Regional bond strength of resins to human root dentine. *J Dent* 1996;24(6):435-42.
- [6] Burrow MF, Nopnakeepong U, Phrukkanon S. A comparison of microtensile bond strengths of several dentine bonding systems to primary and permanent dentine. *Dental Mater* 2002;18:239-45
- [7] Nakabayashi N, Watanabe A, Arao T. A tensile test to facilitate the identification of defects in dentine bonded specimen. *J Dent* 1998;26(4):379-85.
- [8] Capel Cardoso PE, Sadek FT, Placido E, Santos JFF. Microtensile bond strength of current adhesive systems when compared to cohesive strength of sound dentin and a resin-based composite. *Mater Res* 2004;7(4): 575-81.
- [9] Phrukannon S, Burrow MF, Tyas MJ. The influence of cross sectional shape and surface area on the microtensile bond test. *Dent Mater* 1998;14(June):212-21.
- [10] Sinhoreti MA, Consani S, De Goes MF, Sobrinho LC, Knowles JC. Influence of loading types on the shear strength of the dentin-resin interface bonding. *J Mater Sci Mater Med.* 2001; 12: 39-44.
- [11] Rodivan Braz, Mário Alexandre Coelho Sinhoreti, Aloísio Oro Spazzin, Sandro Cordeiro Loretto, Arine Maria Viveros de Castro Lyra1, Agenor Dias de Meira-Júnior. Shear bond

strength test using different loading conditions – a finite element analysis. *Braz J Oral Sci.* October/December 2010 - Volume 9, Number 4.

[12] Al-Salehi SK, Burke FJ. Methods used in dentin bonding tests: an analysis of 50 investigations on bond strength. *Quintessence Int.* 1997; 28: 717-23.

[13] Pecora N, Yaman P, Dennison J, Herrero A. Comparison of shear bond strength relative to two testing devices. *J Prosthet Dent.* 2002; 88: 511-5.

[14] Van Noort R, Cardew GE, Howard IC, Noroozi S. The effect of local interfacial geometry on the measurement of the tensile bond strength to dentin. *J Dent Res.* 1991; 70: 889-93.

[15] Katona TR, Long RW. Effect of loading mode on bond strength of orthodontic brackets bonded with 2 systems. *Am J Orthod Dentofacial Orthop.* 2006; 129: 60-4.

[16] Oilo G, Olsson S. Tensile bond strength of dentin adhesives: a comparison of materials and methods. *Dent Mater.* 1990; 6: 138-44.

[17] Oilo G. Bond strength testing—what does it mean? *Int Dent J* 1993;17(6):492–8.

[18] Sudsangiam S, van Noort R. Do dentin bond strength tests serve a useful purpose. *J Adhesive Dent* 1999;1(1):57–67.

[19] Eliane Placidoa, Josete B.C. Meiraa, Raul Gonza´lez Limab, Antonio Muencha, Roberto Martins de Souzaab, Rafael Yagu¨e Ballester. Shear versus micro-shear bond strength test: A finite element stress analysis. *dental materials* 23 (2 0 0 7) 1086–1092

[20] Tantbirojn D, Cheng Y-S, Versluis A, Hodges JS, Douglas WH. Nominal shear or fracture mechanics in the assessment of composite-dentin adhesion. *J Dent Res* 2000;79(1):41–8.

[21] Van Noort R, Noroozi S, Howard IC, Cardew G. A critique of bond strength measurements. *J Dent* 1989;17(2):61–7.

[22] Rasmussen ST. Analysis of dental shear bond strength tests, shear or tensile? *Int J Adhesives Adhesion* 1996;16(3): 147–54.

[23] Hiraishi N, Kitasako Y, Nikaido T, Nomura S, Burrow MF, Tagami J. Effect of artificial saliva contamination on pH value change and dentin bond strength. *Dent Mater* 2003;19(5):429–34.

[24] McDonough WG, Antonucci JM, He J, Shimada Y, Chiang MY, Schumacher GE, et al. A microshear test to measure bond strengths of dentin-polymer interfaces. *Biomaterials* 2002;23(17):3603–8. [25] Shimada Y, Yamaguchi S, Tagami J. Micro-shear bond strength of dual-cured resin cement to glass ceramics. *Dent Mater* 2002;18(5):380–8.

[26] Tantbirojn D, Cheng Y-S, Versluis A, Hodges JS, Douglas WH. Nominal shear or fracture mechanics in the assessment of composite-dentin adhesion. *J Dent Res* 2000;79(1):41–8.

-
- [27] Felice R. Grassi, Carmine Pappalettere, Mariasevera Di Comite, Massimo Corsalini, Giorgio Mori, Andrea Ballini, Vito Crincoli, Francesco Pettini, Biagio Rapone, Antonio Boccaccio. Effect of Different Irrigating Solutions and Endodontic Sealers on Bond Strength of the Dentin – Post Interface with and without Defects. *Int. J. Med. Sci.* 2012, 9
- [28] Jainan A, Palamara JE, Messer HH. Push-out bond strengths of the dentine-sealer interface with a without a main cone. *Int Endod J.* 2007; 40: 882-90.
- [29] Teixeira CS, Alfredo E, Thomé LH, et al. Adhesion of an endodontic sealer to dentin and gutta-percha: shear and push-out bond strength measurements and SEM analysis. *J Appl Oral Sci.* 2009; 17: 129-35.
- [30] Hashem AA, Ghoneim AG, Lutfy RA, et al. The effect of different irrigating solutions on bond strength of two root canal-filling systems. *J Endod.* 2009; 35: 537-40.